Ferroelectric polycrystals: structural and microstructural levers for property-engineering via domain-wall dynamics

Jan Schultheiß, G. Picht, J. Wang, Y. A. Genenko, L. Q. Chen, J. E. Daniels, J. Koruza

Angaben zur Veröffentlichung / Publication details:

Schultheiß, Jan, G. Picht, J. Wang, Y. A. Genenko, L. Q. Chen, J. E. Daniels, and J. Koruza. 2023. "Ferroelectric polycrystals: structural and microstructural levers for property-engineering via domain-wall dynamics." *Progress in Materials Science* 136: 101101. https://doi.org/10.1016/j.pmatsci.2023.101101.

Progress in Materials Science 136 (2023) 101101

Contents lists available at ScienceDirect

Progress in Materials Science

journal homepage: www.elsevier.com/locate/pmatsci

Ferroelectric polycrystals: Structural and microstructural levers for property-engineering via domain-wall dynamics

J. Schultheiß [a,b,*], G. Picht [c], J. Wang [d], Y.A. Genenko [e], L.Q. Chen [d], J.E. Daniels [f], J. Koruza [g,*]

[a] Department of Materials Science and Engineering, Norwegian University of Science and Technology (NTNU), 7034 Trondheim, Norway
[b] Experimental Physics V, University of Augsburg, 86159 Augsburg, Germany
[c] Corporate Sector Advanced Technology, Advanced Technologies for Chemical and Biological Systems, Robert Bosch GmbH, 71272 Renningen, Germany
[d] Department of Materials Science and Engineering, The Pennsylvania State University, University Park, PA 16802, USA
[e] Institute of Materials Science, Technische Universität Darmstadt, Otto-Berndt-Straße 3, 64287 Darmstadt, Germany
[f] School of Materials Science and Engineering, University of New South Wales, 2052 Sydney, Australia
[g] Institute for Chemistry and Technology of Materials, Graz University of Technology, 8010 Graz, Austria

ARTICLE INFO

Keywords:
Polycrystalline ceramics
Ferroelectric/Ferroelastic
Domain wall dynamics
Dielectric
Piezoelectric

ABSTRACT

Ferroelectrics have a spontaneous electrical polarization that is arranged into domains and can be reversed by an externally-applied field. This high versatility makes them useful in enabling components such as capacitors, sensors, and actuators. Key parameters to tune their dielectric, piezoelectric, and electromechanical performance are the domain structure and the dynamic of the domain walls. In fixed compositions, this is often realized by chemical doping. In addition, structural and microstructural parameters, such as grain size, degree of crystallographic texture and porosity play a key role. An important step forward in the field was the fundamental understanding of the link between the local electric and mechanical driving forces and domain wall motion. Here, the impact of crystal structure and microstructure on these driving forces is reviewed and an engineering toolbox is introduced. An overview of advances in the understanding of domain wall motion on the micro- and nanoscale is provided and discussed in terms of the macroscopic functional performance of polycrystalline ferroelectrics/ferroelastics. In addition, a link to theoretical and computational models is established. The review concludes with a discussion about beyond state-of-the-art characterization techniques, new approaches, and future directions toward non-conventionally ordered ferroelectrics for next-generation nanoelectronic and energy-storage applications.

1. Introduction

Ever since their discovery over 100 years ago, [1] ferroelectric materials have been a fascinating research topic. Their numerous functional and physical properties make them indispensable in various technological products, such as actuators, capacitors, sensors, and transducers. [2,3] The field is continuously growing due to ongoing innovations, ranging from nanotechnology [4] to energy storage, [5] medical applications, [6] flexible electronics, [7] memristors, [8] and neuromorphic computing [9]. The intriguing

* Corresponding authors.
E-mail addresses: jan.schultheiss@ntnu.no (J. Schultheiß), jurij.koruza@tugraz.at (J. Koruza).

https://doi.org/10.1016/j.pmatsci.2023.101101
Received 17 May 2022; Received in revised form 1 February 2023; Accepted 19 February 2023
Available online 3 March 2023

physical properties of these materials are related to a switchable spontaneous polarization, that forms below the Curie temperature on the unit cell level. A coherent alignment of unit cells with uniform polarization direction is referred to as a ferroelectric domain. [11] Domains naturally form in ferroelectric materials to minimize the electrostatic and elastic energy. Ferroelectric 180° domain walls separate volumes where the spontaneous polarization vectors are parallel but of opposite sign, while ferroelectric/ferrolastic non-180° domain walls separate regions with non-parallel polarization vectors (further details on domain types are provided in Section 4.1.1.1). The domain walls may respond to an externally applied field by motion, which we refer to as domain wall dynamics. The mobility defines the proportionality coefficient between the domain wall velocity and the applied external field. [12]

Domain walls and their dynamics are heavily researched, since they co-determine many of the functional properties of ferroelectric materials, such as the switchable polarization, dielectric, or piezoelectric response. In this frame, the functional properties can be disentangled into intrinsic and extrinsic contributions. [11] The intrinsic response is related to the unit cell, i.e., distortions of the crystal lattice in response to some perturbation. The extrinsic response is generally associated with electric and/or mechanical field-induced displacement of domain walls or phase transformations. [13] Extrinsic ferroelectric/ferroelastic domain wall motion may contribute up to 80% to the dielectric and piezoelectric properties in polycrystals [14] and the functional properties of ferroelectrics/ferroelastics can be tuned via engineering the domain structure and the response of ferroelectric/ferroelastic domain walls to an applied external stimulus. In comparison to single crystalline counterparts, intergranular interactions, i.e., elastic strains originating from a rigid coupling between individual grains, and grain boundaries play a key role in polycrystals, impacting intrinsic and extrinsic contributions. [15] The dynamics of domain walls depend on the chemical composition of the polycrystals. Material-specific review articles exist for $BaTiO_3$ (BT)-based, [16] $BiFeO_3$ (BFO)-based, [17] and $(K,Na)NbO_3$ (KNN)-based [18] materials. Beyond the initial parent composition, chemical doping is often used to control domain wall dynamics. By creating defect complexes that interact with the small- and large-scale motion of domain walls, properties can be varied. [19–22]

Here, we move beyond the chemical doping strategy and discuss the general influence of structural and microstructural parameters on the functional properties of polycrystalline ferroelectric/ferroelastic ceramics with a focus on the dynamics of domain walls. We first explain the main driving forces for domain wall motion in single crystalline materials (Section 2.1), followed by a description of the impact of polycrystallinity on these forces (Section 2.2). Next, we summarize selected imaging techniques, driving the field forwards due to their increasingly accurate capability of direct mapping and quantifying the static domain structure of ferroelectrics and the impact of an external stimulation on domain wall motion (Section 3). In the main section, we review the impact of structural and microstructural parameters, including crystal system (Section 4.1), grain size, and orientation (Section 4.2), as well as porosity (Section 4.3) on domain wall dynamics and functional properties with a focus on BT and $Pb(Zr,Ti)O_3$ (PZT) based model systems. We further discuss selected computational methods which allow to shed light on the interplay between the microstructure and domain wall dynamics on different length scales (Section 5). We end our review with an outlook on advanced characterization techniques and outline their potential to disentangle the complex interplay between structure and domain wall dynamics (Section 6.1), more recent approaches to tailor domain wall dynamics using extended defects (Section 6.2), and polycrystalline systems with non-classical ferroelectric order (Section 6.3).

2. Driving forces for domain wall motion in ferroelectrics/ferroelastics

In our review we discuss the impact of structure and microstructure on enhancing and inhibiting domain wall motion and establish a link to the functional properties of ferroelectric/ferroelastic materials. To do this, we first address the question of how domain walls move in the single crystalline model case, and next explain the impact of the more complex boundary conditions found in

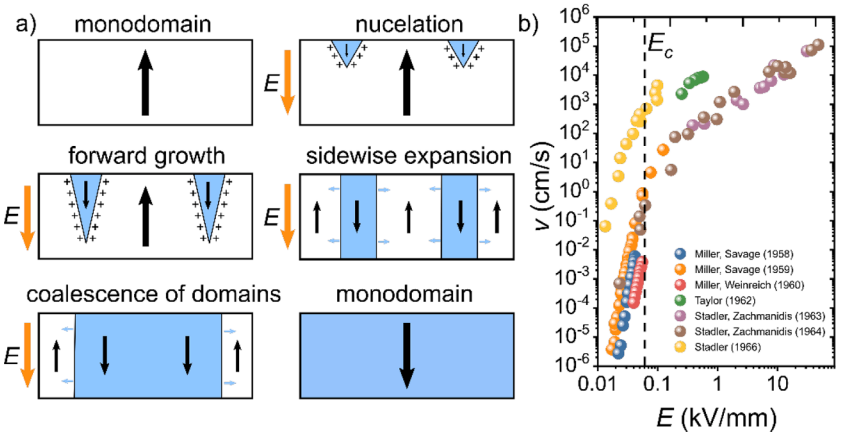

Fig. 1. Polarization reversal in a monodomain single crystal. a) Schematic representation of the polarization reversal process under an applied electric field, *E*. The mechanism includes the nucleation of new domains, forward growth, sidewise expansion, and domain coalescence. [39] b) Field-dependent velocity of 180° domain walls, *v*, in single crystalline BT during the sidewise expansion. [45–51] The coercive field of $E_c = 0.06$ kV/mm of a BT single crystal, obtained from polarization hysteresis measurements, is indicated for comparison by a vertical dashed line. [86]

polycrystalline materials. While the focus of our review is on the mechanisms, the understanding of domain wall dynamics in polycrystalline ferroelectrics/ferroelastics was driven forward by advances in characterization techniques. For a more detail insight and application examples of bulk-averaging characterization techniques, we refer the reader to refs. [13] and [15]. Due to their capability to cover a broad electric field and time range, we focus on time-dependent measurements, which enable distinction between individual types of domain wall motion. In addition to this, an important insight on the interplay between structure/microstructure and domain wall dynamics can be gained from frequency, [23] temperature, [24] and both above- and sub-coercive field-dependent measurements [25,26]. Furthermore, X-Ray (XRD) [15,27–35] and neutron [36–38] diffraction provide in-situ capabilities and access to the domain switching fraction and elastic strains averaged over different grain families, which is one of the keys towards disentangling the intergranular interactions in polycrystalline ferroelectrics/ferroelastics.

2.1. Single crystals

To reveal the main driving forces for domain wall motion, we first recall the polarization reversal process in a single crystal, schematically illustrated in Fig. 1a. Application of an electric field to a monodomain crystal results in the nucleation of new domains, their growth through the crystal, followed by sidewise expansion and domain coalescence. A more detailed description of the individual steps is provided in ref. [39], while a review of the detailed mechanisms for domain wall motion is given in ref. [20]. While in this review we term the entire process polarization reversal, we focus on the impact of the structure and the microstructure on the motion of the domain walls. In addition to the established mechanism presented in Fig. 1a, polarization reversal may occur without domains, if the domain nucleation can be suppressed. This requires ferroelectric single crystals of high purity and electric fields far above the coercive field need to be applied under a high ramp rate. This exotic scenario was experimentally observed in ref. [40] and a more detailed explanation is provided in ref. [41].

To understand the main driving force for domain wall motion, we display electric-field-dependent velocity studies of 180° domain walls in BT single crystals. [42–44] Pioneering experimental results [45–51] are summarized in Fig. 1b. A strong dependence of the velocity of the domain walls on the applied electric field amplitude can be observed. Two regimes are apparent: an exponential relationship was found for low electric fields ($E < 0.1$ kV/mm), [45] while a power law was proposed for high electric fields ($E > 0.1$ kV/mm). [49] The Merz law describes the exponential relationship between the domain wall velocity, $v(E)$, and the applied electric field, E [42]:

$$v(E) = v_0 \cdot \exp[-(E_a/E)]. \tag{1}$$

The coefficient v_0 is the pre-exponential factor, while the parameter E_a is termed the activation field, which is linked to the material-specific activation barrier, U, via

$$E_a = E_{c_0} \cdot \frac{U}{k_b \cdot T}. \tag{2}$$

Here, E_{c_0} is the critical field for domain wall depinning at 0 K, k_b is the Boltzmann constant, and T is the temperature. A ferroelectric domain wall is moving if the interplay between the thermal fluctuation and the external fields is sufficient to overcome the activation barrier. Mechanistically, the domain wall does not move as a whole but by small jumps, [47,52–56] the so called Barkhausen jumps [57]. In an ideal defect-free single crystal, the height of the potential barrier, and thus the parameter E_a, is defined by the Peierls potential of the lattice. [20,58–60] The local energy landscape depends on chemical defects, including electronic charge carriers, ionic defects, defect dipoles, and defect complexes. The interplay between chemical defects and domain wall motion has been studied experimentally, [61,62] as well as theoretically [63,64]. Since the impact of chemical defects on domain wall motion goes beyond the scope of this review, we refer the reader to refs. [19–22] for a more complete literature overview.

While experimental observations on single crystalline materials with a monodomain starting state confirmed the idealized scenario displayed in Fig. 1a, [39,65,66] domain wall dynamics become more complicated if the starting state deviates. For example, polarization reversal occurs via successive non-180° domain switching steps, if non-180° domain walls are present before application of the electric field. [67,68] The motion of non-180° domain walls in single crystals was confirmed by electromechanical, [69,70] acoustical, [71,72] optical, [73–75] and diffraction [76,77] studies. These works outline that besides the electric field, as displayed in Fig. 1 and Equation (1), mechanical driving forces also play a significant role for the motion of domain walls, related to their additional ferroelastic nature. Mechanical stress is known to modify the height of the potential barrier and thus impacts the parameter E_a, [78,79] acting as an additional driving or hindering force for domain wall motion. [80,81] Furthermore, domain wall motion was found to be impacted by other obstacles, such as other domain walls [82,83] or electrode defects [84,85].

2.2. Polycrystals

Similar to their single crystalline counterparts, both 180° [87–89] and non-180° [90–93] domain wall motion were found in polycrystalline ceramics. An important finding in understanding the driving forces for domain wall motion in polycrystalline materials was the revelation of the sequence of domain switching events from time-dependent measurements. This was accomplished using a synergetic approach combining high-energy diffraction, polarization, and strain measurements, [94,95] as well as stochastic modelling [96] on a poled polycrystalline ferroelectric/ferroelastic material. Ferroelectric 180° and ferroelectric/ferroelastic non-180° domain switching events can be disentangled based on their individual contribution to the time evolution of polarization and strain under a constant electric field pulse. [96] A typical time-dependent response of the switched polarization, ΔP, and strain, S, of the

material to a high-voltage pulse applied anti-parallel to the poling direction is schematically displayed in Fig. 2a. Based on this, a sequential mechanistic description of domain wall dynamics featuring three different regimes has been revealed (Fig. 2b): 1) non-180° domain wall movement, 2) main switching phase, and 3) creep-like domain wall movement. First, we discuss the three regimes mechanistically (Section 2.2.1), before we consider the impact of the local electric and mechanical driving forces on the dynamics of domain walls (Section 2.2.2) in detail.

2.2.1. Sequence of domain switching events

As a consequence of high lattice strain after electric poling and a four times lower domain wall energy of non-180° compared to 180° domain walls, [97] a high density of non-180° domain walls exists in the poled state of a polycrystalline material (regime 0 in Fig. 2). [98–102] Application of an external electric field antiparallel to the poling direction results in a rapid shrinkage of the sample and the development of a negative macroscopic strain due to non-180° domain wall movement (Fig. 2a). [15] The driving force for non-180° domain wall movement is the local electric field [103] supported by mechanical driving forces [95] originating from grain-to-grain coupling. [104] In comparison to single crystalline counterparts discussed in Section 2.1, mechanical stress plays a key role during polarization reversal in polycrystalline materials. [94,95] Electric and mechanical driving forces are displayed by orange and green arrows in Fig. 2b, respectively. At the end of regime 1 a critical state within the grains is achieved, defined by the interplay between local mechanical and electric fields. This triggers the main switching phase (regime 2 in Fig. 2), [94] where more than 60% of ΔP reverses. [94,105,106] Mechanistically, two different scenarios, as highlighted in i) and ii) in Fig. 2b, explain the macroscopic polarization and positive strain response: i) 180° domain walls nucleate and move sidewise similar to the situation in single crystals (Fig. 1a) [107] and ii) 180° domain switching occurs by synchronized non-180° domain wall motion. The latter requires the nucleation of a non-180° domain wall, which moves through the domain structure of a grain. [108,109] While current experimental techniques do not allow to distinguish between both suggested paths, microstructural arguments favor synchronized non-180° domain wall motion. For example, a reduced Peierls barrier, [54,97,110,111] crystallographic arguments, [112,113] and reduced activation barriers [114] indicate that non-180° domain wall motion is energetically favorable compared to 180° domain wall motion. At the end of the main switching phase, most domains have reversed, and the material enters regime 3 (Fig. 2). Here, the electric field is parallel to the polarization vector and the time-dependent polarization [115] and strain [116] curves (Fig. 2a) resemble electric creep. The slow increase of polarization and strain in this regime was attributed to the progressive movement of the ferroelectric/ferroelastic domain walls. [117,118]

2.2.2. Local electric and mechanical driving forces for domain wall dynamics

Similar to single crystalline materials (Fig. 1) discussed in Section 2.1, the local electric field is the main driving force for the polarization reversal process in polycrystalline ferroelectric/ferroelastic ceramics (orange arrow in Fig. 2b). In contrast to single crystals, where the value of the local electric field is similar to the externally applied one, [119,120] the local electric field is inhomogeneously distributed in polycrystals, [88,121–125] which is relevant to discuss the impact of structure and microstructure on switching dynamics. The local electric field thereby is a projection of the external field onto the local spontaneous polarization vector of each individual domain inside the grain. [124,125] In a first approach, this distribution can be calculated by considering the dielectric permittivity tensor and the distribution of polarization vectors. [126,127] The statistical distribution of the local electric field values in polycrystals is roughly symmetrically centered around the value of the external applied field. The broadness of the local

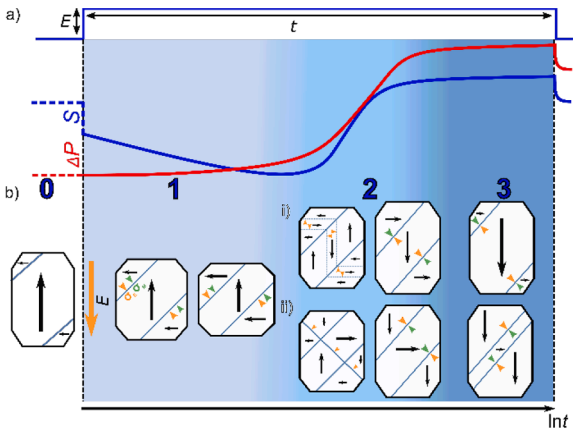

Fig. 2. Domain wall dynamics in ferroelectric/ferroelastic polycrystalline ceramics. a) Schematic response to a high voltage (HV) pulse with height E and time t. Based on the evolution of strain, S, and switched polarization, ΔP, three regimes can be distinguished. The schematic domain response is displayed in b) for a grain with a tetragonal crystal system. The 90° domain walls are displayed as solid lines, while the 180° domain walls are dashed. 1) Initial non-180° domain wall movement, 2) main-switching phase by i) nucleation and sidewise growth of 180° domains, [107] and ii) 180° polarization reversal by a nucleated non-180° domain wall through synchronized non-180° domain-wall movements, [108,109] and 3) creep-like domain wall movement. Electric and mechanical driving forces are displayed by orange and green arrows, respectively. Reprinted from [94], with permission from Elsevier.

electric field distribution is typically quantified by its full width at half maximum (FWHM). [88] For the model case of a dense $Pb(Zr_{0.515}Ti_{0.485})O_3$ material with a tetragonal crystal system, [126] the local electric field is enhanced/reduced by ~ 20% in ~ 85% of the grains, while strong field deviations exceeding 60% enhancement/reduction occur in < 5% of the grains. Crystal system, [126,128–130] degree of crystallographic texture, [131] stress concentrations near grain boundaries, [132] and porosity [106,133] were suggested as engineering levers for tuning the local electric field distribution, as discussed in more details in Section 4.

In comparison to single crystalline materials, where the local deformation related to the piezoelectric effect and the movement of ferroelectric/ferroelastic domain walls is unconstrained, [134] in polycrystalline materials the grains are mechanically coupled over a rigid grain boundary, as demonstrated experimentally. [20,94,104,135–141] Mechanical stress is a direct consequence of the coupling between the grains (green arrow in Fig. 2b). [94] The anisotropy of both intrinsic and extrinsic piezoelectric strains, as well as the elastic anisotropy of the system, causes some grain orientations to drive the response, while others restrict the response due to their requirement for elastic accommodation. A rigorous treatment of these intergranular interactions using the Eshelby approach [142] is provided in ref. [104]. Considerable intergranular stress in the order of 40–100 MPa were reported for polycrystalline ferroelectric/ferroelastics. [143]

3. Imaging techniques

Ferroelectric/ferroelastic polycrystals offer various engineering degrees of freedom, including grain boundaries, [144–146] a locally distributed electric field, [88,125,133] and 3D confinement effects. [94,104] One of the key challenges in the field is therefore to develop suitable methods enabling to visualize the static domain structure, i.e., the shape and size of the ferroelectric domains, and to image the impact of external driving forces on domain wall dynamics. Due to their capability to directly quantify and map the

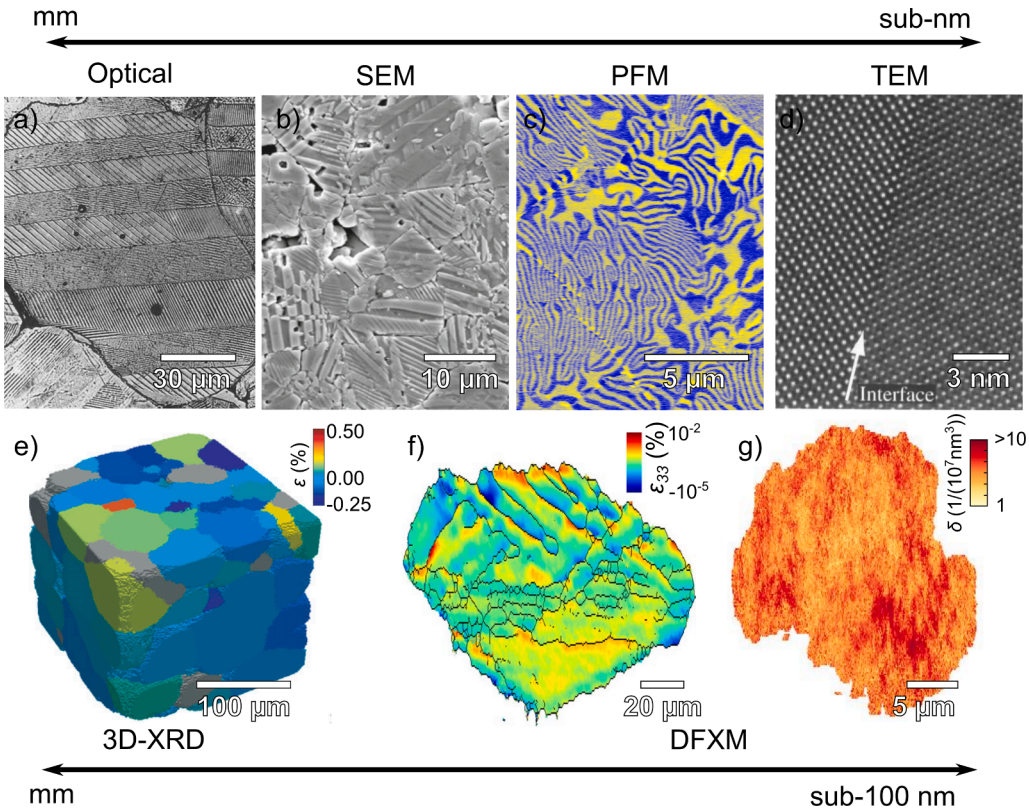

Fig. 3. Selected techniques which enable multilength scale mapping of ferroelectric domains in polycrystalline ferroelectric/ferroelastic materials, providing information on the domain structure and domain wall dynamics. a) Micrograph of polycrystalline BT obtained by optical microscopy. Reprinted by permission from Springer Nature: [182], Copyright 1990. b) SEM micrograph of an etched surface of $(K,Na)_{0.94}Li_{0.06}NbO_3$ featuring a complex domain structure. Reprinted by permission from Springer Nature: [183], Copyright 2018. c) PFM of polycrystalline $ErMnO_3$ displaying the complex domain structure which forms by the interaction of topologically protected vortex/anti-vortex pairs and elastic strain fields. Reprinted from [184] with permission from Wiley. d) High resolution TEM micrograph of a 90° domain wall in $PbTiO_3$. [185], by permission of The Japanese Society of Microscopy. e) Grain maps of a polycrystalline BT sample in the virgin state obtained using 3D-XRD. The average strains, ε, of the individual grains are displayed. Reproduced with permission from [173], Copyright 2017, The American Ceramic Society. f) Cross sectional cut through a BT grain obtained by DFXM. Strain concentrations in the vicinity of interfaces, e.g., domain walls (black lines) are displayed. Reprinted by permission from Springer Nature: [178], Copyright 2018. g) Density of domain variants in a slice of a grain of a polycrystalline BCZT material. The number of domains inside a localized diffraction volume of 10^7 nm^3 is displayed. [179]

correlation between the micro- and domain structure as well as the motion of domain walls, we focus on selected imaging techniques in this section, which, in our opinion, are advancing the fundamental understanding of the interplay between structure and microstructure on domain wall dynamics in polycrystalline ferroelectrics/ferroelastics. To further consider the different chemical and mechanical boundary conditions [147–150] that impact structure–property relationships in polycrystalline ferroelectrics, we have structured the section into surface-sensitive (Section 3.1) and bulk-sensitive (Section 3.2) imaging techniques.

3.1. Surface-sensitive imaging techniques

Classically, domains in ferroelectric/ferroelastic polycrystals were visualized via optical microscopy (Fig. 3a) with the capability to capture domain dynamics in the ms regime. [151] These methods were limited to domain structures with sizes above approximately 0.5 μm. [152] A major achievement in the field was the development of domain imaging techniques pushing the resolution towards the nanoscale. Scanning electron microscopy (SEM) and piezoresponse force microscopy (PFM) have facilitated imaging of the complex coupling between microstructure and domain morphology at length scales well below 100 nm. Selected domain images obtained by SEM and PFM are displayed in Fig. 3b and Fig. 3c, respectively.

SEM provides a direct overview of the domain structure of several grains. The time resolution is given by the scanning speed of the electron beam, which is in the μs range. [153] The domains can be revealed either by chemical or thermal etching or by electron channeling contrast imaging of well-polished samples. A detailed overview of the characterization and experimental parameter ranges of ferroelectric domains by SEM is provided in refs. [153,154]. In comparison to SEM, PFM enables to map the electromechanical properties with nanoscale resolution, facilitating visualization of the ferroelectric domain structure. In addition to mapping the static properties of ferroelectric domains, approaches with sub-100 ns spectroscopic time resolution [155] broaden the measurement capabilities, e.g., by quantifying the impact of electric driving forces on domain wall dynamics on the nanoscale. [156] Comprehensive reviews on the working principle of PFM and examples of domain structures of ferroelectric materials can be found in refs. [157–160]. Tomographic PFM further extends the analysis into subsurface regions of ferroelectric materials. [161] To obtain even higher resolution, transmission electron microscopy (TEM) directly visualizes atomic positions, facilitating atomic-scale structural resolution of a ferroelectric domain wall (Fig. 3d). Due to the ability to identify individual atomic columns with different atomic weight, high angle annular dark field (HAADF) and annular bright field (ABF) scanning transmission electron microscopy (STEM) imaging techniques are particularly interesting for polycrystalline ferroelectric/ferroelastic materials, as reviewed in ref. [162]. In-situ studies in TEM provide time-resolutions down to the ms regime. In addition, photoemission electron microscopy (PEEM), [163] low-energy electron microscopy (LEEM), [164] and confocal Raman spectroscopy, [165] have been explored to widen the experimental parameter range for mapping ferroelectric domain structures.

3.2. Bulk sensitive imaging techniques

Bulk-sensitive microscopy imaging provides a new dimension to the techniques introduced in Section 3.1, since static and dynamic information of the domain structure can be readily obtained under natural mechanical, electrostatic, and chemical boundary conditions in the bulk of ferroelectric/ferroelastic polycrystals. In addition, they are powerful tools to unravel the structure–property relationship since they combine domain imaging with local maps of elastic strain, giving direct access to elasto-morphological correlations in the bulk as a function of an external stimulation.

X-Ray projection ptychography maps the ferroelectric domain structure in thin films, with a spatial resolution down to 5.7 nm. [166] A more detailed explanation of the technique is provided in ref. [167]. Scanning with a highly coherent beam enables to capture the dynamics of ferroelastic domains in nanowires. [168] For ferroelectric polycrystals, 3D grain mapping techniques, such as 3D X-ray diffraction (3D-XRD) [169,170] and diffraction contrast tomography, [171,172] allow a rapid overview of the grain morphology and orientation, and visualize the response of individual grains with a resolution down to 1 μm. Combined with an electric field, this facilitates quantification of the strain response of each individual grain (Fig. 3e). [173,174] Related methods using neutrons open the possibility of probing much larger bulk polycrystalline materials, though the resolution is limited in comparison to XRD-based methods. [175] Dark-field X-Ray microscopy (DFXM) [176–178] allows observation of strain fields (Fig. 3f) together with crystallographic orientation maps, [178] with resolutions in the sub-100 nm regime (Fig. 3g), [179] slowly approaching the spatial resolution of SPM or SEM methods. For a more detailed insight into DFXM, we refer the reader to refs. [180,181].

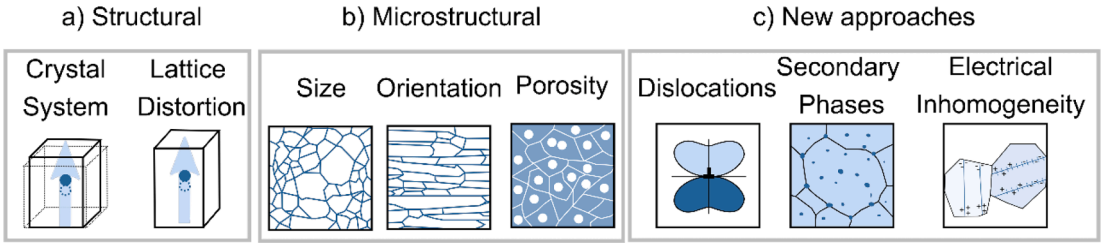

Fig. 4. Structural and microstructural toolbox to tune functional properties in polycrystalline ferroelectric/ferroelastic materials via domain wall dynamics: a) intrinsic structural, b) microstructure-related parameters, and c) new approaches using extended defects.

4. Structural and microstructural toolbox

An overview of the degrees of freedom offered by the structure and microstructure is provided in Fig. 4. In this review, we disentangle the high interdependency between each of the parameters and clarify the individual impacts on the static domain structure and domain wall motion. Note that Fig. 4 focuses on structural and microstructural elements, while composition specific approaches, such as doping or defect chemistry, which are frequently applied to control domain wall motion are not included (the interested reader is referred to refs. [19–22]). Section 4.1 deals with intrinsic structural parameters, i.e., the crystal system and the distortion of the lattice (Fig. 4a). Sections 4.2 and 4.3 discuss the impact of the grain boundaries, the grain-orientation relationship, and the porosity on domain wall dynamics (Fig. 4b). The potential of new approaches using extended defects (Fig. 4c), including dislocations, secondary phases, and electrical inhomogeneities is briefly outlined in Section 6.2.

4.1. Intrinsic structural parameters

While a coexistence of crystallographic phases, e.g., the concept of the morphotropic phase boundary (MPB), is important in terms of an enhancement of dielectric and piezoelectric properties, the exact mechanisms are still under discussion. In this section, we therefore focus on the impact of the individual crystal systems with the goal to establish a mechanistical understanding linking the number of polarization directions and spontaneous strain to the mobility of domain walls (Section 4.1.1.1). Next, we review literature on the impact of the magnitude of the lattice distortion away from the parent paraelectric state and evaluate the domain-wall related response (Section 4.1.1.2). Finally, the mechanisms are demonstrated via two selected case studies (Section 4.1.2), establishing a link between domain wall dynamics and functional performance.

4.1.1. Mechanistic description

4.1.1.1. Tetragonal, orthorhombic, and rhombohedral systems. The polar axes and the amount of equivalent polarization directions vary for the different crystal systems as summarized in Table 1. For perovskite materials, which are of key interest in our review article, the number of equivalent polarization directions is 6, 12, and 8 for tetragonal, orthorhombic, and rhombohedral systems, respectively. [186] Systems with a coexistence of rhombohedral and tetragonal systems have been described by 14, [187] while systems with a coexistence of all three systems (tetragonal, rhombohedral, and orthorhombic) have been described by 26 polarization directions [188]. The crystal system impacts the local electric field, which is one of the driving forces for domain wall dynamics. The correlation between crystal system and electric-field distribution, as quantified by its FWHM defined in Section 2.2.2 (Table 1), was measured [129] and calculated [105,126]. Calculations found that the distribution is broadest for a tetragonal material (FWHM = 0.32), while it is narrowest for a rhombohedral counterpart (FWHM = 0.19). Further, a one-to-one correlation between the crystal system and the switchable polarization exists. In a single crystalline ferroelectric, the entire polarization can be aligned if the external field is applied in the direction of a polar axis, e.g., along [100] in tetragonal materials ($P_{max}/P_S = 1$). In polycrystalline materials, the maximal possible fraction P_{max}/P_S is reduced and scales with the amount of the available polarization directions. [189] As displayed in Table 1, values of $P_{max}/P_S = 0.866$ and $P_{max}/P_S = 0.831$ were calculated for rhombohedral and tetragonal systems, respectively, while a higher value of $P_{max}/P_S = 0.912$ was reported for an orthorhombic crystal system. [124,126,190,191] For comparison, a value of $P_{max}/P_S = 0.922$ was reported for a coexistence of tetragonal and rhombohedral crystal systems. [192,193] Going beyond the impact of the crystal system on electric driving forces and switchable polarization, also mechanical driving forces are impacted via the spontaneous strain of the unit cell. In a polycrystalline ferroelectric/ferroelastic material, the electric-field induced movement of non-180° domain walls comes along with the generation of internal stress, [104] which was found to be higher in tetragonal compared to rhombohedral systems. [194,195]

4.1.1.2. Lattice distortion away from the parent cubic system. The magnitude of the distortion of the lattice away from the parent cubic structure mainly impacts local mechanical driving forces (Section 2.2.2) as can be best understood if the responses of a single- and a polycrystalline material with a high lattice distortion are compared. A good example is $PbTiO_3$ (PT), which has a high tetragonal lattice distortion of $c/a = 1.063$. Macroscopic electric-field-dependent polarization measurements on polycrystalline PT [196,197] did not reveal the development of a polarization hysteresis loop when an electric or mechanical field was applied, indicating that domain wall motion in polycrystalline PT is suppressed due to mechanical stress originating from grain-to-grain interactions. [198] This is

Table 1
Impact of crystal system for perovskite ferroelectric/ferroelastics: Number of equivalent directions, allowed types of non-180° domain walls, maximum possible fraction of single crystal polarization value, which can be achieved in a random polycrystalline state, P_{max}/P_S, and FWHM of the local electric field distribution [After ref. [186]].

Crystal system	Polar axis	Number of equivalent pol. directions	Types of non-180° domain walls	P_{max}/P_s (refs. [190,192])	FWHM of the local electric field distribution (ref. [126])
Tetragonal	⟨001⟩	6	90°	0.831	0.32
Orthorhombic	⟨110⟩	12	90° / 60° / 120°	0.912	0.29
Rhombohedral	⟨111⟩	8	71° / 109°	0.866	0.19

manifested by an unchanged tetragonal domain switching fraction for electric fields as high as 5 kV/mm or under compressive stress as high as 300 MPa. [196] In comparison, measurements on PT single crystals found a low coercive field of 0.64 kV/mm and a high remanent polarization of 74 μC/cm^2, [199,200] which is close to the theoretical value. [201]

The mechanical stress in the vicinity of domain walls scales with the lattice distortion. The reason is that the angle between two adjacent domains deviates from the ideal strain-free 90° configuration of a tetragonal crystal system, [202–204] experimentally resolved for PT thin films. [205] For tetragonal systems, the deviation angle ξ thereby depends on the tetragonal c/a lattice distortion and can be calculated as

$$90^{\circ} - \zeta = \tan^{-1}\left((c/a)^{-1}\right). \tag{3}$$

Calculations for different lattice distortions are in good agreement with experimental results. For example, BT with a low lattice distortion of $c/a = 1.01$ exhibits a deviation angle of $\zeta = 0.5^{\circ}$, [206–208] while PT with a lattice distortion of $c/a = 1.063$ has a higher deviation angle of $\zeta = 3.6^{\circ}$. [209,210] The origin of the internal compatibility stress at a domain wall is derived in Fig. 5a-c. [211] A drawing of the stress-free domain structure for a tetragonal material is schematically depicted in Fig. 5a. This schematic domain structure can be separated into three pieces, as displayed in Fig. 5b. Mechanical stress arises when the domain structure is forced back to be exactly 90° (Fig. 5c). Large tensile and compressive elastic stress is stored in such junctions between different lamellar regions, as indicated by the arrows in Fig. 5c. [212–215] The stress level is plotted as a function of the c/a ratio in Fig. 5d for a tetragonal PZT model system and significant stress levels in the GPa regime were calculated for the junction of 90° domains. [216,217] The blue data points in Fig. 5d represent the theoretically calculated deviation angle according to Equation (3), while the orange data points represent experimentally obtained values. Results obtained by DFXM further demonstrate that the elastic stress fields in the vicinity of domain walls are long ranging and can extend up to several micrometer into the adjacent domains (Fig. 3f). [178]

Besides at domain walls, stress concentrations are also found near grain boundaries. These arise in all polycrystalline materials, e.g., due to the anisotropy of the thermal expansion coefficient, the random orientation of the grains, [179,218,219] and the formation of a

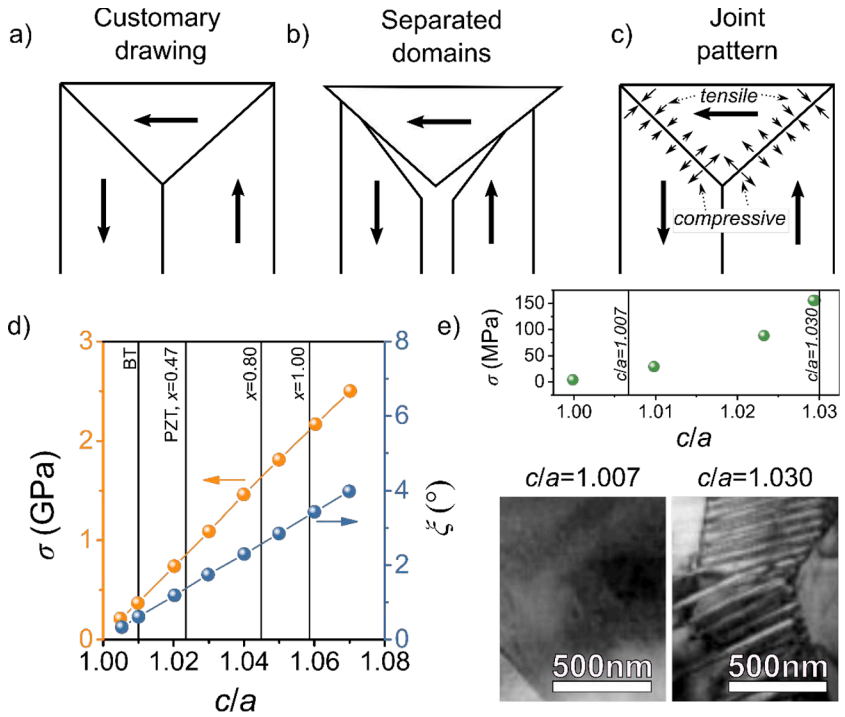

Fig. 5. Interplay between lattice distortion and microstructure. A possible origin of mechanical stress in the vicinity of the domain walls is shown for a simple 2D banded domain structure in a)—c). a) The customary drawing of the domain structure displays the stress-free case. The lattice distortion results in a space mismatch between the domains, as displayed in b). After joining the domain patters, tensile and compressive stress develops at the domain wall, as schematically displayed by the arrows in c). [211] d) The influence of lattice distortion on the maximum stress, σ, at a band junction between two domains and the deviation angle ζ. The stress in the vicinity of the domain wall scales with the magnitude of the lattice distortion. The blue solid line represents the calculation based on Equation (3). The maximum stress in the vicinity of the domain wall increases with increasing deviation angle and c/a ratio. The c/a ratios of example materials, including BT and tetragonal $Pb(Zr_{1-x}Ti_x)O_3$ with different titanium contents x are plotted for comparison as vertical lines. [217] e) Internal stress averaged over the whole polycrystalline body as a function of the c/a ratio for a La-doped PT. Average intrinsic stress increases with increasing the c/a ratio. TEM images of the domain structure are displayed for two different c/a ratios (indicated by the solid line). The TEM images display that the density of domain walls increases with increasing the c/a ratio. [223] Reprinted by permission from Springer Nature: [224], Copyright 2000.

spontaneous strain at the phase transition temperature. [134] For ferroelectric materials with a high lattice distortion, e.g., PT or $YMnO_3$, high stress results in microcracks [220,221] or even in fracture of the polycrystalline material during cooling. [222] The correlation between lattice distortion and stress was systematically studied for La-doped PT. [223] Internal mechanical stress was found to scale with the c/a ratio, as displayed in Fig. 5e. While average internal mechanical stress is absent for a lattice distortion close to cubic ($c/a \sim 1.00$), values of approximately 150 MPa were found for a lattice distortion of 1.03. Furthermore, a correlation between the c/a ratio and the static domain structure was observed. TEM micrographs obtained for two representative lattice distortions of 1.007 and 1.030 of a La-doped PT ceramic are displayed in Fig. 5e. [224] While strain-induced domains were found to be absent for a c/a ratio close to the cubic parent phase ($c/a = 1.007$), a high density of domain walls was observed if the c/a ratio was increased to 1.030. A similar correlation between the lattice distortion and the static domain structure for other systems is also reported in refs. [225,226].

4.1.2. Case studies

We next present two selected case studies, that allow to disentangle the complex interplay between crystal system/lattice distortion and domain wall dynamics and shed light on functional properties.

4.1.2.1. Phase boundary in the Pb(Zr,Ti)O_3 system. Phase boundaries are important, because they are often associated with peaks in functional properties, such as piezoelectric or dielectric coefficients. [11] Various studies exist, which investigate the domain wall dynamics over phase boundaries, e.g., in PZT-, [105,129,227–232] $(Bi_{1/2}Na_{1/2})TiO_3$ (BNT)-, [233–236] KNN- [237,238] or BT- [128,130,239] based ceramic systems. The most prominent phase boundary is most likely the rhombohedral-tetragonal phase boundary in PZT. In this section, we discuss the domain wall dynamics in the rhombohedral and tetragonal phases in the PZT system, while we display the MPB composition for comparison. Multiple studies outlined that domain switching is easier in the rhombohedral phase compared to the tetragonal one, experimentally underlined by a higher activation field for polarization reversal, [105,129] a broader distribution of switching times, [129] a lower Rayleigh coefficient, α, [240,241] a higher coercive field, [105,230,232] and a higher coercive stress [231,242] for tetragonal PZT materials in comparison to rhombohedral counterparts.

While various reports are available on polycrystalline PZT, e.g., refs. [231,243–245], we focus here on the $Pb_{0.985}V_{Pb_{0.005}}La_{0.01}(Zr_{1-x}Ti_x)O_3$ system, [246] since the domain-wall dynamics were characterized using a combination of time-dependent pulse and triangular bipolar HV electric measurements (Fig. 6). [105] The polarization and strain hysteresis loops measured at 1 Hz and the time-dependent evolution of switched polarization and strain are displayed for different titanium contents x in Fig. 6a and b, respectively, facilitating a

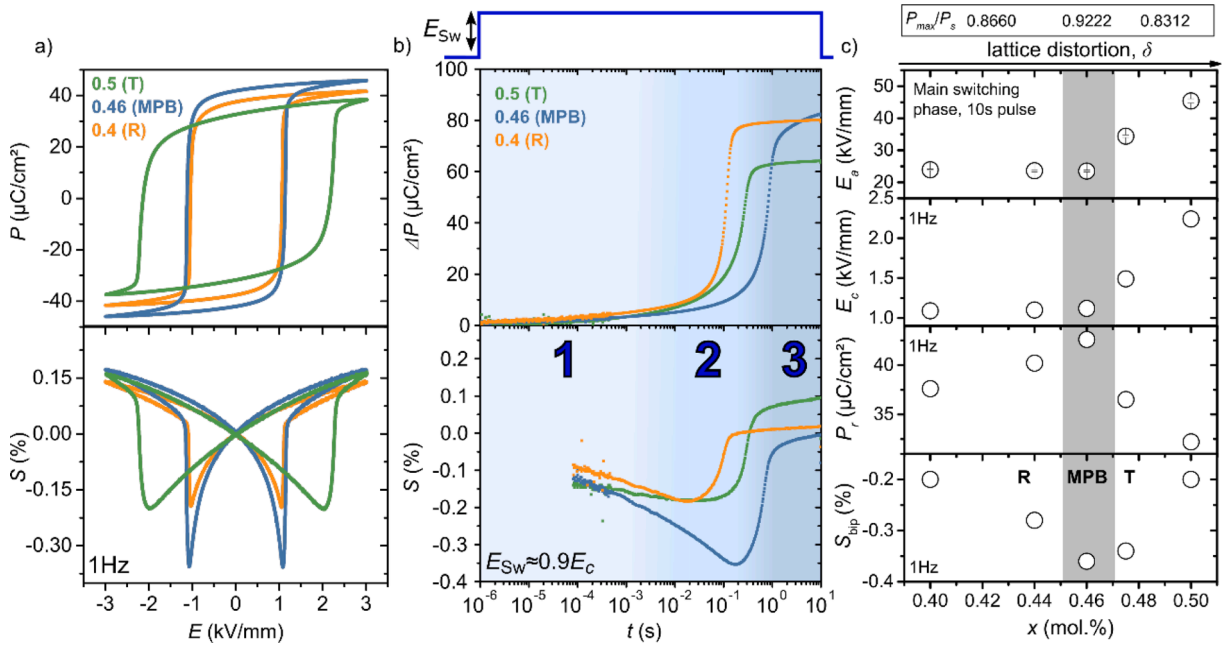

Fig. 6. Domain wall dynamics over the tetragonal (T) - rhombohedral (R) phase transition in a $Pb_{0.985}V_{Pb_{0.005}}La_{0.01}(Zr_{1-x}Ti_x)O_3$ model system. a) Macroscopic polarization and strain hysteresis loops measured at 1 Hz. A tetragonal, rhombohedral, and a composition with a phase mixture are compared. b) Representative time-dependent measurements of switched polarization, ΔP, and macroscopic strain, S, of a poled sample as a response to a HV pulse of height $E_{Sw} \approx 0.9E_C$. The numbers indicate the individual switching regimes according to ref. [94]. The motion of non-180° domain walls govern the first regime, while in the second regime the 180° events are dominant. Reprinted from [105], with the permission of AIP Publishing. c) Evolution of the activation barrier for polarization reversal of the main switching phase (determined from time-dependent measurements [42]), the coercive field, the remanent polarization, and the bipolar strain are displayed as a function of the composition. The change of the lattice distortion is indicated by the arrow. [105]

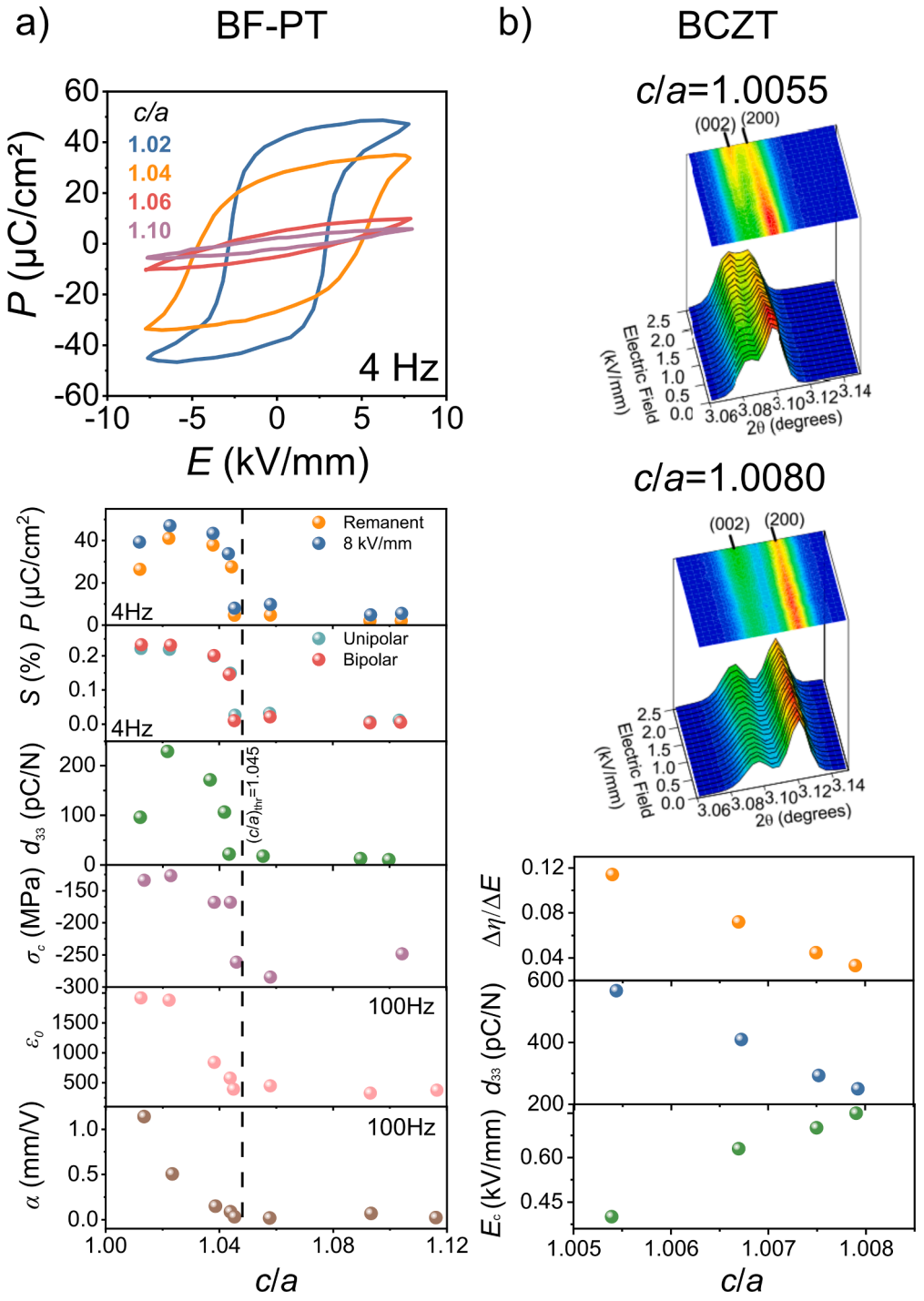

Fig. 7. Impact of the c/a ratio on domain wall dynamics and functional properties in polycrystalline ferroelectric/ferroelastic ceramics. a) The c/a ratio was tailored by changing the La content in tetragonal $BiFeO_3$-$PbTiO_3$ polycrystalline ceramics. Field-dependent macroscopic polarization loops are displayed for different c/a ratios. The polarization, P, macroscopic strain, S, macroscopic piezoelectric coefficient, d_{33}, coercive stress, σ_c, zero field permittivity, ε_0, and Rayleigh coefficient, α, are displayed as a function of the c/a ratio. A threshold value $(c/a)_{thr} = 1.045$ was identified, beyond which polarization reversal was completely suppressed. [253–255] b) The c/a ratio was changed through the composition in the tetragonal $(1\text{-}x)Ba(Zr_{0.2}Ti_{0.8})O_3\text{-}x(Ba_{0.7}Ca_{0.3})TiO_3$ system. Field-induced changes in the pseudo-cubic 002 diffraction peaks are displayed during poling from the virgin state for two different c/a ratios. The change of the domain switching at weak electric fields, $\Delta\eta/\Delta E$ (ΔE is from −0.45 kV/mm to + 0.45 kV/mm), the macroscopic piezoelectric coefficient, d_{33}, and the coercive field are displayed as a function of the c/a ratio. Reprinted from [256], with the permission of AIP Publishing.

comparison between a T and R crystal system. A MPB composition is displayed for comparison. The polarization and strain response of the rhombohedral systems is sharper in comparison to the tetragonal systems, which reflects the narrow distribution of the local electric fields in these materials (FWHM value in Table 1). [105,247] The dependence of the activation barrier for polarization reversal (determined from time-dependent measurements), coercive field, bipolar strain, and remanent polarization are displayed as a function of the titanium content in Fig. 6c. The impact of the crystal system on the switchable polarization can be quantified by the remanent polarization value. [105] A value of $P_r = 32.2\ \mu C/cm^2$ was found for the composition with tetragonal crystal system ($x = 0.5$), while a higher value was found for the rhombohedral crystal system ($x = 0.4$, $P_r = 37.6\ \mu C/cm^2$). The coercive field and the activation barrier for polarization reversal (obtained from field- and time-dependent measurements [42]) in the tetragonal composition is by a factor of 2 higher compared to the rhombohedral counterpart (Fig. 6c), underlining that switching is more difficult in tetragonal materials. Particularly, it can be observed that the coercive field and the activation barrier scale with the distortion of the lattice, as displayed by the arrows in Fig. 6c. The distortion of the tetragonal lattice for $x = 0.5$, for example, is by a factor 3 higher compared to the rhombohedral crystal system at $x = 0.4$. [246] This outlines that domain wall motion gets more difficult with increasing lattice distortion, most likely related to enhanced stress in the vicinity of the interfaces, e.g., domain walls and grain boundaries, as discussed in Section 4.1.1.2 and Fig. 5.

The impact of the crystal system on the fraction/dynamics of non-180° domain walls can be further quantified by the slope of the time-dependent strain curve (Fig. 6b). The slope, which represents the fraction/dynamics of the moving non-180° domain walls (Fig. 2) is lowest for $x = 0.5$ (tetragonal). The motion of non-180° domain walls generates large internal stress in tetragonal materials, [195] making the motion of these types of domain walls unlikely. The measurements provided in Fig. 6b were corroborated by time-resolved synchrotron studies [32,35,94,104,248–250] and theoretical calculations [251]. While these studies confirm the motion of non-180° domain walls in tetragonal PZT compositions, their fraction is much smaller in comparison to rhombohedral or MPB compositions. The contribution of non-180° domain wall movement to the entire domain switching fraction (180° and non-180° domain walls) was for example quantified as 20–25% for undoped rhombohedral PZT systems, while it was found to be lower for their tetragonal counterparts (7–8%). [252]

4.1.2.2. Lattice distortion in La-doped $BiFeO_3$-$PbTiO_3$. The interplay between lattice distortion and domain wall dynamics was systematically studied for La doped tetragonal $BiFeO_3$-$PbTiO_3$ (BF-PT), [253–255] the tetragonal side of the BCZT system, [256] lanthanum doped tetragonal PT, [223,224,226] and KNN-based [257] materials. Results for BF-PT and BCZT are displayed in Fig. 7. These studies outline that switching gets more difficult with increasing the c/a ratio. At the same time, electromechanical properties were found to peak for small lattice distortions, followed by a decrease with increasing distortion away from the paraelectric phase. [244]

We discuss the impact of lattice distortion in more details for the BF-PT and the BCZT systems, as the available data allows to establish a systematic link between the lattice distortion and functional properties. The impact of the c/a ratio on the shape of the polarization hysteresis loops, as well as the ferroelectric and piezoelectric properties [253–255] are displayed in Fig. 7a for the BF-PT system. With increasing the c/a ratio, the polarization hysteresis loops broaden and the ferroelectric behavior gets suppressed. The remanent and maximum polarization (measured at 8 kV/mm) decrease with increasing the c/a ratio. For small lattice distortions, the d_{33} response first peaks, followed by a decrease. The suppression of piezoelectric performance was explained by an incomplete poling of the material related to an increased distortion of the lattice. [253] As indicated by the coercive stress (Fig. 7a), easiest switching was found for small c/a ratios, while switching gets more difficult if the c/a ratio increases. Moreover, a threshold value of $(c/a)_{thr} = 1.045$ was reported, beyond which the ferroelectric/ferroelastic domain wall motion was suppressed under the electric or mechanical fields applied for the studied material. Diffraction measurements, provided in ref. [255], highlight the absence of change in the 002/200 peak intensities as a function of the applied mechanical stress, indicating the suppression of ferroelectric/ferroelastic domain wall motion for materials with a lattice distortion larger than the threshold value. The mobility of the domain walls was further quantified by the Rayleigh parameters, ε_0, and α. As displayed in Fig. 7a, the Rayleigh parameters continuously decrease with increasing the c/a ratio, indicating that reversible and irreversible domain wall motion gets reduced.

The impact of c/a ratio on the functional properties of a tetragonal BCZT material is displayed in Fig. 7b. [256] Macroscopic diffraction measurements show the poling process of two virgin samples with different c/a ratios. As quantified by the change in 002/200 intensities, 90° domain wall motion was found to be easier for a lattice distortion of $c/a = 1.0055$ compared to compositions with a larger lattice distortion of $c/a = 1.0080$. Thereby, the contribution of 90° domain wall motion was found to continuously decrease with increasing the lattice distortion as quantified by the parameter $\Delta\eta/\Delta E$. Similar to polycrystalline BF-PT, the macroscopic d_{33} in BCZT decreases, while the coercive field increases with increased lattice distortion. The continuous decrease of functional properties and the hindering of domain wall motion was related to the large internal stress, which builds up at the domain walls and grain boundaries, suppressing the ability of the polarization to align with the electric field, as mechanistically discussed in Fig. 5.

4.1.3. Summary and further aspects

Intrinsic structural parameters strongly impact the dynamics of ferroelectric/ferroelastic domain walls. In general, domain wall motion was found to be facilitated in materials with a higher number of available polarization directions and a smaller distortion of the lattice. Importantly, the mobility of domain walls, however, is not the only parameter impacting the electromechanical response of polycrystalline ferroelectric/ferroelastic materials. The maximum electromechanical response reflects the interplay between the lattice distortion and the mobility of non-180° domain walls. As outlined in Sections 4.1.2.1 and 4.1.2.2, these parameters are not independent of each other. A practical consequence of this interplay for example is, that the maximum electromechanical response can

be found at the tetragonal side of the MPB in PZT materials. [244] Similar effects are observed in temperature-dependent studies of PZT [258,259] and KNN-based [260] materials. Therefore, to optimize the electromechanical response of ferroelectric/ferroelastic materials, the crystal system and the distortion of the lattice need to be tailored simultaneously.

Besides the dielectric and electromechanical properties discussed so far (Fig. 6 and Fig. 7), also other functional parameters can be engineered via the crystal system and lattice distortion. For example, the fracture toughness was found to be considerably reduced in tetragonal PZT compared to rhombohedral counterparts. [261] Similar to the piezoelectric response, the increase of fracture toughness due to the reorientation of ferroelastic domains, also referred to as the ferroelastic toughening effect, depends on the combined ability of the material for non-180° domain wall motion and the distortion of the unit cell. Furthermore, the mechanical quality factor, Q, which scales inversely with losses and domain wall mobility in PZT, is considerably higher in tetragonal compared to rhombohedral compositions. [262]

4.2. Grain size and grain-orientation relationship

Representative hysteresis loops highlighting the impact of grain size [263] and grain-orientation [264] on domain wall motion are displayed in Fig. 8 for polycrystalline BT. The polarization hysteresis loop of a BT single crystal is displayed in Fig. 8b for comparison. [265] It can be observed that the polarization loops get slimmer if the microstructure of the material contains coarse grains or if the grains are highly aligned, implying facilitated domain wall motion for large grains and highly textured microstructures.

In comparison to previous reviews on the grain size-dependency [266–269] or the impact of crystallographic texturing [270–272] on dielectric and piezoelectric properties, we focus on the domain wall-grain boundary interaction and draw a link to the functional behavior. We start by summarizing the impact of grain size on small- and large signal dielectric and electromechanical properties and discuss them in the framework of the static domain structure and the influence on electric and mechanical driving forces for domain wall dynamics (Section 2.2.2). Next, we apply these concepts in the context of textured polycrystals and outline how domain wall-grain boundary relationships can be used for functional property engineering.

4.2.1. Grain size

4.2.1.1. Domain wall dynamics and domain morphology. The correlation between small/large signal electromechanical properties and grain size, g is displayed in Fig. 9a-d for polycrystalline BT [269,273–292] and PZT [140,144,228,293–303]. The relatively wide spread of absolute values may be related to different chemical compositions, defect states, crystal systems, utilized precursor materials or processing conditions, which we do not discuss further here. However, irrespectively of the spread of the data points, a general trend can be revealed. For both materials, the large signal properties (Fig. 9a and b), i.e., the coercive field and the remanent polarization, are nearly independent of the grain size for large grains, while rapid changes occur if the grain size decreases. For small grain sizes, the coercive field increases, while the remanent polarization decreases with decreasing grain size, indicating the suppression of domain wall motion. Similar dependences can be observed in other ferroelectric/ferroelastic systems, such as KNN, [304–306] $Ba(Zr_{0.2}Ti_{0.8})O_3$, [307] and BCZT [308], suggesting that the grain-size dependence of large signal properties is a general phenomenon.

The grain size-dependence of the small signal properties of BT and PZT is displayed in Fig. 9c and Fig. 9d, respectively. All studies report a peak in ε_r and d_{33} at ~ 1 µm for polycrystalline BT. For polycrystalline PZT, the reports on the dependence of the small signal properties on grain size, however, show much less unified characteristics. While some researchers find a continuous decrease of ε_r, [299] others observe a slight increase with decreasing grain size [144,293,296,303].

To understand the correlation between grain size and large/small signal properties, we display the domain size (δ) as a function of grain size for BT [274,276,277,279] and PZT [140,300,303] in Fig. 9e and f, respectively. Two regions can be distinguished. The critical transition grain size, g_{crit}, between the two regions was calculated by Arlt considering elastic, electric, and surface energy of the domain walls. For polycrystalline BT, $g_{crit} \approx 5$ µm, while for PZT a value of $g_{crit} \approx 1-2$ µm was calculated. [263] Note, that the obtained experimental values of the critical transition grain size were found to be dependent on the chemical composition of the material. [303] Following the nomenclature of Arlt, [182] in the small grain size regime, a lamellar domain structure (contains only non-180° domain walls) is observed, while at large grain sizes, a banded domain structure (contains 180° and non-180° domain walls) develops. Domain images of a lamellar and a banded domain structure for BT [182] and PZT [303] are provided in Fig. 9g and h, respectively.

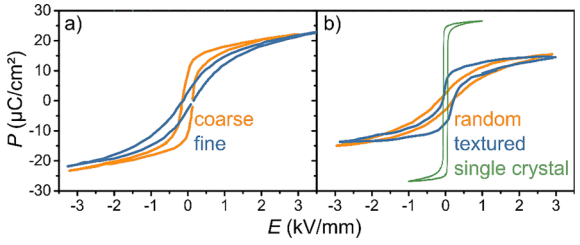

Fig. 8. Impact of grain size and grain-orientation relationship on the shape of polarization loops. a) Polarization loops for polycrystalline BT ceramics with different grain sizes. [263] b) Polarization loops for random and crystallographically-textured polycrystalline BT ceramics. [264] The polarization loop of a BT single crystal is displayed for comparison. [265]

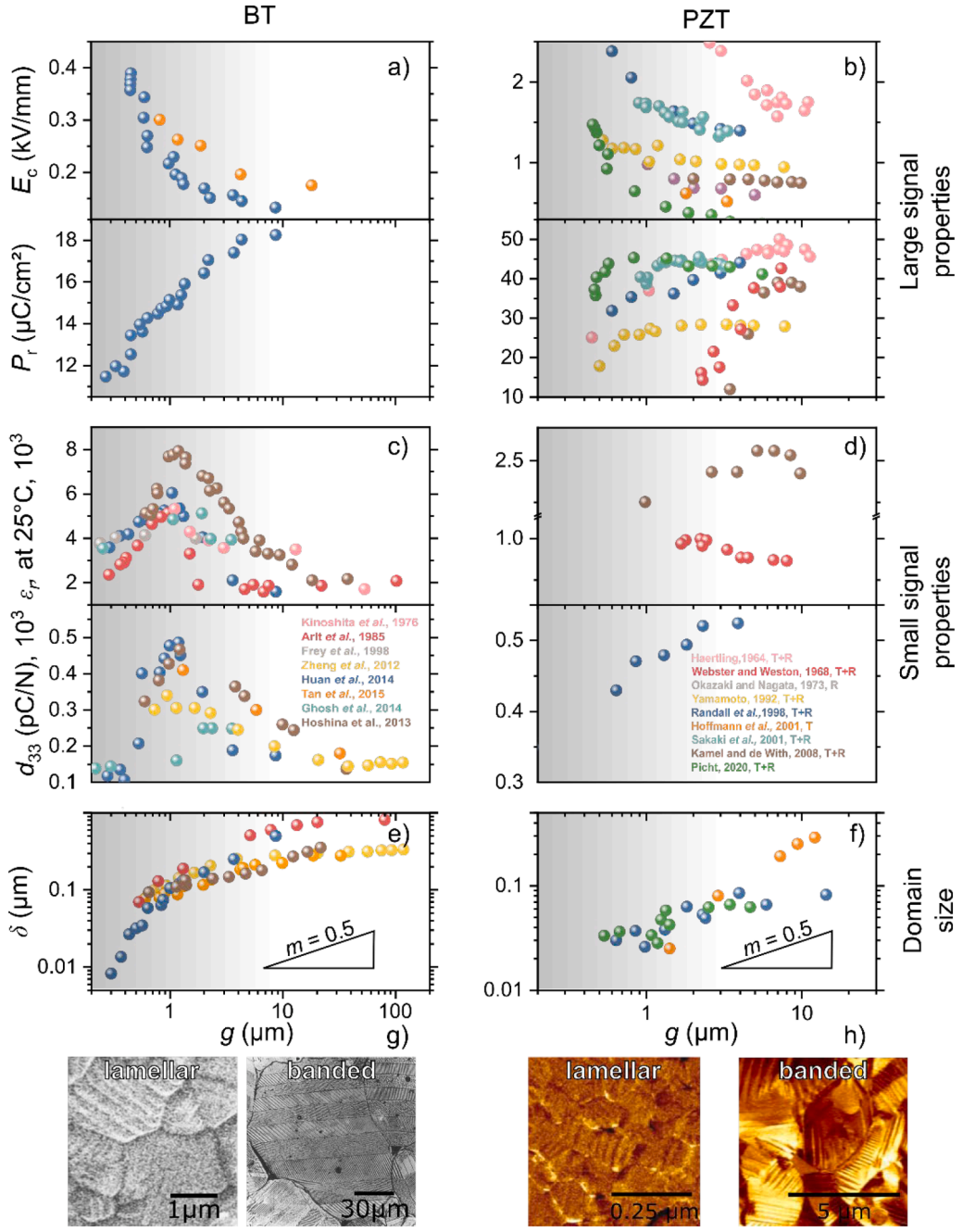

Fig. 9. Impact of grain size on ferroelectric and electromechanical properties, as well as domain sizes for polycrystalline BT and PZT. The dependence of the a), b) large signal properties (coercive field and remanent polarization) and c), d) small signal properties (permittivity and piezoelectric coefficient) is displayed together with the domain size in e) and f). The triangles in e) and f) indicate the typical correlation between grain and domain size, $\delta \propto g^m$, with $m \approx 0.5$, [309] for BT [269,273–280] and PZT [140,295–303]. For PZT the crystal system of the composition is abbreviated with T (tetragonal) and R (rhombohedral). [182] Microscopy images for a lamellar and banded domain structure of polycrystalline BT [182] and of PZT ceramics [303] are displayed in g) and h). g) Reprinted by permission from Springer Nature : [182], Copyright 1990. h) Reprinted from [303], with the permission of AIP Publishing.

The correlation between domain size and grain size is given by $\delta \propto g^m$. [309] For the investigated BT [274] and PZT [83,303] materials $m \approx 0.5$ is typically observed, as displayed by the triangles in Fig. 9e and f. The main driving force for the scaling behavior is the elastic strain, which is released via the formation of ferroelectric/ferroelastic domain walls. [182] A deviation from the scaling behavior can be observed when the grain size is decreased, e.g., for $g < 0.5$ μm in BT (Fig. 9e). At even smaller grain sizes (a

theoretically calculated value for BT is around 40 nm [182]) ferroelectricity vanishes as experimentally proved for both BT and PZT. [299,307,310–312]

4.2.1.2. Grain size dependence of domain wall-related contributions under large and small electric fields. Under large electric fields (Fig. 9a and b), the contribution of non-180° domain wall motion in polycrystalline ferroelectric/ferroelastic materials decreases with decreasing grain size. For PZT, XRD measurements revealed that non-180° domain wall motion is considerably reduced in fine (~1.6 μm) compared to coarse grained (~3.3 μm) ceramics. [300] Similar conclusions were drawn for tetragonal $Pb_{0.9}La_{0.1}TiO_3$ in the grain size range of 1.3–6.0 μm. [313] For polycrystalline BT the domain wall motion is significantly higher for grain sizes of 2.0 μm and 3.5 μm in comparison to counterparts with a smaller grain size of 0.3 μm. [280] In analogy to bulk polycrystalline ceramics, non-180° domain wall motion was found to be negligible in polycrystalline thin films with a grain size smaller than 2 μm, while it was evident for larger (>5 μm) grain sizes. [314]

While domain wall mobility decreases with decreasing grain size under large electric fields, the domain-wall related response under small electric fields is considerably different. The peak in the small signal relative permittivity and piezoelectric coefficient of BT, which is observed for a grain size of ~ 1 μm (Fig. 9c) was explained by enhanced domain-wall-related contributions. [267,268] In this frame, the grain-size dependent small signal response was quantified for BT using XRD [280] and spectroscopic techniques, [269,285] as summarized in Fig. 10. The domain switching fraction, η_{002}, obtained from XRD is displayed as a function of grain size for BT in Fig. 10a. For subcoercive fields (40% of the coercive field) a higher degree of non-180° domain switching fraction ($\Delta\eta = 0.013 \pm 0.02$) was found for materials with a grain size, $g = 1.97 \pm 0.44$ μm, while the sample with a large grain size, $g = 3.52 \pm 0.29$ μm, featured a smaller non-180° domain switching fraction of $\Delta\eta = 0.007 \pm 0.002$. [280] Complementary to XRD measurements, frequency-dependent small-signal measurements facilitate the distinction between intrinsic and extrinsic contributions. The frequency-dependent permittivity up to the terahertz range for polycrystalline BT of different grain sizes is displayed in Fig. 10b. [285] Extrinsic domain wall related contributions feature a characteristic relaxation frequency at $f \sim 10^8$ Hz, while intrinsic contributions vanish at frequencies higher than $f \sim 10^{11}$ Hz. The determined domain-wall related contribution to the permittivity, ε_r^{ext}, are displayed as a function of grain size in the inset of Fig. 10b. A peak contribution was found for a grain size of 1.4 μm, while substantially lower values were reported for BT materials with larger (13.0 μm) and smaller (0.7 μm) grain sizes

4.2.1.3. Interplay between elastic strains and domain wall dynamics in the vicinity of grain boundaries. In order to understand why the impact of grain size on the large and small signal response is different, we continue with an explanation of the interplay between domain wall motion, elastic strains, and grain size. The impact of grain size on lattice strains (quantified by the *c/a* ratio) is displayed for polycrystalline BT with different grain sizes in Fig. 11a. Above a grain size of ~ 1.5 μm, lattice distortion was found to be independent of the grain size in polycrystalline BT, [274,315] while below ~ 1.5 μm, the lattice distortion continuously drops. A similar behavior is found in polycrystalline PZT and composition-dependent critical grain sizes in the range of 0.6 μm [303] to 1.5 μm [294] were reported. In polycrystalline BT the drop in the lattice distortion comes along with a decrease of the Curie temperature, corroborating the decreased stability of the tetragonal phase. As displayed in Fig. 11b, the Curie temperature rapidly decreases when the grain size is reduced into the submicrometer range, [278,286] while it remains unchanged for larger grain sizes [273,288,316,317]. At the same time, the orthorhombic-rhombohedral phase transition temperature slightly increases with decreasing grain size. [276,318] Interestingly, in comparison to the discussed impact of the *c/a* ratio (Section 4.1.2.2), the coercive field and remanent polarization do not decrease with decreasing grain size (Fig. 9a and b), indicating that the decreasing *c/a* ratio is not the dominant mechanism.

The impact of grain size on microstrains was quantified by the broadness of the diffraction peaks in XRD measurements. [144,319] The broadness of the (222) peak, β, which is proportional to the microstrains, [320] increases with decreasing grain size, as displayed for polycrystalline BT materials over a grain size range of 0.15–50 μm (Fig. 11c). [319] A qualitatively similar behavior was found for a polycrystalline $Pb(Zr_{0.7}Ti_{0.3})O_3$ over a grain size range of 3.9–10.4 μm. [144] An additional feature, which is frequently revealed by XRD measurements, is the occurrence of diffuse scattering between the tetragonal (002) and (200) peaks [276,280–282] when the

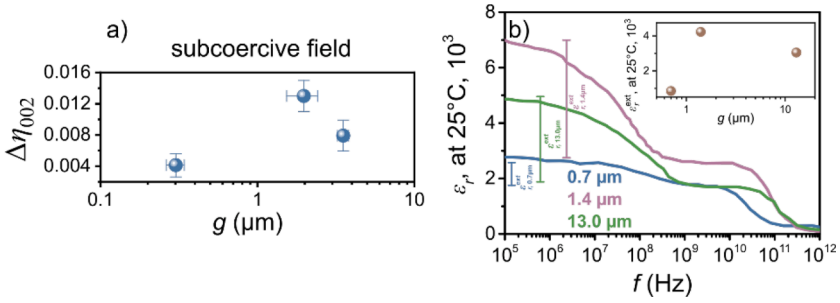

Fig. 10. Impact of grain size on extrinsic contributions in polycrystalline materials under small electric fields. a) Domain switching as a function of grain size during subcoercive electric field application in polycrystalline BT (applied $E = \pm 0.2$ kV/mm, $E_c = 0.5$ kV/mm). [280] b) Frequency dependence of the dielectric constant for polycrystalline BT materials with different grain sizes. The grain-size dependence of the extrinsic contribution is quantified in the inset. [285]

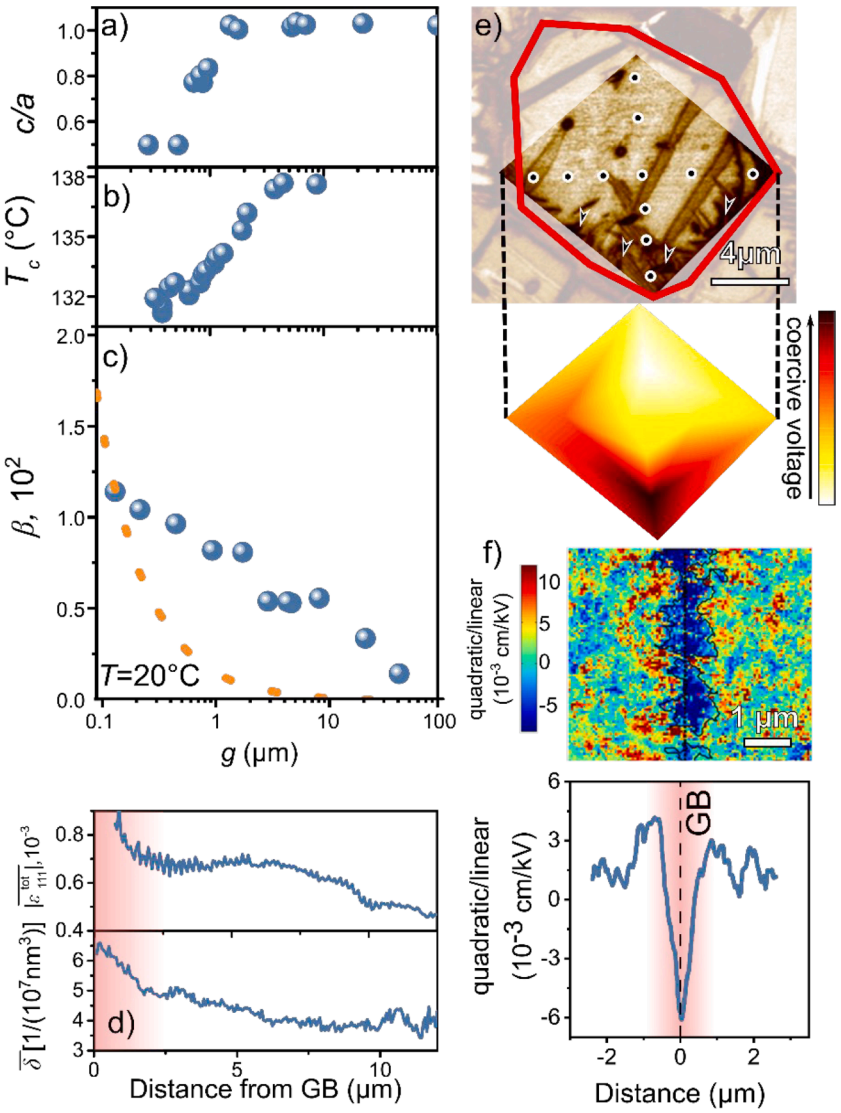

Fig. 11. Correlations between elastic strain and ferroelectric/ferroelastic domain walls. Variation of a) the lattice distortion, [274] b) the Curie temperature [278] and c) the broadness, β, of the (222) diffraction peak, [319] as a function of grain size of polycrystalline BT. Contributions of the crystallite size (Scherrer broadening) to the broadening of the diffraction peaks are indicated by the orange line and cannot explain the peak broadening alone. d) Dependence of the total strain, ε_{111}^{tot}, and the density of domain variants, δ, measured as a function of the distance of the grain boundary of a slice of a 30 μm large grain for a BCZT polycrystal in the virgin state. Data is taken from ref. [179]. The red shaded area indicates the impact of the grain boundary on the simultaneous enhancement of the local strains and domain wall density. e) PFM image of a grain of a polycrystalline rhombohedral PZT ceramic. The red line indicates the position of the grain boundary. Areas of high domain wall density are indicated by arrows. Local coercive voltages were determined by local switching measurements (measurement positions are indicated by dots) and are displayed as a contour plot for the same grain region. Reprinted from [144], with the permission from Elsevier. f) Maps of the nonlinear response measured across a grain boundary of a $Pb(Zr_{0.45}Ti_{0.55})O_3$ thin film. The dashed line indicates the position of the grain boundary, while the area shaded in red indicates the substantial impact of the grain boundary on domain-wall mobility. Reproduced from [327], with the permission of Wiley.

grain size is decreased. Such features were observed for BT [203,204,274,282] and PZT [202] polycrystals and explained by microstrains located in the vicinity of ferroelectric/ferroelastic domain walls.

While it is clear that the lattice and microstrains increase with decreasing grain size, maps of the resulting strain state were obtained spatially resolved. Strained regions were found to be located in the vicinity of domain walls [178,321,322] or grain boundaries [179,323,324]. The strain profile is displayed as a function of the distance from the grain boundary in Fig. 11d for a grain with a diameter of 30 μm embedded in a polycrystalline BCZT matrix. The strains in the vicinity of the grain boundary are about twice as high as the strains in the center of the grain. [218,219,325] Together with the spatial variation of strain, the spatial variation of the density of domain variants, δ, is displayed in Fig. 11d. As displayed by the red shaded area, both parameters peak in the vicinity (2–3 μm) of the grain boundary, and the domain density is enhanced by 30% in comparison to deep inside the grain, [179] related to the strain

releasing effects of ferroelectric/ferroelastic domain walls. The findings displayed in Fig. 11d agree well with bulk polycrystalline [144,326] and thin film PZT materials, [327] for which the domain wall density was found to be substantially enhanced in the vicinity of a grain boundary.

The domain wall density directly impacts the mobility of the domain walls and calculations predict a reduced domain wall mobility in finer domain structures than in coarser ones. [215,274,328] Fig. 11e displays a PFM image of a grain of a polycrystalline $Pb(Zr_{0.7}Ti_{0.3})O_3$ ceramic with the grain boundary highlighted as a red line, [144] facilitating to quantify coercive voltages spatially resolved. The coercive voltage map highlights that domain wall dynamics are hindered in volumes in the vicinity of the grain boundary, in particular in areas with high domain wall density. The findings on polycrystalline bulk materials are in good agreement to reports on polycrystalline PZT thin films (Fig. 11f), where domain wall motion was found to be impacted in a range of 450 ± 30 nm in the vicinity of a 24° tilt grain boundary in a rhombohedral $Pb(Zr_{0.52}Ti_{0.48})O_3$ bicrystal. [329] Maps of the nonlinear domain-wall related response along the grain boundary are displayed in Fig. 11f and a significant dip can be found at the position of the grain boundary. Furthermore, local hysteresis loops measured at the grain boundary were reported to have a considerably larger coercive field, [139,330] display a strong imprint, [137,331] and incomplete domain reorientation even under high electric fields [332]. In addition, domain wall pinning at the grain boundary is frequently reported experimentally [331,333–335] and by simulations [336]. The volume influenced in the vicinity of the grain boundary thereby can be tuned by the composition of the material, boundary orientation angle, as well as temperature. [146,327,329] Domain wall continuity over grain boundaries, as experimentally demonstrated for grain boundaries in polycrystalline BT [337,338] and PZT [145,339,340] may further facilitate domain wall dynamics for specific grain configurations. For example, one of the grain boundaries that allows domain continuity in tetragonal materials is the 111 boundary, allowing 110 plane matching. [341,342] For more insights into detailed grain configurations, we refer the reader to refs. [343,344] and a review article (ref. [345]).

4.2.1.4. Summary and further aspects. The impact of grain size has been intensively studied for polycrystalline BT and PZT. For both materials, the large-signal coercive field increases, while the remanent polarization and the non-180° domain switching fraction continuously decrease with decreasing grain size (Fig. 9a and b). This effect was related to strained volumes in the micrometer vicinity of the grain boundary, which come along with a considerably enhanced domain wall density (Fig. 11d). [179] As a consequence, domain wall motion gets locally reduced in the vicinity of the grain boundary (Fig. 11e and f). [144,327] For grain sizes below the critical transition grain size, discussed in Section 4.2.1.1, the inhomogeneous stress state occupies the entire grain. This is reflected in a rapid decrease in the lattice distortion (Fig. 11a) and the development of a lamellar domain structure (Fig. 9g and h), which nearly completely suppresses domain wall motion under large electric signals. [346] Macroscopically, the coercive field and remanent polarization significantly change in the small grain size regime (Fig. 9a and b). In order to obtain enhanced large-signal electromechanical properties, polycrystalline materials with large grain sizes featuring a limited amount of grain boundaries are therefore desirable. In applications of ferroelectrics/ferroelastics in multilayer actuators, however, additional design criteria, such as the thickness of each layer, need to be considered to avoid leakage currents or device failures. [347] Going beyond the discussed impact on the electromechanical response, also fracture toughness, [348,349] electric fatigue, [324,350] and high-power behavior [301] can be tailored by grain size engineering.

The dependence of small-signal properties on the grain size is more complex (Fig. 9c and d). With decreasing grain size, the non-180° domain density is considerably enhanced (Fig. 9e and f), and particularly regions in the vicinity of the grain boundary are

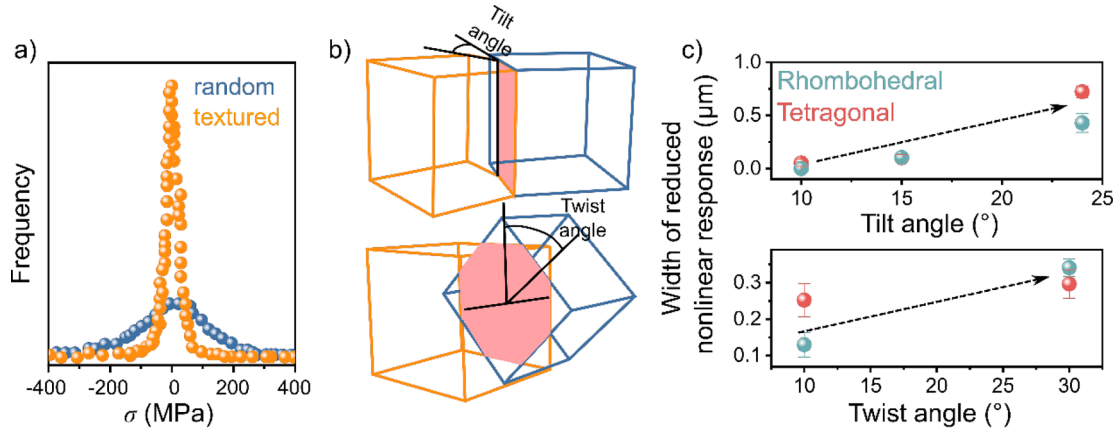

Fig. 12. Impact of crystallographic texture on the stress and domain wall mobility. a) Residual stress distribution in textured and random polycrystalline Al_2O_3. The stress is significantly reduced in a polycrystalline ceramic with textured grains compared to a random counterpart. [219] b) Schematic representation of a tilt and a twist grain boundary separating two grains. The grain boundary area between two grains is indicated by the red area. The tilt and twist angles are schematically displayed. c) Experimental results summarizing the impact of twist and tilt angle on the width of the region with reduced nonlinear response in the vicinity of a grain boundary for a rhombohedral $Pb(Zr_{0.52}Ti_{0.48})O_3$ and tetragonal $Pb(Zr_{0.45}Ti_{0.55})O_3$ bicrystal model system. As indicated by the dashed arrows, the width of the region increases with increasing tilt/twist angle for both crystal systems. [146]

impacted (Fig. 11d and e). Vibrational motion of these non-180° domain walls under low voltages are the main reason for the enhancement of the small signal dielectric permittivity and piezoelectric response (Fig. 10a and b). [280,285] The decrease of the c/a ratio (Fig. 11a) may further enhance domain wall mobility under small electric fields, as discussed in Section 4.1.2.2. Since the grain-size-dependence of small signal properties is temperature-independent, [263] grain size induced structural changes, e.g., an orthorhombic/tetragonal phase coexistence in polycrystalline BT, [292,318] originating from the grain-size-dependency of the phase transition temperatures contribute as a secondary effect to the enhancement of the small signal properties. A similar grain-size-

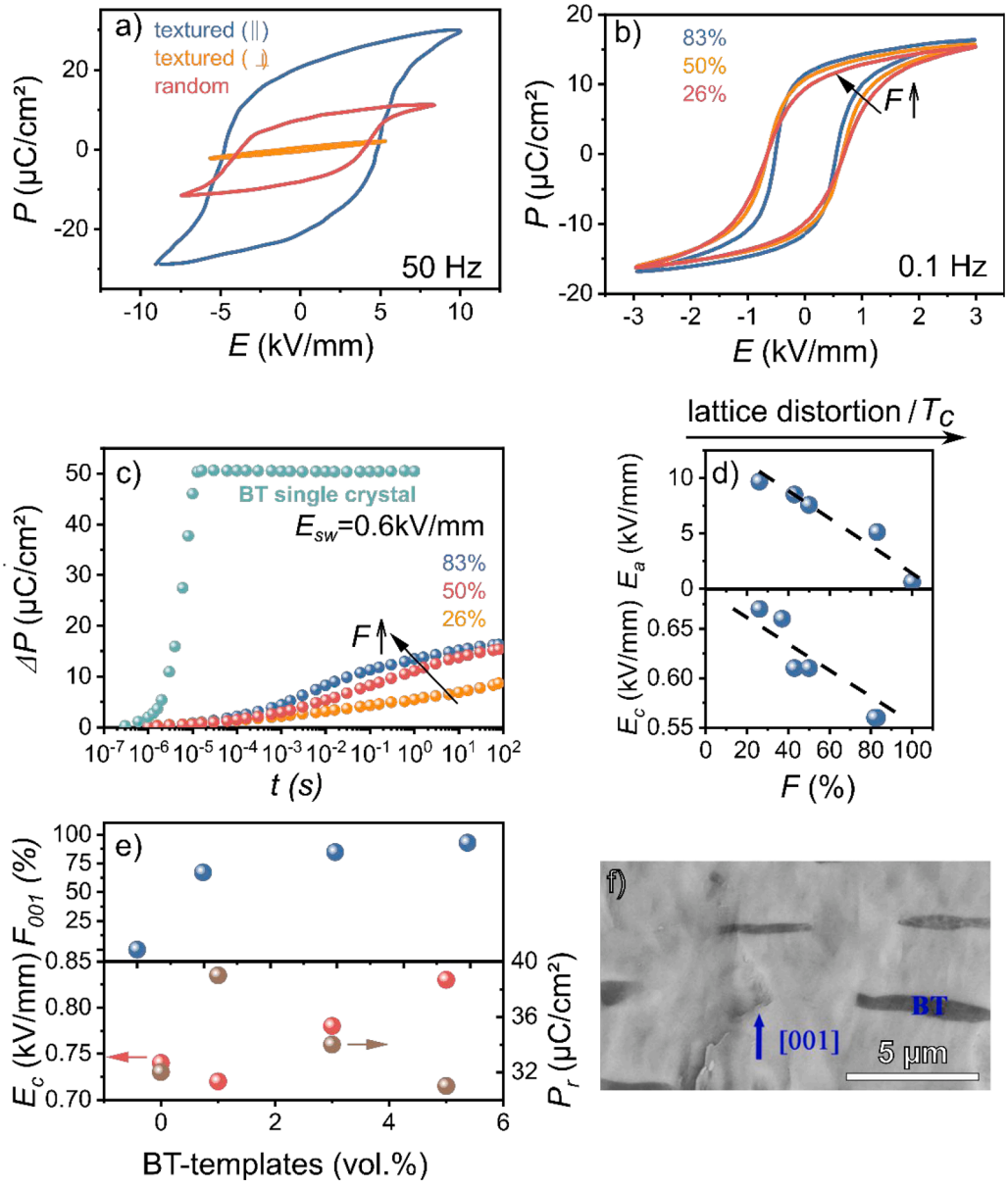

Fig. 13. Experimental results on the impact of crystallographic texture on domain wall dynamics: a) Impact of the orientation of texture on the polarization hysteresis loops (measured at 200 °C) in textured $Na_{0.5}Bi_{4.5}Ti_4O_{15}$. The orientation of the crystallographic texture is parallel and perpendicular to the electric field. A polycrystalline material with random grain orientation is displayed for comparison. [365] b) Large signal polarization and strain loops for polycrystalline BCT with different degrees of crystallographic texture (the degree of texture is quantified by the Lotgering factor, F [373]). [354] c) Time-dependent polarization measurements for polycrystalline BCT with different degrees of crystallographic texture (measured under an electric field pulse of height $E_{Sw} = 0.6$ kV/mm). A BT single crystal is displayed for comparison. [131] d) The coercive field [354] and the activation barrier [131] for polarization reversal for polycrystalline BCT are displayed as a function of the Lotgerging factor. The change of the lattice distortion and the Curie temperature is indicated by the arrow. e) The impact of the amount of BT templates in polycrystalline PMT-PT on the Lotgering factor, F_{001} is displayed. The effects on the coercive field, and the remanent polarization are highlighted as well. A micrograph of the material with 5 vol.% BT templates is displayed in f). Reprinted from [360], with the permission of AIP Publishing.

dependence of the crystal system was also observed for polycrystalline KNN-based materials. [306] Decreasing the grain size further below 1 μm leads to a rapidly increasing mechanical stress (Fig. 11a-c) and a suppression of the domain wall motion, which comes along with a decrease of dielectric and piezoelectric performance and the subsequent loss of ferroelectricity in the sub-100 nm range. While the enhancement of the small signal properties naturally occurs in polycrystalline BT materials at a grain size of ~ 1 μm, a similar, but much less emphasized behavior was observed for polycrystalline PZT materials. [144,296,303] For example, the solid solution $Pb(Zr,Ti)O_3$-$Sr(K_{0.25}Nb_{0.75})O_3$ displays a peak of the dielectric permittivity in the grain size range of 2–3 μm. [293]

4.2.2. Crystallographic texture

As we have outlined in Section 4.2.1, elastic strains substantially influence domain wall dynamics in polycrystalline ferroelectric/ferroelastic ceramics with a random grain orientation. Crystallographic texturing impacts elastic strains, as reported for structural [219,351,352] and functional [137,353,354] polycrystals. To visualize this effect, we display representative stress distributions comparing a random and a highly textured Al_2O_3 in Fig. 12a. [219] The distribution is narrow for a textured material and the absolute value of stress is substantially lower in comparison to a non-textured counterpart, which was explained by lower grain boundary misorientation angles and energies. [219] Model experiments on thin films [146] supported by phase field simulations [355] have investigated the resulting impact on domain wall dynamics, suggesting a pronounced dependency on the misorientation angle. A summary of this effect is provided in Fig. 12b and c. Fig. 12b provides a schematic drawing of two grains highlighting the tilt and twist angle, while the impact of the tilt and twist angle on the width of the region with reduced domain wall mobility is outlined in Fig. 12c for a rhombohedral $Pb(Zr_{0.52}Ti_{0.48})O_3$ and a tetragonal $Pb(Zr_{0.45}Ti_{0.55})O_3$ composition. [146] For small misorientation angles, typically found in textured polycrystalline materials, the width of the region with reduced nonlinear response is nearly zero and domain wall mobility is not impacted. With increasing misorientation angle, the width of the region continuously increases to ~ 0.3 and ~ 0.6 μm for a tilt and twist grain boundary, respectively, indicating a more pronounced impact on domain wall dynamics.

Literature on the impact of crystallographic texture on the mobility of domain walls, however, is inconsistent. Some reports find that crystallographic texturing facilitates domain wall motion, [264,354,356] while others find hindering effects [357–359]. Again, others report that domain wall dynamics are not impacted by crystallographic texturing [360–362]. To disentangle different experimental results, we review the impact of orientation of the grains with respect to the electric field (Section 4.2.2.1), the degree of crystallographic orientation (Section 4.2.2.2), and the impact of reactive templates (Section 4.2.2.3) on the domain wall mobility and functional performance in the following.

4.2.2.1. Anisotropy. The domain wall dynamics depend on the orientation of the crystallographic texture with respect to the external electric field. This was demonstrated for an Aurivillius oxide bismuth titanate ($Na_{0.5}Bi_{4.5}Ti_4O_{15}$) model system, which has a highly anisotropic unit cell (the *c* axis is 7.5 times the *a/b* axis [363]) and allows 180° and 90° domain switching. [364,365] Polarization hysteresis loops of samples with grains oriented parallel and perpendicular to the *c*-axis are compared to a random counterpart in Fig. 13a. A high remanent polarization of 21 $\mu C/cm^2$ was found if the electric field was applied parallel to the *c*-axis, while the domain wall motion was completely suppressed for electric fields perpendicular to it. The enhanced switchable polarization for the sample with polarization parallel to the *c*-axis in comparison to the random counterpart was attributed to a synergistic alignment of the ferroelectric distortion directions in each grain during domain switching. [364] In analogy to clamping effects due to in-plane stress in thin films, [366,367] the absence of domain wall motion was related to the highly anisotropic unit cell, preventing domain reorientation. Similar results were observed for textured $Sr_{0.53}Ba_{0.47}Nb_2O_6$ (SBN) [368] and KNN, [369] indicating that domain wall motion is easiest if the long axis is oriented parallel to the applied electric field.

4.2.2.2. Degree of crystallographic texture. Quantifying the degree of crystallographic texture in polycrystalline ferroelectrics/ferroelastics is crucial for optimizing processing parameters. The most common methods of evaluating the degree of crystallographic texture are based on X-ray diffraction or stereographical methods and include pole figure measurements, [370] X-ray rocking curve analysis, [371] Rietveld refinement of X-ray diffraction data (March-Dollas factor) [372] or the Lotgering analysis [373]. A comprehensive comparison of texture analysis techniques is provided in ref. [374], while a critical evaluation of the Lotgering factor is given in ref. [363]. Experimental techniques and material-specific challenges in polycrystalline ferroelectric/ferreolastics to enhance the degree of crystallograhic texture are provided in refs. [272] and [375].

The impact of the degree of crystallographic texture was systematically investigated on a series of $(Ba_{0.85}Ca_{0.15})TiO_3$ (BCT) samples with different degrees of crystallographic texture in refs. [131,354]. The description of the processing of the textured BCT samples utilizing reactive templates is provided in ref. [376]. Fig. 13b displays polarization loops of samples with different degrees of crystallographic texture, quantified by the Lotgering factor, *F*. [373] A highly textured sample is characterized by *F* with values close to 100%, while a sample with random grain orientation has a value of $F = 0\%$. For the BCT series, with increasing *F*, the squareness of the polarization loops increases indicating enhanced and facilitated domain wall dynamics. Similar behavior was also observed in KNN-based materials with a high degree of crystallographic texture, [377,378] textured SBN, [368] as well as in textured thin films [379,380].

Further information on the impact of crystallographic texture on the dynamics of domain walls in polycrystalline BCT was obtained from time-dependent polarization switching measurements. Fig. 13c displays the time dependence of the switched polarization of the BCT samples with different degrees of crystallographic orientation under an applied electric field pulse of height $E_{Sw} = 0.6$ kV/mm. A (0 0 1)-oriented BT single crystal is displayed for comparison. With increasing the degree of crystallographic texture, the switching time of the sample with a high degree of crystallographic texture ($F = 83\%$) is 2–3 orders of magnitude smaller in comparison to a sample

with a low degree of crystallographic texture ($F = 26\%$). The response of the polycrystalline samples, however, remain far behind the BT single crystal. The impact of the degree of crystallographic texture on domain wall dynamics was quantified by the coercive field and the activation barrier for polarization reversal. These parameters are displayed as a function of the Lotgering factor in Fig. 13d. The coercive field of the highly textured samples (0.55 kV/mm) is about 18% lower compared to counterparts with a low degree of crystallographic texture (0.60–0.67 kV/mm). For comparison the coercive field of a BT single crystal was found to be about 0.05 kV/mm, [381] which is about an order of magnitude lower. Similar as the coercive field, also the activation barrier for polarization reversal decreases with increasing Lotgering factor (Fig. 13d).

As outlined in Fig. 12a, the internal stress decreases with increasing the degree of crystallographic texture, allowing a facilitated cooperative alignment of the polarization vectors during the application of an electric field. For the series of BCT, reduced internal stress can be manifested by an increased c/a ratio, which comes along with an increased Curie temperature, as indicated by the arrow in Fig. 13d. As discussed in Section 4.1.2.2, high lattice distortion in polycrystalline materials with a random orientation of grains hinders domain wall motion. However, as displayed in Fig. 13d, this effect is different, if the microstructure is textured and a high lattice distortion in combination with a high degree of crystallographic texture was found to be beneficial for domain wall dynamics.

4.2.2.3. Non-reactive templates. Beyond the orientation relationship and the degree of crystallographic texture discussed so far, the interactions between the templates and the ferroelectric matrix are important if non-reactive templates are utilized, i.e., templates that remain present in the matrix after sintering. While these templates promote the grain-orientation, they reduce domain wall mobility. This impact of the non-reactive templates on domain wall dynamics and functional properties was studied systematically in $Pb(In_{1/2}Nb_{1/2})O_3$-$Pb(Mg_{1/3}Nb_{2/3})O_3$-$PbTiO_3$ polycrystals, which were textured by BT templates (Fig. 13e and f). [360] Fig. 13e displays the impact of the volume fraction of BT templates on the Lotgering factor, the coercive field, and remanent polarization. It was found that the Lotgering factor continuously increases with increasing BT concentration. At the same time the coercive field increases and the remanent polarization drops, if the concentration of BT templates exceeds 1 vol.%. This indicates that with increasing BT template concentration, domain wall motion gets more difficult, even though the degree of crystallographic texture is increasing, which is different to the behavior discussed in Section 4.2.2.2.

To understand the different behavior, the microstructure containing the BT templates is displayed in Fig. 13f. [360] In comparison to the results presented in Section 4.2.2.2, where reactive templates were used to fabricate the textured polycrystals, [376] BT templates are not reacting with the matrix material. Non-reactive templates impact the distribution of elastic stress in the matrix and thus the mobility of the domain walls. Using finite element simulations, local stress up to 8 MPa were calculated, located in the vicinity of an $SrTiO_3$ template in a $Pb(Mg_{1/3}Nb_{2/3})O_3$-$PbTiO_3$ (PMN-PT) matrix. [271] These elastic stresses were further found to result in a self-poling effect, i.e., the development of a preferential ferroelastic texture already during processing. [382]

4.2.2.4. Summary and further aspects. Crystallographic texturing enables tailoring the mobility of domain walls as a consequence of a stress reduction (Fig. 12a), facilitating domain wall motion. A side effect, coming along with the stress reduction during the electric field-application is an enhancement of the dielectric breakdown field of textured materials in comparison to random counterparts, [383] increasing their energy density. [375] Crystallographic texturing was further reported to be beneficial for the fatigue behavior and temperature stability of polycrystalline ferroelectrics/ferroelastics. [384,385] Textured polycrystalline ferroelectrics/ferroelastics make full use of the intrinsic dielectric and piezoelectric properties, mimicking the behavior of single crystals. Even though domain wall motion is facilitated, experiments [386] and simulations [387] find only small contributions of extrinsic ferrolectric/ferroelastic domain wall motion to small signal properties in poled textured ceramics. Phase field simulations, for example, suggest that domain walls contribute about 50% to the small signal piezoelectric and permittivity in randomly oriented polycrystals, while the contribution was found to be negligible in textured counterparts. [387]

For single crystalline materials it is known that the small signal piezoelectric coefficient increases with decreasing domain size. [388,389] Building up on this, a strategy was suggested to combine crystallographic texturing and domain engineering in polycrystalline ceramics to improve their small signal response. This was demonstrated for two textured BT materials with approximately the same degree of crystallographic texturing ($F \sim 83\%$) and different grain sizes. [390] For a grain size of 1.2 μm a piezoelectric response of 507 pC/N was reported, while a higher value of 788 pC/N was found for a reduced grains size of 0.8 μm. Interestingly, this value is substantially higher than the reported values for all grain sizes in Fig. 9a, indicating the potential for an additional boost in functional properties if grain size and crystallographic texture are engineered simultaneously. Colossal piezoelectric coefficients of up to 10 000 pC/N were foreshadowed using a synergetic approach of domain engineering and crystallographic texturing. [390]

So far, only fey studies shed light on domain wall dynamics in textured polycrystalline ferroelectrics/ferroelastics. [375] To exploit the domain-wall related contributions to the dielectric and piezoelectric performance in textured polycrystals further, future studies should optimize the angle between the applied electric field and the orientation of the crystallographic texture. To study the relationship between domain wall dynamics and crystallographic texture on the nanoscale, studies on the impact of crystallographic texture on the ferroelectric domain structure via domain imaging and spectroscopic techniques are highly desirable. These should be combined with residual stresses and chemical gradient mapping near the template-matrix interface and the grain boundary.

4.3. Porosity

In comparison to grain size (Section 4.2.1) and crystallographic texture (Section 4.2.2), porosity relieves mechanical constraints and broadens the distribution of the local electric field. The latter effect is mainly related to a large difference in the relative

permittivity between the ferroelectric matrix (e.g., $\varepsilon_r =$ 1500 for PZT [106]) and the pores ($\varepsilon_r = 1.0006$ for air). This effect is particularly enhanced for regions in the vicinity of the pores. [391] Typically, finite element methods (FEM) facilitate calculation of the distribution of the local electric field. A comprehensive FEM study of the impact of porosity on the distribution of the local electric field is displayed in Fig. 14 for different degrees of porosity and pore morphologies. [133] Here, E_{app} is the externally applied electric field to the porous body and the simulated distribution of the local electric field, E_{loc}, is displayed. Independent of the pore morphology, the presence of porosity shifts the distribution of the local electric field towards lower values and broadens it. The degree of porosity, shape, and orientation of the pores are levers to tune the local electric field distribution.

The degree of porosity, p, quantifies the volume fraction of porosity of a material. Fig. 14a displays the impact of the degree of porosity ($p =$ 5–27 %) on the local electric field distribution. The simulations reveal a broadening of the distribution with increasing degree of porosity. [392–394] The impact of the radius of isometric pore size under a constant total porosity on the distribution of the local electric field is displayed in Fig. 14b. For pore radii in the range of 20–120 μm, the local electric field distribution was found to be unaffected by the pore radius. Complementary studies find an impact of pore diameter on the distribution of the local electric field, if the pore radius is extended towards the nanometer range. [395] Finally, the interplay between the orientation angle of anisometric pores and the distribution of the local electric field is displayed in Fig. 14c. With increasing pore orientation angle, the distribution of the local electric field shifts towards lower electric fields and broadens. [106,133,391,393,396]

Besides the local electric driving forces discussed so far, porosity also impacts local mechanical driving forces for domain wall dynamics. The domain switching fraction of ferroelectric/ferroelastic domains was enhanced in porous PZT thin films [397–399] compared to dense counterparts, which was related to declamping effects in the vicinity of the pores. [400–402] Corroborating this mechanism, theoretical results outline facilitated domain switching in the vicinity of surfaces in general. [403] According to a synchrotron study on porous BT, residual stress decreases from 70 MPa to 40 MPa with increasing porosity, [404] indicating that porosity reduces intergranular stress in ceramic polycrystals. Such declamping of individual grains was demonstrated to result in giant functional properties, e.g., piezoelectric response and energy-harvesting figures of merit. [405]

4.3.1. *Degree of total isometric porosity*

To discuss the impact of total isometric porosity on domain wall dynamics and functional properties, we present experimental results on samples with different degree of total isometric porosity. SEM micrographs of a dense and a porous ($p =$ 40%) BCZT ($0.5Ba(Ca_{0.8}Zr_{0.2})O_3$-$0.5(Ba_{0.7}Ca_{0.3})TiO_3$) material are compared in Fig. 15a. Polarization loops of the same material with different degrees of isometric porosity are displayed in Fig. 15b. [394] With increasing the degree of porosity, the remanent and saturated polarization continuously decrease, while at the same time the polarization loops broaden. Similar results have been reported for porous PZT [133,392,406–409] and other BCZT [410] compositions. The impact of porosity on the dynamics of domain walls during polarization reversal was studied for a dense and a porous ($p =$ 40%) PZT material and the switched polarization as a function of time is

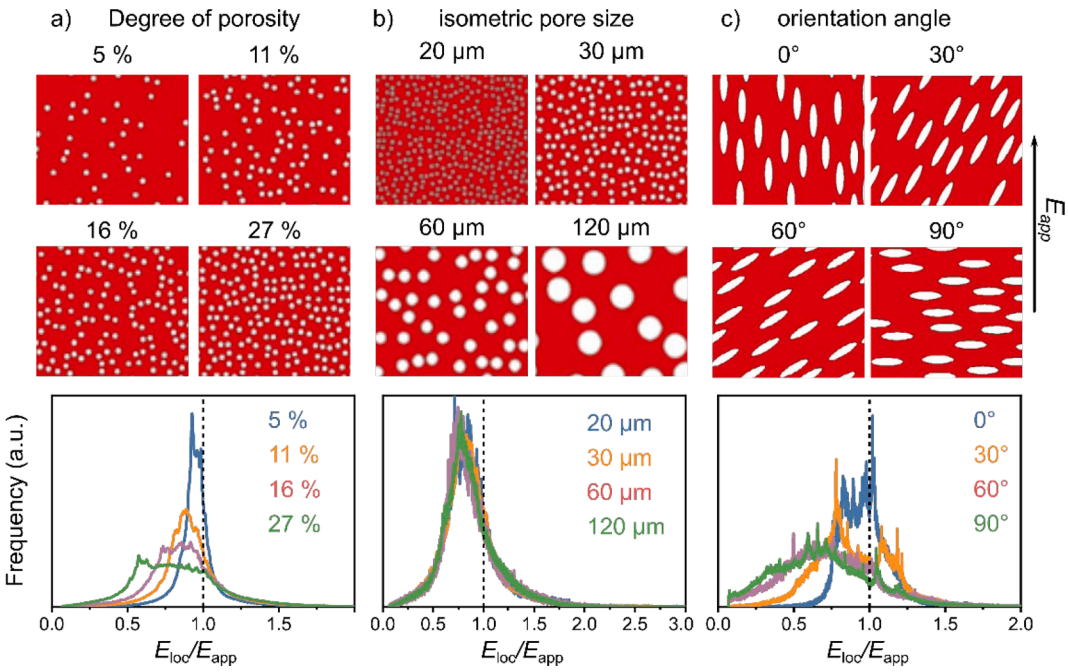

Fig. 14. The impact of pores on the statistical distribution of the local electric field, E_{loc}. The pore morphologies consider changes in a) degree of porosity, b) isometric pore size, and c) orientation angle with respect to the electric field, E_{app}. The 2D FEM simulations take into account the impact of the porosity on the distribution of the local electric field. [127] For a completely dense material, the local electric field would be equal to the applied electric field as displayed by the dashed line.

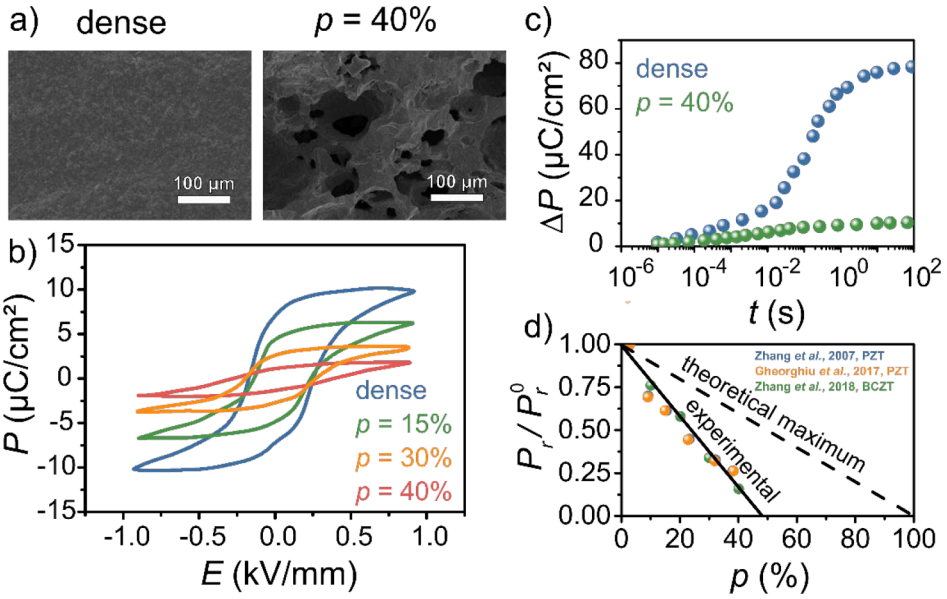

Fig. 15. Impact of the degree of isometric porosity on domain wall dynamics. a) Micrographs of a dense material and a material with isometric pores ($p = 40\%$) of a BCZT samples are displayed. The impact of porosity on the polarization hysteresis loops of porous BCZT materials with different degrees of porosity is displayed in b). Reprinted from [394], with permission from Elsevier. c) Time-dependent development of the switched polarization, ΔP, of a dense and a porous ($p = 40\%$) PZT ceramic material. [133] d) Dependence of the remanent polarization, P_r, of selected porous materials with porosity, p, normalized to the remanent polarization of a dense counterpart, P_r^0. [392,394,407] The experimental data of the selected porous materials follow the solid line. The theoretical maximum, which displays the real available material, is displayed by the dashed line (Eq. 4).

displayed in Fig. 15c. [133] The results indicate that the switched polarization and the mobility of domain walls gets reduced for the material with isometric pores. The latter is reflected by the decreased slope at the inflection point of the polarization curves, as highlighted in Fig. 15c. The shape of the field- and time dependent polarization response in porous materials (Fig. 15b and c) was explained by the distribution of the local electric field, which shifts to lower values and broadens with increasing the degree of isometric porosity, as displayed in Fig. 14a. [133]

An additional effect observed in the polarization hysteresis loops in Fig. 15b is the reduction in the remanent polarization with increasing volume fraction of isometric porosity. The fraction of the remanent polarization of a porous material, P_r, normalized to the remanent polarization of a dense counterpart, P_r^0, is displayed for different materials in Fig. 15d. [392,394,407] The decrease of P_r/P_r^0 was interpreted as a reduced degree of poling and is responsible for the reduced piezoelectric coefficient of porous materials compared to dense counterparts. [411–413] If the entire porous material would be polarized, the fraction P_r/P_r^0 should follow the dashed line, as displayed in Fig. 15d. The experimentally measured fraction of porous materials, however, is significantly lower, as indicated by the solid line. The difference indicates that a substantial amount of the material remains unpoled after the application of the electric field. The difference between the experimentally observed and the theoretical limit is considered mathematically by the depolarization factor, d_p. [394,414] In the framework of this theory, the fraction of the remanent polarization of a porous material compared to a dense counterpart is expressed as:

$$P_r/P_r^0 = d_p(p, E_{\text{app}}) \cdot (1 - p). \tag{4}$$

The local electric field in some volumes of the material is too low to initiate domain wall motion (Fig. 14a). Consequently, the depolarization factor and thus the volume fraction of active material can be tuned by tailoring the local electric field distribution, e.g., through microstructural engineering the degree of porosity or its shape [106,394] or by increasing the applied electric field [106]. A higher applied electric field shifts the local electric field distribution to higher values and activates previously inactive volumes. Adjusting the externally applied electric field thus offers the potential to tailor the degree of poling and the piezoelectric response of porous ferroelectrics/ferroelastics.

Another consequence of the gap between experimentally measured and theoretically predicted values of the remanent polarization in Fig. 15d is, that a direct comparison between the coercive fields obtained from polarization measurements of different porous materials should be undertaken with care, since the polarization reversal remains incomplete in most cases (Fig. 15d). This may explain the previously revealed discrepancies in trends of the coercive fields of porous materials with increasing degree of isometric porosity [394]. Some authors claim that the coercive field decreases with increasing total porosity, [392,407,415] others find an increase, [409,414] while again others observe no effect [406,410]. Other reports find that the coercive field first decreases before it increases again. [394,416] Calculations predict a more realistic increase of the coercive field with increasing total porosity if a sufficiently high electric field is applied to activate the entire material. [417,418]

4.3.2. Orientation angle of anisometric pores

Materials with oriented anisometric pores can be obtained by freeze casting [419,420] or paper-derived approaches [413,421]. The impact of pore orientation angle with respect to the electric field on domain wall dynamics and performance has been systematically studied in ref. [106]. Micrographs of a freeze-cast polycrystalline PZT ceramic are displayed in Fig. 16a. The individual porous channels are magnified in Fig. 16b, highlighting the high degree of pore alignment achievable by freeze-casting. Macroscopic polarization and strain loops of samples with different orientation angles of anisometric pores, Θ, with respect to the electric field are displayed in Fig. 16c and d. A dense counterpart of the same grain size is displayed for comparison. Increasing Θ away from the direction of the applied electric field results in a reduction of the remanent and saturation polarization, which comes along with a reduction in bipolar strain. This effect was related to statistical local electric field distributions, (Fig. 14c) shifting towards lower values and broadening with increasing Θ away from the applied electric field. [106,133,391,393,396] This reduces the amount of actively switched material, and thus the obtainable remanent polarization and bipolar strain. Interestingly, at the same time, the sample with anisometric pores oriented parallel to the applied electric field ($\Theta = 0^{\circ}$) has comparable electromechanical properties to a dense counterpart. This is a consequence of the comparable local electric field distributions, which allows to activate the porous material with pores oriented parallel to the applied electric field nearly completely (Fig. 14c). In this frame small signal piezoelectric coefficient and permittivity decrease with increasing pore orientation angle, which is the key to obtain high figures of merit for sensing (g_{33}) and energy harvesting ($d_{33} \cdot g_{33}$), as summarized in Fig. 16d. [391,419,422]

4.3.3. Summary and further aspects

Experiments and simulations have revealed the role of porosity on the local electric driving forces for domain wall motion. While the impact of the degree of total porosity and the pore orientation angle on domain wall dynamics and functional properties have been heavily researched, experimental studies on the impact of pore radius/shape are lacking. To further reveal the impact of mechanical driving forces on the static domain structure and domain wall dynamics, imaging of the domains in porous materials are highly desirable. Orienting highly anisotropic pores has been further identified as an effective mean to engineer domain wall dynamics via local electric field distributions. Combining porous ferroelectric/ferroelastic materials with other microstructural engineering parameters, such as grain size (Section 4.2.1) and crystallographic texturing (Section 4.2.2), further broadens the playground for

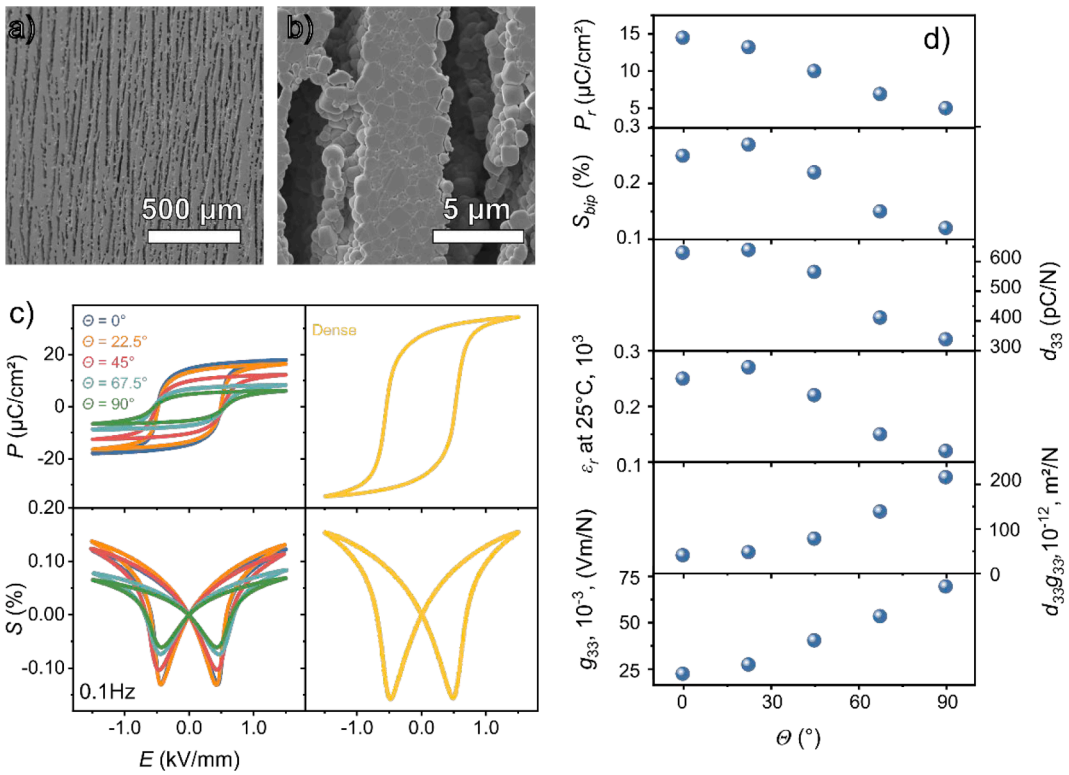

Fig. 16. Impact of pore orientation angle on domain wall dynamics and functional properties. The microstructure of porous (34 vol.%) PZT samples containing anisometric pores is displayed in a) and a magnification of the porous channels is provided in b). Macroscopic polarization and strain loops are displayed in c) for porous materials with different pore orientation angles. The angle Θ represents the pore orientation angle with respect to the external electric field. The response of a dense polycrystalline material with the same grain size is displayed for comparison. The dependence of functional properties (remanent polarization, P_r, bipolar strain, S_{bip}, small-signal piezoelectric charge coefficient, d_{33}, relative permittivity, ε_r, piezoelectric voltage coefficient, g_{33}, figure of merit for energy harvesting, $d_{33}g_{33}$) on the pore orientation angle Θ is displayed in d). [106]

property engineering. Freeze casting in combination with the templated grain growth process, for example, provides full control over the pore orientation together with the orientation of the grains. [423] While first materials were manufactured, the dielectric and piezoelectric performance has not yet been characterized. Processing routines to control the porosity together with the grain size are also on the way, [424] giving porous ferroelectric/ferroelastic materials a new dimension to engineer the functional performance via microstructural engineering.

5. Computational approaches

In this section we summarize selected computational approaches, which allow insight on different aspects of the relationship between domain wall motion and structure/microstructure in ferroelectric/ferroelastic polycrystals. We start in Section 5.1 with phase field simulations, which give insights into structure-property relationships on the mesoscale. Complementary, stochastic (Section 5.2) and micromechanical modelling (Section 5.3) shed light on the time- and field-dependent response of ferroelectric/ferroelastic materials on the macroscopic scale. Going beyond the approaches summarized in this review, the domain wall dynamics utilizing effective Hamiltonian approaches and molecular dynamic simulations are discussed in refs. [425–427], while a more general overview of atomistic models can be found in refs. [428,429]. Homogenized energy models [79,430–432] or atomistic dummy models [433,434] allow to study further specific aspects of domain wall dynamics in polycrystalline ferroelectrics/ferroelastics.

5.1. Phase field method

The phase-field method has been established as an effective tool to predict the domain structure evolution and its correlations with material properties and behaviors in ferroelectric ceramics, single crystals, and thin films. [435,436] The method is based on the thermodynamics and kinetics of materials at the mesoscale. The total free energy of a ferroelectric polycrystal includes contributions from the bulk, elastic, electric, and domain wall energies. [435,436] To describe more specific aspects of ferroelectrics, it is also possible to include other contributions, e.g., from charged defects, [437] flexoelectric coupling, [438] and antiferrodistortive ordering [439]. Table 2 summarizes these energy expressions and the material parameters together with possible sources of experimental methods and/or density functional theory (DFT) calculations to obtain material parameters needed in phase-field simulations. In the phase-field model of polycrystalline ferroelectric/ferroelastic materials, all tensor parameters are grain orientation-dependent and thus the properties within different grains are related by the corresponding matrix rotation operation. [440] However, the structures and properties of grain boundaries are largely unknown and thus require future extensive experimental and theoretical exploration. [329] Phase-field simulations can be employed to model and predict the domain structure evolution, as well as the equilibrium domain structures under externally applied thermal, mechanical, and electric stimuli by numerically solving the time-dependent evolution equations for polarization along with mechanical and electrostatic equilibrium equations. [435,436]

Phase-field modelling has been extensively utilized to model the equilibrium domain structures, [441,442] domain dynamics, [443,444] mechanical behavior, [445] piezoelectric responses, [446,447] and electrostatic energy-storage properties [387]. There have also been phase-field simulations to understand the effect of grain morphology, [448] crack propagation, [449] and mobile defects [437,450–453] such as oxygen vacancies in ferroelectric ceramics. The models found that grain boundaries, structural, and charge defects in ferroelectric polycrystals result in strongly inhomogeneous internal electric and stress fields, leading to complex polar configurations and material behavior considerably different from their single-crystalline counterparts. [454,455]

Table 2
Energy terms and necessary material parameters in the phase-field model of ferroelectrics. Possible approaches to obtaining the material parameters are also provided.

Energy Term	Expression	Variables	Key Parameters and Possible Sources
f_{bulk}	$\alpha_i P_i^2 + \alpha_{ij} P_i^2 P_j^2 + \alpha_{ijk} P_i^2 P_j^2 P_k^2$	P_i: Spontaneous polarization α_i, α_{ij}, α_{ijk}: Landau Coefficients	α_i, α_{ij}, α_{ijk} relating to different-order dielectric stiffness [463,464]
$f_{elastic}$	$\frac{1}{2} c_{ijkl}(\varepsilon_{ij} - Q_{ijmn} P_m P_n)(\varepsilon_{kl} - Q_{klmn} P_m P_n)$	ε_{ij}: total strain c_{ijkl}: stiffness tensor coefficients Q_{ijkl}: electrostrictive coefficients	c_{ijkl}, Q_{ijkl} inelastic neutron scattering [465]; plate resonance measurements [466]; DFT calculations [467]
$f_{electric}$	$-P_i E_i - \frac{1}{2} \epsilon \kappa_{ij}^b E_i E_j$	E_i: electric field κ_{ij}^b: background dielectric constant	κ_{ij}^b, high-temperature dielectric measurement [468]
$f_{gradient}$	$\frac{1}{2} \gamma_{ijkl} \frac{\partial P_i}{\partial x_j} \frac{\partial P_k}{\partial x_l}$	γ_{ijkl}: gradient energy coefficients	γ_{ijkl}, neutron diffuse scattering experiment [466]
$f_{defects}$	$nE_C - pE_V + N_i E_i - T(s_n + s_p + s_{trap})$	E_C: conduction band bottom E_V: valence band top n: electron concentration p: hole concentration N_i, E_i: concentration and electron level of the ith defect species s: entropy	E_C, E_V, N_C, N_V, E_i electrical conductance measurements [469–471]
f_{flexo}	$\frac{1}{2} F_{ijkl} \left(\frac{\partial P_k}{\partial x_l} \sigma_{ij} - \frac{\partial \sigma_{ij}}{\partial x_l} P_k \right)$	F_{ijkl}: flexoelectric coefficients σ_{ij}: stress	F_{ijkl}: neutron diffuse scattering [472,473]
$f_{antiferrodistortion}$	$\beta_i q_i^2 + \beta_{ij} q_i^2 q_j^2 + \beta_{ijk} q_i^2 q_j^2 q_k^2$	q_i: structural order parameter β_i, β_{ij}, β_{ijk}: Landau Coefficients	β_i, β_{ij}, β_{ijk}temperature-dependent Raman spectrum measurement [474]

As an example, modelling results for the impact of grain size in a polycrystalline BT materials and degree of crystallographic texture in a polycrystalline PMN-PT are displayed in Fig. 17a and b, respectively, and is discussed with respect to the experimental results presented in Sections 4.2.1 and 4.2.2. In agreement with experimentally measured polarization loops displayed in Fig. 8a, phase field simulations predict slimmer polarization loops for ceramics with larger (100 nm) grain sizes than for smaller (20 nm) ones. Furthermore, the grain size dependence of the coercive field and the remanent polarization obtained from phase-field simulations are in good qualitative agreement with experimental results discussed in Fig. 9a. However, phase field simulations do not yet cover all experimentally observed aspects, e.g., the peak in the small signal permittivity and piezoelectric coefficient observed for BT in Fig. 9c. The dependence of the piezoelectric coefficient on the degree of crystallographic texture in PMN-PT is displayed in Fig. 17b. [448] The experimental piezoelectric response of a PMN-PT material is presented for comparison. [456,457] The results obtained from phase field simulations largely agree with experimental observations, as discussed in Section 4.2.2.2. Fig. 17b further displays the spatial distribution of local electric field and mechanical stress concentrations obtained from simulations, highlighting concentrations at the boundary between misoriented grains.

The advantage of phase-field modeling in understanding the experimental observations at the mesoscale lies in its ability to resolve multi-physical fields and quantify different energy contributions. More details about the phase-field model of ferroelectrics and its applications, challenges, and prospects are reviewed in ref. [435]. Phase-field method can be employed to not only help to understand experimental observations and measurements, but also to guide the design of materials, e.g., ultrahigh piezoelectric response in relaxor ceramics, [458] enhanced dielectric response in tricritical ferroelectrics, [459] enhanced energy-storage performance in solid-solution polycrystalline films, [460] and giant electrocaloric effect in relaxor ceramics-polymer nanocomposites [461]. Moreover, phase field simulations have been employed to reveal the impact of dislocations, [265] precipitates [462] or more complex topological defects [184] on the domain structures in ferroelectric materials.

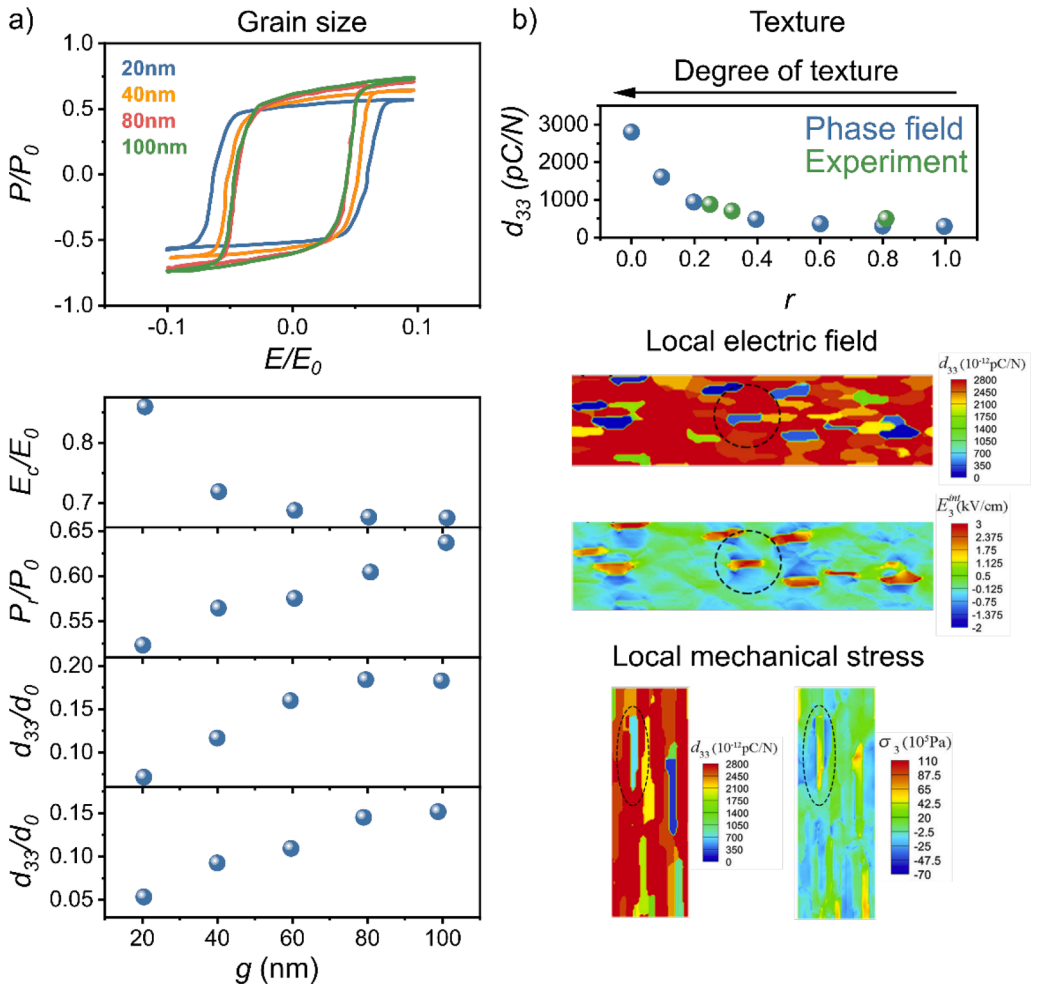

Fig. 17. Insights obtained by phase field modelling on the impact of microstructure on domain wall dynamics and functional properties of polycrystalline ferroelectric/ferroelastic materials: a) Simulated impact of grain size on polarization hysteresis in polycrystalline BT. [443]. b) Impact of degree of crystallographic texture (quantified by the March Dollas parameter, *r* [372]) on piezoelectric properties in PMN-PT polycrystalline ceramics. The experimental reference values, obtained from refs. [456,457], are plotted for comparison. To highlight local electric and mechanical stress concentrations, misoriented grains are indicated by dashed circles in b). Reprinted from [448], with permission from Elsevier.

5.2. Stochastic modelling

Stochastic models are based on the theories developed by Johnson and Mehl [475] and independently by Avrami [476]. Isibashi and Takagi systematically applied the theoretical approaches to study domain wall dynamics in ferroelectric single crystals, [120] using the mathematical concept of Kolmogorov, [477] which is commonly used to describe crystallization kinetics in metals. According to the classical Avrami approach, the driving force for domain wall motion is the difference in the free energies between the starting and the new phases. In the framework of the Kolmogorov-Avrami-Ishibashi (KAI) model, it is assumed that the mean size of individually transformed regions is small in comparison to the sample size, that the nucleation probability for new domains is spatially uniform, and that the value of domain wall velocity is the same in all regions. Additionally, the domain wall motion is considered as the time-dependent step. [119] In the KAI model, a temporal dependence of the reversed polarization is presented as

$$\Delta P(t, \tau_{E_{Sw}}) = \Delta P_{max}\left\{1 - \exp\left[-\left(\frac{t}{\tau_{E_{Sw}}}\right)^{\zeta}\right]\right\}. \quad (5)$$

Here, $\tau_{E_{Sw}}$ is a unique time constant related to the motion of the domain walls after nucleation, ΔP_{max} is the amount of the reversed polarization reached at saturation, and ζ is the Avrami exponent. The latter depends on the dimensionality of the domain and is expected to take only integer values from 1 to 4. In this frame, it is distinguished between one-step-nucleation (no additional nuclei form and the domain walls move with a constant velocity, $\zeta = \delta_{dim}$) and continuous nucleation (additional nuclei form during the switching process with a constant rate and domain walls move with a constant velocity, $\zeta = \delta_{dim} + 1$). The value ζ can be related to the dimensionality of the growing domain δ_{dim}. Stripe domains ($\delta_{dim} = 1$), circular domains ($\delta_{dim} = 2$), and spherical domains ($\delta_{dim} = 3$) are distinguished (Fig. 18a). The correlation between the exponent ζ and the dimensionality of the growing domain has not yet been confirmed experimentally.

The KAI model is commonly used to describe the time-dependent polarization evolution of single crystalline ferroelectrics/ferroelastics. Studied materials include BT, [131,381] $(CH_3NH_3)_5Bi_2Br_{11}$, [478,479] TGS, [480,481] and $KTiOPO_4$ (KTP) [482]. A representative example of the time-dependent switched polarization of a [111] oriented BT single crystal is provided in Fig. 18b. Here, the solid lines reveal fits according to Equation (5). The Avrami exponents were found to be field-dependent and non-integer. [381] To account for non-integer Avrami coefficients, the KAI model was modified to take finite sample sizes [483,484] into account and a new mathematical treatment was suggested. When the growing domain touches a boundary, it stops growing in that direction, resulting in a time-dependent change of the Avrami exponent, referred to as "geometrical catastrophe" [44,485]. Non-integer Avrami coefficients were also explained by a mixing of one step and continuous nucleation. [482]

The KAI model was applied to describe domain wall dynamics in more complex systems, characterized by a higher degree of disorder than single crystals. For example, domain wall dynamics in certain copolymers revealed values as large as $\zeta = 5$. [486]

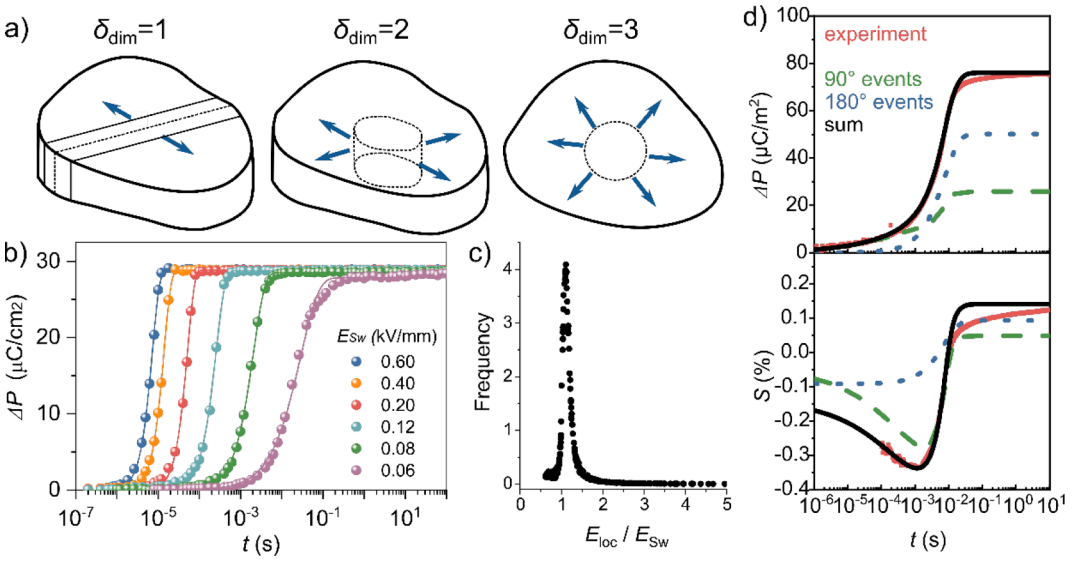

Fig. 18. The description of domain wall dynamics in polycrystalline ferroelectrics/ferroelastics using stochastic modelling. a) The shape of domains with different dimensionality according to the KAI approach are visualized. [120] The blue arrows indicate the direction of growth. b) Switched polarization as a function of time for a [111] oriented BT single crystal. The symbols correspond to the experimental results obtained at a constant switching field of pulse height E_{Sw}, as indicated, while the solid lines represent fits according to Equation (5). [381] c) Weighted statistical distribution of the local electric field of a polycrystalline PZT ceramic sample obtained from the IFM Model (Equation (6)). [88] d) Switched polarization and strain variation as a function of time for a tetragonal $Pb_{0.985}\ V_{Pb_{0.005}}\ La_{0.01}(Zr_{0.475}Ti_{0.525})O_3$ polycrystalline ceramic at a constant applied electric field. Fits to the experimental data according to the MSM model display the calculated contribution of 90° and 180° switching events using the MSM model. [96,105]

Equation (5) was utilized to describe the domain wall dynamics also in polycrystalline [487–489] and epitaxial [490,491] thin films. By comparing the domain wall dynamics of polycrystalline thin films to single crystalline counterparts, it was found that thin films exhibit a broadened distribution of switching times. [492] This finding led to an extension of the KAI model by an aggregation of regions with different switching dynamics, while the domain wall dynamics in the entire sample is a superposition of all these regions. [493] In the nucleation limited switching (NLS) model, switching of one region is limited by the nucleation of new domains rather than by domain wall motion, and a smooth and exponentially broad distribution of nucleation waiting times was suggested to describe the switching process in a polycrystalline thin film best. Individual regions thereby correspond to single grains or clusters of grains and grain boundaries act as frontiers to limit the propagation of the switched region. [335,494] This extended model was successfully applied to study polarization reversal dynamics in polycrystalline thin films. [495,496]

Building up on the NLS model, domain wall dynamics in polycrystalline bulk ceramics were described by the inhomogeneous field mechanism (IFM) model. The IFM model assumes that the distribution of switching times is related to an inhomogeneous distribution of the local electric field, as discussed in Section 2.2.2. [88,122] In this context, the time-dependent switched polarization

$$\Delta P(E_{Sw}, t) = \Delta P_{max} \int_0^{E_{Sw}/E_{max}(t)} \frac{du}{u} \Phi(u) \tag{6}$$

can be calculated for any high voltage field pulse E_{Sw}, if the functions $E_{max}(t)$ and $\Phi(u)$, which represent a fingerprint of the domain wall dynamics of the ferroelectric material, are known. The functions $E_{max}(t)$ and $\Phi(u)$ can be extracted from polarization dynamic measurements performed at different field pulses, E_{Sw}, as described in refs. [88,129]. This model was applied to study the impact of crystallographic system, [128–130] degree of crystallographic texture, [354] and porosity [133] on domain wall dynamics in polycrystalline ferroelectrics/ferroelastics and is even applicable to ferroelectric polymers. [497,498]

Experimental advances allowed to measure the dynamics of macroscopic strain simultaneously with the switched polarization, which allows to distinguish 180° and non-180° domain wall dynamics (Section 2.2 and Fig. 2). [94,105] These findings helped to improve stochastic models further. In contrast to the classical KAI approach, the multi-step stochastic mechanism (MSM) [96] model includes two parallel channels of switching for materials with a tetragonal system: 180°-polarization reversal and sequential two-step 90° switching events. This allows to calculate the time-dependence of the switched polarization and strain, as schematically indicated in Fig. 18d. Here, experimental curves are highlighted by red symbols, while calculated contributions from 180° and 90° switching events are displayed by dotted lines. The sum is represented by the black solid line and describes the experimental observation well. An important finding of the MSM model is, that 90° switching events account for 34% of the switched polarization in a tetragonal $Pb_{0.985}$ $V_{Pb_{0.005}}$ $La_{0.01}(Zr_{0.475}Ti_{0.525})O_3$ polycrystalline ceramic. In the framework of the MSM model, the domain dynamics in polycrystalline ferroelectrics/ferroelastics are related to the dimensionality of the growing domain, [96] as well as the inhomogeneous distribution of the local electric field. [123] An extension of the MSM model to polycrystalline orthorhombic [499] and rhombohedral [247] materials also exists.

5.3. Micromechanical modelling

In early micromechanical models, [500,501] the polycrystalline material was constructed by many randomly oriented tetragonal and single-domain grains and the switching behavior of each individual grain was described by an idealized rectangular hysteresis behavior. To simulate the response of the polycrystalline material, each grain was subjected to the same externally applied field and stress. The applied field was increased stepwise and for each step the change in energy, related to a possible 180° or 90° switching event, was calculated. When the sum of the electric and the mechanical work exceeded a critical value, the direction of the spontaneous polarization has switched:

$$E_i \Delta P_i + \sigma_{jk} \Delta S_{jk} \geq 2 P_s E_c \tag{7}$$

Here, ΔP_i is the change in remanent polarization and ΔS_{jk} is the change in remanent strain of the switching domain. The first set of micromechanical models assumed a very simplified behavior. Individual grains were described as monodomain states and domain walls were neglected. [501–503] Also, inhomogeneities in the electric field and mechanical stress, which are both a key feature of polycrystalline materials (Section 2.2), were ignored. [504] Later, interactions between grains were implemented via the Eshelby approach [316,505,506] or finite element solutions. [507] The models were further extended and domain configurations [508,509] and interaction between domains [510] were taken into account. Beyond tetragonal materials, extensions to rhombohedral crystal systems [506] or materials with a phase coexistence [511] are available. For a more detailed description of micromechanical models, we refer the reader to ref. [512].

6. Conclusions, current challenges, and future perspectives

Domain wall motion has been identified as one of the main contributions to the dielectric and electromechanical properties of ferroelectric/ferroelastic materials. While the dynamics of the walls can be tuned via the defect chemistry, the impact of structure and microstructure on the functional properties of polycrystalline ferroelectric/ferroelastic materials has been intensively studied. In this frame, polycrystals offer many degrees of freedom, including crystallographic system, degree of crystallographic orientation, grain size, and porosity. The impact of each of these parameters on ferroelectric/ferroelastic domain wall motion needs to be understood. The main challenge is to disentangle the high interdependency between parameters governing the formation of the static domain

structure and domain wall dynamics. In this review article, we addressed this challenge by explaining domain formation and domain wall motion by electric and mechanical driving forces, which have been revealed to govern domain wall dynamics in polycrystalline ferroelectrics/ferroelastics. [94–96] To generate a comprehensive understanding of the complex structure–property relationship in ferroelectric/ferroelastic materials in the future, dielectric and electromechanical measurements need to be combined with advanced structural and nanoscale dynamic characterization.

6.1. Advanced characterization methods

High-energy diffraction and advanced SPM techniques are particularly interesting for this purpose. Advanced X-Ray microscopy techniques visualize and quantify domain wall dynamics, spatially resolved on the nanoscale. State-of-the-art synchrotron sources achieve sub-100 nm spatial resolutions [179] and time-resolutions in the nanosecond-range in stroboscopic modes were reported in bulk geometry. [513] Furthermore, X-Ray free electron lasers (XFEL) enable ultrafast time resolutions, which allow capturing polarization rotation phenomena occurring at picoseconds. [514] In this frame, it is also known that ferroelectric materials are suffering from radiation damage. [515–517] Defined boundary conditions, such as the interplay between radiation time and electric field amplitude or the influence of different chemical elements on the interactions between ferroelectric/ferroelastic materials and high-energy synchrotron radiation therefore need to be established.

Besides X-Ray diffraction, SPM-based techniques and spectroscopic approaches are highly attractive to get insights into the ferroelectric/ferroelastic domain structure since they offer nanoscale spatial resolution. The ferroelectric/ferroelastic domain size and domain morphology can be quantified together with the local coercive voltages, relaxation times or Rayleigh behavior. For polycrystalline materials, which feature a complex domain structure and a random orientation of the individual crystallites, advances towards automated SPM experiments and the use of machine learning approaches are of particular interest. [518] Such measurements provide the possibility to quantify the dynamics of individual types of domain walls, providing a new pathway to study the impact of microstructure on domain wall dynamics in polycrystalline ferroelectrics/ferroelastics. [519]

Besides the structural and microstructural features discussed so far, the domain structure and the mobility of domain walls may be influenced by ordered chemical defects. [520,521] Atom probe tomography (APT) combines a high chemical sensitivity and accuracy with three-dimensional spatial resolution, and is therefore frequently applied in metallurgy to characterize subtle changes in defect concentrations along precipitates or dislocations. [522] Mapping and quantifying point defects via APT will be important to characterize the impact of chemistry on the local domain structure and domain wall dynamics in the future and will be of further interest the nanoscale chemistry of polycrystalline ferroelectrics/ferroelastics in general.

6.2. New microstructural approaches using extended defects

Going beyond the structural and microstructural tools introduced in Fig. 4a and b, new approaches are well on the way now. The local interaction of domain walls with strain fields originating from designed extended defects, such as secondary phases, [523,524] dislocations, [265,525] or precipitates [462] have been outlined, providing new levers to control the static domain structure, domain wall back-switching or domain wall pinning in polycrystalline ferroelectrics/ferroelastics. Pioneering studies on BT single crystals, for example, outline a giant electric-field dependent permittivity (5800) and large-signal piezoelectric coefficient (1890 pm/V), indicating that controlling the domain wall dynamics via mechanical dislocation imprint will be a powerful tool for functional property engineering. [265]

Besides strain fields, advances in nanoscale electric characterization have created a fundamental understanding on the electronic transport properties of ferroelectric domain walls. [160,526] Bulk ferroelectric materials strongly benefit from the ongoing advance in characterization and understanding of the electronic response on the domain wall level. First intriguing examples suggest domain wall networks as reconfigurable barrier layer capacitors in single crystalline $ErMnO_3$. [527,528] In addition, the unusual low frequency enhanced electromechanical properties in polycrystalline BFO were explained by conductive domain walls [529,530]. New physical phenomena, e.g., the uncoupling of lattice strain and domain wall switching, [531] not available in classical materials such as PZT or BT, in addition provide new degrees of freedom to control the frequency-dependent properties of bulk ferroelectric materials. While charged ferroelectric domain walls have been identified as a general phenomenon appearing in many ferroelectrics, [532] utilizing their collective electronic transport behavior in bulk application in polycrystals is unchartered territory. An outlook on the application potential of charged ferroelectric domain walls in macroscopic capacitor or actuator applications is provided in ref. [160].

6.3. Ferroelectric materials with more complex correlation phenomena

The response of polar materials to an electric field can also be fundamentally different as in the classical ferroelectrics discussed in this review. Examples of ferroelectric materials with a more complex electronic correlation include improper ferroelectrics, [533–535] incipient ferroelectrics, [536] antiferroelectrics, [537] ferrielectrics, [538] and relaxor ferroelectrics [539]. For example, the electric-field-induced phase transition enables an improved energy density, making ferrielectrics and antiferroelectric materials interesting for dielectric energy-storage applications. [540] In improper ferroelectrics, the spontaneous polarization is not the primary order parameter, [541,542] which leads to much more flexible electronic and mechanical boundary conditions of the domain walls. As a consequence, the materials exhibit a large variety of unusual physical phenomena at the level of ferroelectric domain walls. Intriguing examples range from domain walls with unique functional electronic properties, ranging from individual domain walls acting as binary switches or rectifiers [533–535,543,544] to the collective macroscopic response for next-generation capacitors [527].

Ferroelectric materials with more complex correlation phenomena may be beneficial rather than detrimental for domain engineering and domain wall dynamics. Similar to the reduction of coercive field with degree of crystallographic texture discussed in Section 4.2.2.2, electric-field-induced phase transformations in relaxors ferroelectrics [545–547] can get promoted by crystallographic texturing. Another good example are improper ferroelectric ternary hexagonal manganites, $R\mathrm{MnO_3}$ (R = Sc, Y, In, and Dy – Lu). In $R\mathrm{MnO_3}$, the polarization emerges as a symmetry enforced by-product of a structurally driven phase transition. [548] Most of the research so far, however, focused on single crystals and thin films, whereas only few studies were performed on polycrystalline systems. [549–552] In particular the possibility to utilize the microstructure to engineer the ferroelectric domain structure via naturally occurring topologically protected vortex/anti-vortex pairs remains to be explored. A novel domain scaling behavior in polycrystalline $\mathrm{ErMnO_3}$ materials was discovered, demonstrating that the established scaling behavior in BT or PZT (Fig. 9e and f) can be suppressed and inverted. [184] This behavior was related to the interaction of topologically protected vortex/anti-vortex pairs with long-ranging elastic strain fields. Combining microstructural engineering with more complex correlation phenomena provides an exciting playground to engineer the functional behavior of polycrystalline ferroelectrics via the domain structure and domain wall dynamics in the future.

Declaration of Competing Interest

The authors declare that they have no known competing financial interests or personal relationships that could have appeared to influence the work reported in this paper.

Data availability

Data will be made available on request.

Acknowledgements

J.S. acknowledges the support of the Feodor Lynen Research Fellowship of the Alexander von Humboldt Foundation and NTNU Nano for the support through the NTNU Nano Impact fund. This work was partially supported by the Deutsche Forschungsgemeinschaft (DFG) under the Grant Nr. 270195408 (KO5100/1-1) and 405631895 (GE-1171/8-1). L.Q.C. would like to acknowledge the Alexander von Humboldt Foundation for the Humboldt Research Award and the US National Science Foundation under the grant number DMR-213373.

References

[1] Valasek J. Piezo-electric and allied phenomena in Rochelle salt. Phys Rev 1921;17:475. https://doi.org/10.1103/PhysRev.17.475.
[2] Uchino K. Ferroelectric. Devices: CRC Press; 2009.
[3] Troiler-McKinstry S. Impact of ferroelectricity. Am Cer Soc Bull 2020;99:22–3.
[4] Meier D, Selbach SM. Ferroelectric domain walls for nanotechnology. Nat Rev Mater 2021;7:157. https://doi.org/10.1038/s41578-021-00375-z.
[5] Yang L, Kong X, Li F, Hao H, Cheng Z, Liu H, et al. Perovskite lead-free dielectrics for energy storage applications. Prog Mat Sci 2019;102:72–108. https://doi.org/10.1016/j.pmatsci.2018.12.005.
[6] Blázquez-Castro A, García-Cabañes A, Carrascosa M. Biological applications of ferroelectric materials. Appl Phys Rev 2018;5:041101. https://doi.org/10.1063/1.5044472.
[7] Tsikriteas ZM, Roscow JI, Bowen CR, Khanbareh H. Flexible ferroelectric wearable devices for medical applications. Iscience 2021;24:101987. https://doi.org/10.1016/j.isci.2020.101987.
[8] Chanthbouala A, Garcia V, Cherifi RO, Bouzehouane K, Fusil S, Moya X, et al. A ferroelectric memristor. Nat Mater 2012;11:860–4. https://doi.org/10.1038/nmat3415.
[9] Oh S, Hwang H, Yoo I. Ferroelectric materials for neuromorphic computing. APL Mater 2019;7:091109. https://doi.org/10.1063/1.5108562.
[11] Damjanovic D. Ferroelectric, dielectric and piezoelectric properties of ferroelectric thin films and ceramics. Rep Prog Phys 1998;61:1267–324. https://doi.org/10.1088/0034-4885/61/9/002.
[12] Kleemann W. Universal domain wall dynamics in disordered ferroic materials. Annu Rev Mater Res 2007;37:415–48. https://doi.org/10.1146/annurev.matsci.37.052506.084243.
[13] Hall DA. Review nonlinearity in piezoelectric ceramics. J Mater Sci 2001;36:4575–601. https://doi.org/10.1023/A:1017959111402.
[14] Zhang QM, Wang H, Kim N, Cross LE. Direct Evaluation of Domain-Wall and Intrinsic Contributions to the Dielectric and Piezoelectric Response and Their Temperature-Dependence on Lead-Zirconate-Titanate Ceramics. J Appl Phys 1994;75:454–9. https://doi.org/10.1063/1.355874.
[15] Pramanick A, Damjanovic D, Daniels JE, Nino JC, Jones JL. Origins of Electro-Mechanical Coupling in Polycrystalline Ferroelectrics During Subcoercive Electrical Loading. J Am Ceram Soc 2011;94:293–309. https://doi.org/10.1111/j.1551-2916.2010.04240.x.
[16] Acosta M, Novak N, Rojas V, Patel S, Vaish R, Koruza J, et al. $BaTiO_3$-based piezoelectrics: Fundamentals, current status, and perspectives. Appl Phys Rev 2017;4:041305. https://doi.org/10.1063/1.4990046.
[17] Otonicar M, Dragomir M, Rojac T. Dynamics of domain walls in ferroelectrics and relaxors. J Am Ceram Soc 2022;105(11):6479–507. https://doi.org/10.1111/jace.18623.
[18] Wu J, Xiao D, Zhu J. Potassium–sodium niobate lead-free piezoelectric materials: past, present, and future of phase boundaries. Chem Rev 2015;115:2559–95. https://doi.org/10.1021/cr5006809.
[19] Genenko YA, Glaum J, Hirsch O, Kungl H, Hoffmann MJ, Granzow T. Aging of poled ferroelectric ceramics due to relaxation of random depolarization fields by space-charge accumulation near grain boundaries. Phys Rev B. 2009;80:224109, https://doi.org/10.1103/PhysRevB.80.224109.
[20] Pramanick A, Prewitt AD, Forrester JS, Jones JL. Domains, Domain Walls and Defects in Perovskite Ferroelectric Oxides: A Review of Present Understanding and Recent Contributions. Crit Rev Solid State Mater Sci 2012;37:243–75. https://doi.org/10.1080/10408436.2012.686891.
[21] Ren X. Large electric-field-induced strain in ferroelectric crystals by point-defect-mediated reversible domain switching. Nat Mater 2004;3:91–4. https://doi.org/10.1038/nmat1051.
[22] Rojac T, Damjanovic D. Domain walls and defects in ferroelectric materials. Jpn J Appl Phys 2017;56:10PA01. https://doi.org/10.7567/JJAP.56.10PA01.

[23] Kersten O, Hofmann M, Schmidt G. Dielectric-Dispersion of Mn Doped Ceramics. Ferroelectrics Lett 1986;6:75–80. https://doi.org/10.1080/00150198608245022.
[24] Herbiet R, Robels U, Dederichs H, Arlt G. Domain-Wall and Volume Contributions to Material Properties of PZT Ceramics. Ferroelectrics 1989;98:107–21. https://doi.org/10.1080/00150198908217575.
[25] Lewis B. Energy loss processes in ferroelectric ceramics. Proc Phys Soc 1959;73:17. https://doi.org/10.1088/0370-1328/73/1/304.
[26] Mueller V, Zhang Q. Nonlinearity and scaling behavior in donor-doped lead zirconate titanate piezoceramic. Appl Phys Lett 1998;72:2692–4. https://doi.org/10.1063/1.121101.
[27] Daniels JE, Pramanick A, Jones JL. Time-Resolved Characterization of Ferroelectrics Using High-Energy X-Ray Diffraction. IEEE T Ultrason Ferr. 2009;56:1539-45. https://doi.org/10.1109/TUFFC.2009.1218.
[28] Jones JL, Nino JC, Pramanick A, Daniels JE. Time-Resolved, Electric-Field-Induced Domain Switching and Strain in Ferroelectric Ceramics and Crystals. In: Eckold G, Schober H, Nagler SE, editors. Studying Kinetics with Neutrons: Prospects for Time-Resolved Neutron Scattering. Springer, Berlin Heidelberg: Berlin, Heidelberg; 2010. p. 149–75.
[29] Jones JL, Daniels JE, Ustundag E. Advances in the characterisation of domain switching in ferroelectric ceramics. Z Kristallogr 2007:441–6. https://doi.org/10.1524/9783486992540-069.
[30] Kugel VD, Cross LE. Behavior of soft piezoelectric ceramics under high sinusoidal electric fields. J Appl Phys 1998;84:2815–30. https://doi.org/10.1063/1.368422.
[31] Subbarao E, McQuarrie M, Buessem W. Domain effects in polycrystalline barium titanate. J Appl Phys 1957;28:1194–200. https://doi.org/10.1063/1.1722606.
[32] Hall DA, Steuwer A, Cherdhirunkorn B, Mori T, Withers PJ. Analysis of elastic strain and crystallographic texture in poled rhombohedral PZT ceramics. Acta Mater 2006;54:3075–83. https://doi.org/10.1016/j.actamat.2006.02.043.
[33] Endriss A, Hammer M, Hoffmann MJ, Kolleck A, Schneider GA. Microscopic and macroscopic ferroelectric-ferroelastic and piezoelectric behavior of PZT ceramics. J Eur Ceram Soc 1999;19:1229–31. https://doi.org/10.1016/S0955-2219(98)00408-7.
[34] Guo R, Cross LE, Park SE, Noheda B, Cox DE, Shirane G. Origin of the high piezoelectric response in $PbZr_{1-x}Ti_xO_3$. Phys Rev Lett 2000;84:5423–6. https://doi.org/10.1103/PhysRevLett.84.5423.
[35] Reszat JT, Glazounov AE, Hoffmann MJ. Analysis of intrinsic lattice deformation in PZT-ceramics of different compositions. J Eur Ceram Soc 2001;21:1349–52. https://doi.org/10.1016/S0955-2219(01)00016-4.
[36] Jones JL, Hoffman M, Daniels JE, Studer AJ. Direct measurement of the domain switching contribution to the dynamic piezoelectric response in ferroelectric ceramics. Appl Phys Lett 2006;89:092901. https://doi.org/10.1063/1.2338756.
[37] Daniels JE, Finlayson TR, Studer AJ, Hoffman M, Jones JL. Time-resolved diffraction measurements of electric-field-induced strain in tetragonal lead zirconate titanate. J Appl Phys 2007;101:094104. https://doi.org/10.1063/1.2720255.
[38] Eßlinger S, Neumeister P, Schönecker A, Hoffman M, Studer A, Hinterstein M. In situ neutron diffraction studies on poling of the hard PZT ceramic PIC181. Adv Eng Mater 2019;21:1900159. https://doi.org/10.1002/adem.201900159.
[39] Shur VY. Fast polarization reversal process: evolution of ferroelectric domain structure in thin films. In: Paz de Araujo CA, Scott JF, Taylor GW, editors. Ferroelectric Thin Films: Synthesis and Basic Properties. London, UK: Gordon & Breach Science Publ; 1996.
[40] Zhang L. Field-induced phase transitions and dielectric energy density in poly (vinylidene fluoride-trifluoroethylene-chlorofluoroethylene) terpolymer. Europhys Lett 2010;91:47001. https://doi.org/10.1209/0295-5075/91/47001.
[41] Scott JF. Switching of ferroelectrics without domains. Adv Mater 2010;22:5315–7. https://doi.org/10.1002/adma.201003264.
[42] Merz WJ. Domain formation and domain wall motions in ferroelectric $BaTiO_3$ single crystals. Phys Rev 1954;95:690–8. https://doi.org/10.1103/PhysRev.95.690.
[43] Little EA. Dynamic Behavior of Domain Walls in Barium Titanate. Phys Rev 1955;98:1201–2. https://doi.org/10.1103/PhysRev.98.978.
[44] Shur VY, Rumyantsev EL. Kinetics of ferroelectric domain structure during switching: theory and experiment. Ferroelectrics 1994;151:171–80. https://doi.org/10.1080/00150199408244739.
[45] Miller RC, Savage A. Velocity of Sidewise 180° Domain-Wall Motion in $BaTiO_3$ as a Function of the Applied Electric Field. Phys Rev 1958;112:755–62. https://doi.org/10.1103/PhysRev.112.755.
[46] Miller RC, Savage A. Further Experiments on the Sidewise Motion of 180° Domain Walls in $BaTiO_3$. Phys Rev 1959;115:1176–80. https://doi.org/10.1063/1.1736077.
[47] Miller RC, Weinreich G. Mechanism for the Sidewise Motion of 180° Domain Walls in Barium Titanate. Phys Rev 1960;117:1460–6. https://doi.org/10.1103/PhysRev.117.1460.
[48] Taylor GW. High Field Polarization Reversals in Liquid Electroded Barium Titanate Crystals. Aust J Phys 1962;15:549–67. https://doi.org/10.1071/PH620549.
[49] Stadler HL, Zachmanidis PJ. Nucleation and Growth of Ferroelectric Domains in $BaTiO_3$ at Fields from 2 to 450 kV/cm. J Appl Phys 1963;34:3255–60. https://doi.org/10.1063/1.1729173.
[50] Stadler HL, Zachmand PJ. Temperature Dependence of 180° Domain Wall Velocity in $BaTiO_3$. J Appl Phys 1964;35:2895–9. https://doi.org/10.1063/1.1713125.
[51] Stadler HL. Forward Velocity of 180° Ferroelectric Domain Walls in $BaTiO_3$. J Appl Phys 1966;37:1947–8. https://doi.org/10.1063/1.1708644.
[52] Drougard ME. Detailed Study of Switching Current in Barium Titanate. J Appl Phys 1960;31:352–5. https://doi.org/10.1063/1.1735571.
[53] Abe R. Theoretical Treatment of the Movement of 180° Domain in $BaTiO_3$ Single Crystal. J Phys Soc Jpn 1959;14:633–42. https://doi.org/10.1143/JPSJ.14.633.
[54] Burtsev EV, Chervonobrodov SP. Some Problems of 180° Switching in Ferroelectrics. Ferroelectrics 1982;45:97–106. https://doi.org/10.1080/00150198208208287.
[55] Shin YH, Grinberg I, Chen IW, Rappe AM. Nucleation and growth mechanism of ferroelectric domain-wall motion. Nature 2007;449:881–4. https://doi.org/10.1038/nature06165.
[56] Liu S, Grinberg I, Rappe AM. Intrinsic ferroelectric switching from first principles. Nature 2016;534:360–3. https://doi.org/10.1038/nature18286.
[57] Chynoweth A. Barkhausen pulses in barium titanate. Phys Rev 1958;110:1316. https://doi.org/10.1103/PhysRev.110.1316.
[58] Paruch P, Giamarchi T, Triscone JM. Domain wall roughness in epitaxial ferroelectric $PbZr_{0.2}Ti_{0.8}O_3$ thin films. Phys Rev Lett 2005;94:197601. https://doi.org/10.1103/PhysRevLett.94.197601.
[59] Pertsev NA, Petraru A, Kohlstedt H, Waser R, Bdikin IK, Kiselev D, et al. Dynamics of ferroelectric nanodomains in $BaTiO_3$ epitaxial thin films via piezoresponse force microscopy. Nanotechnology 2008;19:375703. https://doi.org/10.1088/0957-4484/19/37/375703.
[60] Tagantsev AK, Cross LE, Fousek J. Domains in ferroic crystals and thin films. Heidelberg, Germany: Springer; 2010.
[61] Morozov MI, Damjanovic D. Hardening-softening transition in Fe-doped $Pb(Zr,Ti)O_3$ ceramics and evolution of the third harmonic of the polarization response. J Appl Phys 2008;104:034107. https://doi.org/10.1063/1.2963704.
[62] Morozov MI, Damjanovic D. Charge migration in $Pb(Zr,Ti)O_3$ ceramics and its relation to ageing, hardening, and softening. J Appl Phys 2010;107:034106. https://doi.org/10.1063/1.3284954.
[63] Erhart P, Traskelin P, Albe K. Formation and switching of defect dipoles in acceptor-doped lead titanate: A kinetic model based on first-principles calculations. Phys Rev B 2013;88:024107. https://doi.org/10.1103/PhysRevB.88.024107.
[64] Robels U, Calderwood JH, Arlt G. Shift and Deformation of the Hysteresis Curve of Ferroelectrics by Defects - Electrostatic Model. J Appl Phys 1995;77:4002–8. https://doi.org/10.1063/1.359511.
[65] Kumada A. Domain Switching in $Gd_2(MoO_4)_3$. Phys Lett A 1969;A 30:186–7. https://doi.org/10.1016/0375-9601(69)90926-8.

[66] Ayoub M, Futterlieb H, Imbrock J, Denz C. 3D imaging of ferroelectric kinetics during electrically driven switching. Adv Mater 2017;29:1603325. https://doi.org/10.1002/adma.201603325.
[67] Li YW, Li FX. The effect of domain patterns on 180° domain switching in $BaTiO_3$ crystals during antiparallel electric field loading. Appl Phys Lett 2014;104:042908. https://doi.org/10.1063/1.4863672.
[68] Li YW, Li FX. The effect of multi-rank domain pattern on the polarization response of $BaTiO_3$ crystal during electric field loading. J Appl Phys 2015;117:244101. https://doi.org/10.1063/1.4922970.
[69] Pan W, Zhang Q, Bhalla AS, Cross LE. Field-Induced Strain in Single-Crystal $BaTiO_3$. J Am Ceram Soc 1988;71:C302–5. https://doi.org/10.1111/j.1151-2916.1988.tb05909.x.
[70] Zhu W, Cross LE. Direct evidence of ferroelastic participation in 180° polarization switching and fatigue for 111 oriented rhombohedral ferroelectric 0.955Pb$(Zn_{1/3}Nb_{2/3})O_3$:0.045$PbTiO_3$ single crystals. Appl Phys Lett 2004;84:2388–90. https://doi.org/10.1063/1.1690869.
[71] Cao WW. Switching mechanism in single crystal 0.955$PbZn_{1/3}Nb_{2/3}O_3$-0.045$PbTiO_3$. Ferroelectrics 2003;290:107–14. https://doi.org/10.1080/00150190390222349.
[72] Yin J, Cao W. Polarization reversal study using ultrasound. Appl Phys Lett 2001;79:4556–8. https://doi.org/10.1063/1.1428629.
[73] Jiang B, Bai Y, Chu WY, Su YJ, Qiao LJ. Direct observation of two 90° steps of 180° domain switching in $BaTiO_3$ single crystal under an antiparallel electric field. Appl Phys Lett 2008;93:152905. https://doi.org/10.1063/1.3000634.
[74] Liu X, Zhao Y, Hu Q, Ushakov AD, Luan P, Fu X, et al. Different domain switching kinetics in tetragonal PMN-PT single crystal studied by in situ observation and current analysis. J Eur Ceram Soc 2020;40:2922–8. https://doi.org/10.1016/j.jeurceramsoc.2020.03.013.
[75] Ushakov A, Esin A, Akhmatkhanov A, Hu Q, Liu X, Zhao Y, et al. Direct observation of domain kinetics in rhombohedral PMN-28PT single crystals during polarization reversal. Appl Phys Lett 2019;115:102903. https://doi.org/10.1063/1.5114885.
[76] Qi XY, Liu HH, Duan XF. In situ transmission electron microscopy study of electric-field-induced 90° domain switching in $BaTiO_3$ single crystals. Appl Phys Lett 2006;89:092908. https://doi.org/10.1063/1.2345231.
[77] Daniels JE, Finlayson TR, Davis M, Damjanovic D, Studer AJ, Hoffman M, et al. Neutron diffraction study of the polarization reversal mechanism in [111] c-oriented $Pb(Zn_{1/3}Nb_{2/3})O_3$−$x$$PbTiO_3$. J Appl Phys 2007;101:104108. https://doi.org/10.1063/1.2733636.
[78] Li YW, Wang J, Li FX. Intrinsic polarization switching in $BaTiO_3$ crystal under uniaxial electromechanical loading. Phys Rev B 2016;94:184108. https://doi.org/10.1103/PhysRevB.94.184108.
[79] Smith RC, Seelecke S, Ounaies Z, Smith J. A free energy model for hysteresis in ferroelectric materials. J Intell Material Syst Struct 2003;14:719–39. https://doi.org/10.1177/1045389X03038841.
[80] Li YW, Li FX. Domain switching criterion for ferroelectric single crystals under uni-axial electromechanical loading. Mech Mater 2016;93:246–56. https://doi.org/10.1016/j.mechmat.2015.11.005.
[81] Mueller R, Gross D, Lupascu D. Driving forces on domain walls in ferroelectric materials and interaction with defects. Comput Mater Sci 2006;35:42–52. https://doi.org/10.1016/j.commatsci.2005.02.014.
[82] Li W, Alexe M. Investigation on switching kinetics in epitaxial $Pb(Zr_{0.2}Ti_{0.8})O_3$ ferroelectric thin films: Role of the 90° domain walls. Appl Phys Lett 2007;91:262903. https://doi.org/10.1063/1.2825414.
[83] Randall CA, Barber DJ, Whatmore RW. Ferroelectric Domain Configurations in a Modified-PZT Ceramic. J Mater Sci 1987;22:925–31. https://doi.org/10.1007/BF01103531.
[84] Schrade D, Mueller R, Gross D, Utschig T, Shur VY, Lupascu DC. Interaction of domain walls with defects in ferroelectric materials. Mech Mater 2007;39:161–74. https://doi.org/10.1016/j.mechmat.2006.04.002.
[85] Lupascu DC, Shur VY, Shur AG. Dynamics of a single-planar domain wall in ferroelectric-ferroelastic $Gd_2(MoO_4)_3$. Appl Phys Lett 2002;80:2359–61. https://doi.org/10.1063/1.1464665.
[86] Eng LM. Nanoscale domain engineering and characterization of ferroelectric domains. Nanotechnology 1999;10:405–11. https://doi.org/10.1088/0957-4484/10/4/308.
[87] Roelofs A, Böttger U, Waser R, Schlaphof F, Trogisch S, Eng LM. Differentiating 180° and 90° switching of ferroelectric domains with three-dimensional piezoresponse force microscopy. Appl Phys Lett 2000;77:3444–6. https://doi.org/10.1063/1.1328049.
[88] Genenko YA, Zhukov S, Yampolskii SV, Schütrumpf J, Dittmer R, Jo W, et al. Universal Polarization Switching Behavior of Disordered Ferroelectrics. Adv Funct Mater 2012;22:2058–66. https://doi.org/10.1002/adfm.201102841.
[89] Fancher CM, Brewer S, Chung CC, Rohrig S, Rojac T, Esteves G, et al. The contribution of 180° domain wall motion to dielectric properties quantified from in situ X-ray diffraction. Acta Mater ;126:36–43. https://doi.org/10.1016/j.actamat.2016.12.037.
[90] Li SP, Bhalla AS, Newnham RE, Cross LE, Huang CY. 90° Domain Reversal in $Pb(Zr_xTi_{1-x})O_3$ Ceramics. J Mater Sci 1994;29:1290–4. https://doi.org/10.1080/07315179308204255.
[91] Jing YY, Blendell JE, Bowman KJ. Three dimensional piezoresponse force microscopy polarization difference maps. J Appl Phys 2011;109:074110. https://doi.org/10.1063/1.3560773.
[92] Kamel TM, de With G. Double-peak switching current in soft ferroelectric lead zirconate titanate. J Appl Phys 2007;102:044118. https://doi.org/10.1063/1.2767188.
[93] Berlincourt D, Krueger HHA. Domain Processes in Lead Titanate Zirconate and Barium Titanate Ceramics. J Appl Phys 1959;30:1804–10. https://doi.org/10.1063/1.1735059.
[94] Schultheiß J, Liu L, Kungl H, Weber M, Kodumudi Venkataraman L, Checchia S, et al. Revealing the sequence of switching mechanisms in polycrystalline ferroelectric/ferroelastic materials. Acta Mater 2018;157:355–63. https://doi.org/10.1016/j.actamat.2018.07.018.
[95] Daniels JE, Cozzan C, Ukritnukun S, Tutuncu G, Andrieux J, Glaum J, et al. Two-step polarization reversal in biased ferroelectrics. J Appl Phys 2014;115:224104. https://doi.org/10.1063/1.4881835.
[96] Genenko YA, Khachaturyan R, Schultheiß J, Ossipov A, Daniels JE, Koruza J. Stochastic multistep polarization switching in ferroelectrics. Phys Rev B 2018;97:144101. https://doi.org/10.1103/PhysRevB.97.144101.
[97] Meyer B, Vanderbilt D. Ab initio study of ferroelectric domain walls in $PbTiO_3$. Phys Rev B 2002;65:104111. https://doi.org/10.1103/PhysRevB.65.104111.
[98] Keve ET, Bye KL. Phase Identification and Domain-Structure in PLZT Ceramics. J Appl Phys 1975;46:810–8. https://doi.org/10.1063/1.321651.
[99] Hardiman B, Zeyfang R, Reeves C. Direct Observation of Ferroelectric Domains in Modified PZT Ceramics by Transmission Electron-Microscopy. J Appl Phys 1973;44:5266–7. https://doi.org/10.1063/1.1662141.
[100] Lucuta PG, Teodorescu V, Vasiliu F. SEM, SAED, and TEM Investigation of Domain-Structure in PZT Ceramics at Morphotropic Phase-Boundary. Appl Phys A: Mater Sci Process 1985;37:237–42. https://doi.org/10.1007/BF00614823.
[101] Wang ZY, Blendell JE, White GS, Jiang Q. Atomic force microscope observations of domains in fine-grained bulk lead zirconate titanate ceramics. Smart Mater Struct 2003;12:217–22. https://doi.org/10.1088/0964-1726/12/2/309.
[102] Zhu XH, Zhu JM, Zhou SH, Li Q, Meng ZY, Ming NB. Configurations of ferroelectric domains in bismuth- and zinc-modified $Pb(Ni_{1/3}Nb_{2/3})O_3$-$PbTiO_3$-$PbZrO_3$ ceramics. J Mater Sci 1999;34:1533–41. https://doi.org/10.1023/A:1004564213417.
[103] Gerthsen P, Krüger G. Coercive Field in Fine-Grained PLZT Ceramics. Ferroelectrics 1976;11:489–92. https://doi.org/10.1080/00150197608237783.
[104] Hall DA, Steuwer A, Cherdhirunkorn B, Mori T, Withers PJ. A high energy synchrotron x-ray study of crystallographic texture and lattice strain in soft lead zirconate titanate ceramics. J Appl Phys 2004;96:4245–52. https://doi.org/10.1063/1.1787590.
[105] Schultheiß J, Kungl H, Koruza J. Influence of crystallographic structure on polarization reversal in polycrystalline ferroelectric/ferroelastic materials. J Appl Phys 2019;125:174101. https://doi.org/10.1063/1.5081086.
[106] Schultheiß J, Roscow JI, Koruza J. Orienting anisometric pores in ferroelectrics: Piezoelectric property engineering through local electric field distributions. Phys Rev Mater 2019;3:084408. https://doi.org/10.1103/PhysRevMaterials.3.084408.
[107] Wersing W. Hystereseeigenschaften ferroelektrischer Keramiken. Ber Dtsch Keram Ges 1974;51:318–23.

[108] Arlt G. A model for switching and hysteresis in ferroelectric ceramics. Integr Ferroelectr 1997;16:229–36. https://doi.org/10.1080/10584589708013045.
[109] Arlt G. Switching and Dielectric Nonlinearity of Ferroelectric Ceramics. Ferroelectrics 1996;189:91–101. https://doi.org/10.1080/00150199608213409.
[110] Kinase W, Takahasi H. On the 180° Type Domain Wall of $BaTiO_3$ Crystal. J Phys Soc Jpn 1957;12:464–76. https://doi.org/10.1143/JPSJ.12.464.
[111] Kinase W, Okayama H, Yoshikawa A, Taguchi N. On the 90°-Type Domain Wall of $BaTiO_3$ Crystal. J Phys Soc Jpn 1970;28(Supplement):383–5. https://doi.org/10.1007/s42452-019-0304-z.
[112] Kubel F, Schmid H. Structure of a Ferroelectric and Ferroelastic Monodomain Crystal of the Perovskite $BiFeO_3$. Acta Crystallogr, Sect B 1990;46:698–702. https://doi.org/10.1107/S0108768190006887.
[113] Ng YS, McDonald AD. X-Ray-Diffraction Studies of Domain Alignments in Modified PZT. Ferroelectrics 1985;62:167–78. https://doi.org/10.1080/00150198508225990.
[114] Tadmor EB, Waghmare UV, Smith GS, Kaxiras E. Polarization switching in $PbTiO_3$: an ab initio finite element simulation. Acta Mater 2002;50:2989–3002. https://doi.org/10.1016/S1359-6454(02)00127-1.
[115] Liu QD, Huber JE. Creep in ferroelectrics due to unipolar electrical loading. J Eur Ceram Soc 2006;26:2799–806. https://doi.org/10.1016/j.jeurceramsoc.2005.07.051.
[116] Zhou DY, Kamlah M. Determination of room-temperature creep of soft lead zirconate titanate piezoceramics under static electric fields. J Appl Phys 2005;98:104107. https://doi.org/10.1063/1.2136207.
[117] Viola G, Chong KB, Guiu F, Reece MJ. Role of internal field and exhaustion in ferroelectric switching. J Appl Phys 2014;115:034106. https://doi.org/10.1063/1.4856235.
[118] Fett T, Thun G. Determination of room-temperature tensile creep of PZT. J Mater Sci Lett 1998;17:1929–31. https://doi.org/10.1063/1.2136207.
[119] Fatuzzo E. Theoretical Considerations on Switching Transient in Ferroelectrics. Phys Rev 1962;127:1999–2005. https://doi.org/10.1103/PhysRev.127.1999.
[120] Ishibashi Y, Takagi Y. Note on Ferroelectric Domain Switching. J Phys Soc Jpn 1971;31:506–10. https://doi.org/10.1143/JPSJ.31.506.
[121] Genenko YA, Wehner J, von Seggern H. Self-consistent model of polarization switching kinetics in disordered ferroelectrics. J Appl Phys 2013;114:084101. https://doi.org/10.1063/1.4818951.
[122] Zhukov S, Genenko YA, von Seggern H. Experimental and theoretical investigation on polarization reversal in unfatigued lead-zirconate-titanate ceramic. J Appl Phys 2010;108:014106. https://doi.org/10.1063/1.3380844.
[123] Khachaturyan R, Schultheiß J, Koruza J, Genenko YA. Stochastic model of dispersive multi-step polarization switching in ferroelectrics due to spatial electric field distribution. Appl Phys Lett 2019;114:222902. https://doi.org/10.1063/1.5099235.
[124] Redin RD, Marks GW, Antoniak CE. Symmetry Limitations to Polarization of Polycrystalline Ferroelectrics. J Appl Phys 1963;34:600–10. https://doi.org/10.1063/1.1729316.
[125] Lupascu DC, Fedosov S, Verdier C, Rödel J, von Seggern H. Stretched exponential relaxation in perovskite ferroelectrics after cyclic loading. J Appl Phys 2004;95:1386–90. https://doi.org/10.1063/1.1636528.
[126] Khachaturyan R, Genenko YA. Correlated polarization-switching kinetics in bulk polycrystalline ferroelectrics. II. Impact of crystalline phase symmetries. Phys Rev B 2018;98:134106. https://doi.org/10.1103/PhysRevB.98.134106.
[127] Khachaturyan R, Wehner J, Genenko YA. Correlated polarization-switching kinetics in bulk polycrystalline ferroelectrics: A self-consistent mesoscopic switching model. Phys Rev B 2017;96:054113. https://doi.org/10.1103/PhysRevB.96.054113.
[128] Zhukov S, Genenko YA, Acosta M, Humburg H, Jo W, Rödel J, et al. Polarization dynamics across the morphotropic phase boundary in $Ba(Zr_{0.2}Ti_{0.8})O_3$–x$(Ba_{0.7}Ca_{0.3})TiO_3$ ferroelectrics. Appl Phys Lett 2013;103:152904. https://doi.org/10.1063/1.4824730.
[129] Zhukov S, Kungl H, Genenko YA, von Seggern H. Statistical electric field and switching time distributions in PZT1Nb2Sr ceramics: Crystal- and microstructure effects. J Appl Phys 2014;115:014103. https://doi.org/10.1063/1.4860335.
[130] Zhukov S, Acosta M, Genenko YA, von Seggern H. Polarization dynamics variation across the temperature- and composition-driven phase transitions in the lead-free $Ba(Zr_{0.2}Ti_{0.8})O_3$-x$(Ba_{0.7}Ca_{0.3})TiO_3$ ferroelectrics. J Appl Phys 2015;118:134104. https://doi.org/10.1063/1.4932641.
[131] Zhukov S, Genenko YA, Koruza J, Schultheiß J, von Seggern H, Sakamoto W, et al. Effect of texturing on polarization switching dynamics in ferroelectric ceramics. Appl Phys Lett 2016;108:012907. https://doi.org/10.1063/1.4939684.
[132] Anton EM, García RE, Key TS, Blendell JE, Bowman KJ. Domain switching mechanisms in polycrystalline ferroelectrics with asymmetric hysteretic behavior. J Appl Phys 2009;105:024107. https://doi.org/10.1063/1.3068333.
[133] Khachaturyan R, Zhukov S, Schultheiß J, Galassi C, Reimuth C, Koruza J, et al. Polarization-switching dynamics in bulk ferroelectrics with isometric and oriented anisometric pores. J Phys D: Appl Phys 2017;50:045303. https://doi.org/10.1088/1361-6463/aa519c.
[134] Buessem WR, Cross LE, Goswami AK. Phenomenological Theory of High Permittivity in Fine-Grained Barium Titanate. J Am Ceram Soc 1966;49:33–6. https://doi.org/10.1111/j.1151-2916.1992.tb04362.x.
[135] Ivry Y, Chu DP, Scott JF, Durkan C. Domains Beyond the Grain Boundary. Adv Funct Mater 2011;21:1827–32. https://doi.org/10.1002/adfm.201002142.
[136] Ivry Y, Scott JF, Salje EKH, Durkan C. Nucleation, growth, and control of ferroelectric-ferroelastic domains in thin polycrystalline films. Phys Rev B 2012;86:205428. https://doi.org/10.1103/PhysRevB.86.205428.
[137] Wicks S, Seal K, Jesse S, Anbusathaiah V, Leach S, Garcia RE, et al. Collective dynamics in nanostructured polycrystalline ferroelectric thin films using local time-resolved measurements and switching spectroscopy. Acta Mater 2010;58:67–75. https://doi.org/10.1016/j.actamat.2009.08.057.
[138] Gruverman A, Kholkin A, Kingon A, Tokumoto H. Asymmetric nanoscale switching in ferroelectric thin films by scanning force microscopy. Appl Phys Lett 2001;78:2751–3. https://doi.org/10.1063/1.1366644.
[139] Wicks S, Anbusathiah V, Nagarajan V. Nanoscale domain switching behaviour in polycrystalline ferroelectric thin films. Nanotechnology 2007;18:465502. https://doi.org/10.1088/0957-4484/18/46/465502.
[140] Cao WW, Randall CA. Grain size and domain size relations in bulk ceramic ferroelectric materials. J Phys Chem Solids 1996;57:1499–505. https://doi.org/10.1016/0022-3697(96)00019-4.
[141] García RE, Huey BD, Blendell JE. Virtual piezoforce microscopy of polycrystalline ferroelectric films. J Appl Phys 2006;100:064105. https://doi.org/10.1063/1.2336073.
[142] Eshelby JD. The Determination of the Elastic Field of an Ellipsoidal Inclusion, and Related Problems. Proc R Soc London 1957;241:376–96. https://doi.org/10.1098/rspa.1957.0133.
[143] Daniel L, Hall D, Withers P. A multiscale modelling analysis of the contribution of crystalline elastic anisotropy to intergranular stresses in ferroelectric materials. J Phys D: Appl Phys 2014;47:325303. https://doi.org/10.1088/0022-3727/47/32/325303.
[144] Schultheiß J, Checchia S, Uršič H, Frömling T, Daniels J, Malič B, et al. Domain wall-grain boundary interactions and functionality of polycrystalline $Pb(Zr_{0.7}, Ti_{0.3})O_3$ ceramics. J Eur Ceram Soc 2020;40:3965–73. https://doi.org/10.1016/j.jeurceramsoc.2020.03.054.
[145] Gruverman A, Auciello O, Tokumoto H. Nanoscale investigation of fatigue effects in $Pb(Zr,Ti)O_3$ films. Appl Phys Lett 1996;69:3191–3. https://doi.org/10.1063/1.117957.
[146] Marincel DM, Zhang HR, Jesse S, Belianinov A, Okatan MB, Kalinin SV, et al. Domain Wall Motion Across Various Grain Boundaries in Ferroelectric Thin Films. J Am Ceram Soc 2015;98:1848–57. https://doi.org/10.1111/jace.13535.
[147] Coufova P, Arend H. On the relation between the thickness dependence of optical absorption and the surface layers of barium titanate single crystals. Cechoslovackij Fiziceskij Z B 1960;10:663–9. https://doi.org/10.1007/BF01604266.
[148] Hossain MJ, Wang ZY, Khansur NH, Kimpton JA, Oddershede J, Daniels JE. The effect of inter-granular constraints on the response of polycrystalline piezoelectric ceramics at the surface and in the bulk. Appl Phys Lett 2016;109:092905. https://doi.org/10.1063/1.4962125.
[149] Xu G, Gehring PM, Stock C, Conlon K. The anomalous skin effect in single crystal relaxor ferroelectric PZN-xPT and PMN-xPT. Phase Transit 2006;79:135–52. https://doi.org/10.1080/02652030600558682.
[150] Kong S, Kumar N, Checchia S, Cazorla C, Daniels J. Defect-Driven Structural Distortions at the Surface of Relaxor Ferroelectrics. Adv Funct Mater 2019;29:1900344. https://doi.org/10.1002/adfm.201900344.

[151] Shishkina E, Chuvakova M, Yuzhakov V, Akhmatkhanov A, Pelegova E, Nebogatikov M, et al. Domain structure evolution during polarization reversal in calcium orthovanadate single crystals. J Appl Phys 2022;132:184101. https://doi.org/10.1063/5.0120792.
[152] Potnis PR, Tsou N-T, Huber JE. A review of domain modelling and domain imaging techniques in ferroelectric crystals. Materials 2011;4:417–47. https://doi.org/10.3390/ma4020417.
[153] Hunnestad K, Roede ED, van Helvoort AT, Meier D. Characterization of ferroelectric domain walls by scanning electron microscopy. J Appl Phys 2020;128:191102. https://doi.org/10.1063/5.0029284.
[154] Ikeda S, Uchikawa Y. SEM imaging of ferroelectric domains. Microscopy 1980;29:209–17. https://doi.org/10.1093/oxfordjournals.jmicro.a050236.
[155] Gruverman A, Wu D, Scott J. Piezoresponse force microscopy studies of switching behavior of ferroelectric capacitors on a 100-ns time scale. Phys Rev Lett 2008;100:097601. https://doi.org/10.1103/PhysRevLett.100.097601.
[156] Jesse S, Baddorf AP, Kalinin SV. Switching spectroscopy piezoresponse force microscopy of ferroelectric materials. Appl Phys Lett 2006;88:062908. https://doi.org/10.1063/1.2172216.
[157] Soergel E. Piezoresponse force microscopy (PFM). J Phys D Appl Phys 2011;44:464003. https://doi.org/10.1088/0022-3727/44/46/464003.
[158] Gruverman A, Alexe M, Meier D. Piezoresponse force microscopy and nanoferroic phenomena. Nat Commun 2019;10:1661. https://doi.org/10.1038/s41467-019-09650-8.
[159] Kalinin SV, Rar A, Jesse S. A decade of piezoresponse force microscopy: progress, challenges, and opportunities. IEEE T Ultrason Ferr 2006;53:2226–52. https://doi.org/10.1109/TUFFC.2006.169.
[160] Schultheiß J, Rojac T, Meier D. Unveiling Alternating Current Electronic Properties at Ferroelectric Domain Walls. Adv Electron Mater 2022;8:2100996. https://doi.org/10.1002/aelm.202100996.
[161] Song J, Zhou Y, Huey BD. 3D structure–property correlations of electronic and energy materials by tomographic atomic force microscopy. Appl Phys Lett 2021;118:080501. https://doi.org/10.1063/5.0040984.
[162] Li L, Xie L, Pan X. Real-time studies of ferroelectric domain switching: a review. Rep Prog Phys 2019;82:126502. https://doi.org/10.1088/1361-6633/ab28de.
[163] Schaab J, Trassin M, Scholl A, Doran A, Yan Z, Bourret E, et al. Ferroelectric domains in the multiferroic phase of $ErMnO_3$ imaged by low-temperature photoemission electron microscopy. J Phys Conf Ser: IOP Publishing 2015;592:012120. https://doi.org/10.1088/1742-6596/592/1/012120.
[164] Nataf G, Grysan P, Guennou M, Kreisel J, Martinotti D, Rountree C, et al. Low energy electron imaging of domains and domain walls in magnesium-doped lithium niobate. Sci Rep 2016;6:1–9. https://doi.org/10.1038/srep33098.
[165] Berth G, Hahn W, Wiedemeier V, Zrenner A, Sanna S, Schmidt WG. Imaging of the ferroelectric domain structures by confocal Raman spectroscopy. Ferroelectrics 2011;420:44–8. https://doi.org/10.1080/00150193.2011.594774.
[166] Hruszkewycz S, Highland M, Holt M, Kim D, Folkman C, Thompson C, et al. Imaging local polarization in ferroelectric thin films by coherent x-ray Bragg projection ptychography. Phys Rev Lett 2013;110:177601. https://doi.org/10.1103/PhysRevLett.110.177601.
[167] Shi X, Shi J, Fohtung E. Applicability of coherent x-ray diffractive imaging to ferroelectric, ferromagnetic, and phase change materials. J Appl Phys 2022;131:040901. https://doi.org/10.1063/5.0072399.
[168] Marçal LA, Oksenberg E, Dzhigaev D, Hammarberg S, Rothman A, Björling A, et al. In situ imaging of ferroelastic domain dynamics in $CsPbBr_3$ perovskite nanowires by nanofocused scanning X-ray diffraction. ACS Nano 2020;14:15973–82. https://doi.org/10.1021/acsnano.0c07426.
[169] Poulsen HF, Nielsen SF, Lauridsen EM, Schmidt S, Suter R, Lienert U, et al. Three-dimensional maps of grain boundaries and the stress state of individual grains in polycrystals and powders. J Appl Crystallogr 2001;34:751–6. https://doi.org/10.1107/S0021889801014273.
[170] Schmidt S, Nielsen SF, Gundlach C, Margulies L, Huang X, Jensen DJ. Watching the growth of bulk grains during recrystallization of deformed metals. Science 2004;305:229–32. https://doi.org/10.1126/science.1098627.
[171] King A, Johnson G, Engelberg D, Ludwig W, Marrow J. Observations of intergranular stress corrosion cracking in a grain-mapped polycrystal. Science 2008;321:382–5. https://doi.org/10.1126/science.1156211.
[172] Ludwig W, Reischig P, King A, Herbig M, Lauridsen E, Johnson G, et al. Three-dimensional grain mapping by x-ray diffraction contrast tomography and the use of Friedel pairs in diffraction data analysis. Rev Sci Instrum 2009;80:033905. https://doi.org/10.1063/1.3100200.
[173] Majkut M, Daniels JE, Wright JP, Schmidt S, Oddershede J. Electromechanical response of polycrystalline barium titanate resolved at the grain scale. J Am Ceram Soc 2017;100:393–402. https://doi.org/10.1111/jace.14481.
[174] Daniels JE, Majkut M, Cao QG, Schmidt S, Wright J, Jo W, et al. Heterogeneous grain-scale response in ferroic polycrystals under electric field. Sci Rep 2016;6:22820. https://doi.org/10.1038/srep22820.
[175] Cereser A, Strobl M, Hall SA, Steuwer A, Kiyanagi R, Tremsin AS, et al. Time-of-Flight three dimensional neutron diffraction in transmission mode for mapping crystal grain structures. Sci Rep 2017;7:9561. https://doi.org/10.1038/s41598-017-09717-w.
[176] Simons H, King A, Ludwig W, Detlefs C, Pantleon W, Schmidt S, et al. Dark-field X-ray microscopy for multiscale structural characterization. Nat Commun 2015;6:6098. https://doi.org/10.1038/ncomms7098.
[177] Simons H, Jakobsen AC, Ahl SR, Detlefs C, Poulsen HF. Multiscale 3D characterization with dark-field x-ray microscopy. MRS Bull 2016;41:454–9. https://doi.org/10.1557/mrs.2016.114.
[178] Simons H, Haugen AB, Jakobsen AC, Schmidt S, Stöhr F, Majkut M, et al. Long-range symmetry breaking in embedded ferroelectrics. Nat Mater 2018;17:814–9. https://doi.org/10.1038/s41563-018-0116-3.
[179] Schultheiß J, Porz L, Venkataraman LK, Höfling M, Yildirim C, Cook P, et al. Quantitative mapping of nanotwin variants in the bulk. Scr Mater 2021;199:113878. https://doi.org/10.1016/j.scriptamat.2021.113878.
[180] Poulsen HF. Multi scale hard x-ray microscopy. Curr Opin Solid State Mater Sci 2020;24:100820. https://doi.org/10.1016/j.cossms.2020.100820.
[181] Yildirim C, Cook P, Detlefs C, Simons H, Poulsen HF. Probing nanoscale structure and strain by dark-field x-ray microscopy. MRS Bull 2020;45:277–82. https://doi.org/10.1557/mrs.2020.89.
[182] Arlt G. Twinning in Ferroelectric and Ferroelastic Ceramics - Stress Relief. J Mater Sci 1990;25:2655–66. https://doi.org/10.1007/BF00584864.
[183] Rödel J, Li J-F. Lead-free piezoceramics: Status and perspectives. MRS Bull 2018;43:576–80. https://doi.org/10.1557/mrs.2018.181.
[184] Schultheiß J, Xue F, Roede E, Ånes HW, Danmo FH, Selbach SM, et al. Confinement-driven inverse domain scaling in polycrystalline $ErMnO_3$. Adv Mater 2022;34:2203449. https://doi.org/10.1002/adma.202203449.
[185] Foeth M, Sfera A, Stadelmann P, Buffat P-A. A comparison of HREM and weak beam transmission electron microscopy for the quantitative measurement of the thickness of ferroelectric domain walls. Microscopy 1999;48:717–23. https://doi.org/10.1093/oxfordjournals.jmicro.a023740.
[186] Jaffe B. Piezoelectric ceramics. Elsevier 1971.
[187] Li FX, Li YW. Modeling on domain switching in ferroelectric ceramics near the morphotropic phase boundary. J Appl Phys 2009;105:124105. https://doi.org/10.1063/1.3153282.
[188] Ryo H-S, Ryo I-G. Analytical calculation of saturated polarization and equilibrium composition near tetragonal-rhombohedral morphotropic phase boundary of polycrystalline ferroelectrics. J Electroceram 2017;38:92–9. https://doi.org/10.1007/s10832-017-0066-1.
[189] Uchida N, Ikeda T. Electrostriction in Perovskite-Type Ferroelectric Ceramics. Jpn J Appl Phys 1967;6:1079–88. https://doi.org/10.1143/JJAP.6.1079.
[190] Mesnard G, Eyraud L. Sur les cycles d'hystérésis des céramiques au titanate de baryum. J Phys Appl 1956;17:78–80. https://doi.org/10.1051/jphysap:0195600170607800.
[191] Baerwald HG. Thermodynamic Theory of Ferroelectric Ceramics. Phys Rev 1957;105:480–6. https://doi.org/10.1103/PhysRev.105.480.
[192] Isupov V. Calculation of orientational dielectric polarization of ferroelectric ceramics with different types of crystal structure. Izv Akad Nauk, Ser Fiz 1967;31:1836–40.
[193] Smolenskii G, Isupov V, Ktitorov S, Trepakov V, Yushin N. The state of ferroelectric physics. Phys Solid State 1979;22:3–30. https://doi.org/10.1007/BF00890540.
[194] Li YW, Zhou XL, Miao HC, Cai HR, Li FX. Mechanism of crystal-symmetry dependent deformation in ferroelectric ceramics: Experiments versus model. J Appl Phys 2013;113:214111. https://doi.org/10.1063/1.4809979.

[195] Tang W, Fang DN, Li JY. Two-scale micromechanics-based probabilistic modeling of domain switching in ferroelectric ceramics. J Mech Phys Solids 2009;57:1683–701. https://doi.org/10.1016/j.jmps.2009.07.004.
[196] Feronov A, Kuleshov V, Dudkevich V, Fesenko E. Properties of a dense chemically pure $PbTiO_3$ ceramic. SPTP 1980;25:621–3.
[197] Shirane G, Hoshino S. On the Phase Transition in Lead Titanate. J Phys Soc Jpn 1951;6:265–70. https://doi.org/10.1143/JPSJ.6.265.
[198] Carl K. Ferroelectric Properties and Fatiguing Effects of Modified $PbTiO_3$ Ceramics. Ferroelectrics 1975;9:23–32. https://doi.org/10.1080/00150197508240077.
[199] Fontana M, Abdi F, Wojcik K. Electro-optical properties of a single domain $PbTiO_3$ crystal. J Appl Phys 1995;77:2102–6. https://doi.org/10.1063/1.358853.
[200] Gavrilyachenko VG, Spinko RI, Martynen.Ma, Fesenko EG.. Spontaneous Polarization and Coercive Field of Lead Titanate. Fiz Tverd Tela+ 1970;12:1203–8.
[201] Haun MJ, Furman E, Jang SJ, Mckinstry HA, Cross LE. Thermodynamic Theory of $PbTiO_3$. J Appl Phys 1987;62:3331–8. https://doi.org/10.1063/1.339293.
[202] Daniels JE, Jones JL, Finlayson TR. Characterization of domain structures from diffraction profiles in tetragonal ferroelastic ceramics. J Phys D Appl Phys 2006;39:5294–9. https://doi.org/10.1088/0022-3727/39/24/029.
[203] Floquet N, Valot CM, Mesnier MT, Niepce JC, Normand L, Thorel A, et al. Ferroelectric domain walls in $BaTiO_3$: Fingerprints in XRPD diagrams and quantitative HRTEM image analysis. J Phys 1997;III(7):1105–28. https://doi.org/10.1051/jp3:1997180.
[204] Floquet N, Valot C. Ferroelectric domain walls in $BaTiO_3$: Structural wall model interpreting fingerprints in XRPD diagrams. Ferroelectrics 1999;234:107–22. https://doi.org/10.1080/00150199908225285.
[205] Stemmer S, Streiffer SK, Ernst F, Ruhle M. Atomistic Structure of 90° Domain-Walls in Ferroelectric $PbTiO_3$ Thin-Films. Philos Mag A 1995;71:713–24. https://doi.org/10.1080/01418619508244477.
[206] Hamazaki SI, Shimizu F, Kojima S, Takashige M. AFM Observation of 90° Domains of $BaTiO_3$ Butterfly Crystals. J Phys Soc Jpn 1995;64:3660–3. https://doi.org/10.1143/JPSJ.64.3660.
[207] Takashige M, Hamazaki SI, Fukurai N, Shimizu F, Kojima S. Atomic force microscope observation of ferroelectrics: Barium titanate and Rochelle salt. Jpn J Appl Phys 1996;1(35):5181–4. https://doi.org/10.1143/JJAP.35.5181.
[208] Balakumar S, Xu JB, Ma JX, Ganesamoorthy S, Wilson IH. Surface morphology of ferroelectric domains in $BaTiO_3$ single crystals: An atomic force microscope study. Jpn J Appl Phys 1997;1(36):5566–9. https://doi.org/10.1143/JJAP.36.5566.
[209] Wang YG, Dec J, Kleemann W. Study on surface and domain structures of $PbTiO_3$ crystals by atomic force microscopy. J Appl Phys 1998;84:6795–9. https://doi.org/10.1063/1.369011.
[210] Takashige M, Hamazaki S, Fukurai N, Shimizu F. Surface morphology of tetragonal $PbTiO_3$ and $BaTiO_3$ observed by atomic force microscopy. J Phys Soc Jpn 1997;66:1848–9. https://doi.org/10.1143/JPSJ.66.1848.
[211] Arlt G, Sasko P. Domain Configuration and Equilibrium Size of Domains in $BaTiO_3$ Ceramics. J Appl Phys 1980;51:4956–60. https://doi.org/10.1063/1.328372.
[212] Pertsev N, Arlt G. Theory of the banded domain structure in coarse-grained ferroelectric ceramics. Ferroelectrics 1992;132:27–40. https://doi.org/10.1080/00150199208009068.
[213] Hennings D. Barium titanate based ceramic materials for dielectric use. Int J High Technol Ceram 1987;3:91–111. https://doi.org/10.1016/0267-3762(87)90031-2.
[214] Arlt G, Dederichs H. Complex Elastic, Dielectric and Piezoelectric Constants by Domain-Wall Damping in Ferroelectric Ceramics. Ferroelectrics 1980;29:47–50. https://doi.org/10.1080/00150198008009006.
[215] Arlt G, Pertsev NA. Force-Constant and Effective Mass of 90° Domain-Walls in Ferroelectric Ceramics. J Appl Phys 1991;70:2283–9. https://doi.org/10.1063/1.349421.
[216] Farooq MU, Villaurrutia R, MacLaren I, Burnett TL, Comyn TP, Bell AJ, et al. Electron backscatter diffraction mapping of herringbone domain structures in tetragonal piezoelectrics. J Appl Phys 2008;104:024111. https://doi.org/10.1063/1.2956704.
[217] MacLaren I, Schmitt LA, Fuess H, Kungl H, Hoffmann MJ. Experimental measurement of stress at a four-domain junction in lead zirconate titanate. J Appl Phys 2005;97:094102. https://doi.org/10.1063/1.1886910.
[218] Zimmermann A, Fuller ER, Rödel J. Residual stress distributions in ceramics. J Am Ceram Soc 1999;82:3155–60. https://doi.org/10.1111/j.1151-2916.1999.tb02217.x.
[219] Vedula VR, Glass SJ, Saylor DM, Rohrer GS, Carter WC, Langer SA, et al. Residual-stress predictions in polycrystalline alumina. J Am Ceram Soc 2001;84:2947–54. https://doi.org/10.1111/j.1151-2916.2001.tb01119.x.
[220] Chung HT, Kim HG. Characteristics of Domain in Tetragonal Phase PZT Ceramics. Ferroelectrics 1987;76:327–33. https://doi.org/10.1080/00150198708016953.
[221] Tomczyk M, Senos AM, Vilarinho PM, Reaney IM. Origin of microcracking in $YMnO_3$ ceramics. Scr Mater 2012;66:288–91. https://doi.org/10.1016/j.scriptamat.2011.11.014.
[222] Rice RW, Pohanka RC. Grain-Size Dependence of Spontaneous Cracking in Ceramics. J Am Ceram Soc 1979;62:559–63. https://doi.org/10.1111/j.1151-2916.1979.tb12730.x.
[223] Yamamoto T, Igarashi H, Okazaki K. Dielectric, Electromechanical, Optical, and Mechanical-Properties of Lanthanum-Modified Lead Titanate Ceramics. J Am Ceram Soc 1983;66:363–6. https://doi.org/10.1111/j.1151-2916.1983.tb10050.x.
[224] Choi SK, Kim SR, Choi DG. Effect of tetragonality ratio on photo-induced domain switching in poled $(Pb_{1-x}La_x)TiO_3$ ferroelectric ceramics. J Mater Sci: Mater Electron 2000;11:603–7. https://doi.org/10.1023/A:1008976628303.
[225] King G, Goo EK. Effect of the c/a Ratio on the Domain-Structure in $(Pb_{1-x},Ca_x)TiO_3$. J Am Ceram Soc 1990;73:1534–9. https://doi.org/10.1111/j.1151-2916.1990.tb09792.x.
[226] Choi DG, Choi SK. Dynamic behaviour of domains during poling by acoustic emission measurements in La-modified $PbTiO_3$ ferroelectric ceramics. J Mater Sci 1997;32:421–5. https://doi.org/10.1023/A:1018513718921.
[227] Chen XF, Dong XL, Zhang HL, Cao F, Wang GS, Gu Y, et al. Frequency Dependence of Coercive Field in Soft $Pb(Zr_{1-x}Ti_x)O_3$ ($0.20<x<0.60$) Bulk Ceramics. J Am Ceram Soc 2011;94:4165–8. https://doi.org/10.1111/j.1551-2916.2011.04913.x.
[228] Kungl H, Hoffmann MJ. Effects of sintering temperature on microstructure and high field strain of niobium-strontium doped morphotropic lead zirconate titanate. J Appl Phys 2010;107:054111. https://doi.org/10.1063/1.3294648.
[229] Haertling G, Zimmer W. An Analysis of Hot-Pressing Parameters for Lead Zirconate-Lead Titanate Ceramics containing 2 Atom Percent Bismuth. Am Ceram Soc Bull 1966;45:1084–9.
[230] Chen XF, Dong XL, Cao F, Wang JX, Wang GS. Field and Frequency Dependence of the Dynamic Hysteresis in Lead Zirconate Titanate Solid Solutions. J Am Ceram Soc 2014;97:213–9. https://doi.org/10.1111/jace.12609.
[231] Seo YH, Franzbach DJ, Koruza J, Benčan A, Malič B, Kosec M, et al. Nonlinear stress-strain behavior and stress-induced phase transitions in soft $Pb(Zr_{1-x}Ti_x)O_3$ at the morphotropic phase boundary. Phys Rev B 2013;87:094116. https://doi.org/10.1103/PhysRevB.87.094116.
[232] Schmidt NA. Coercive Force and 90° Domain-Wall Motion in Ferroelectric PLZT Ceramics with Square Hysteresis Loops. Ferroelectrics 1981;31:105–11. https://doi.org/10.1080/00150198108201980.
[233] Yoshii K, Hiruma Y, Nagata H, Takenaka T. Electrical properties and depolarization temperature of $(Bi_{1/2}Na_{1/2})TiO_3$-$(Bi_{1/2}K_{1/2})TiO_3$ lead-free piezoelectric ceramics. Jpn J Appl Phys 2006;45:4493. https://doi.org/10.1143/JJAP.45.4493.
[234] Xu C, Lin D, Kwok K. Structure, electrical properties and depolarization temperature of $(Bi_{0.5}Na_{0.5})TiO_3$–$BaTiO_3$ lead-free piezoelectric ceramics. Solid State Sci 2008;10:934–40. https://doi.org/10.1016/j.solidstatesciences.2007.11.003.
[235] Chen M, Xu Q, Kim BH, Ahn BK, Ko JH, Kang WJ, et al. Structure and electrical properties of $(Na_{0.5}Bi_{0.5})_{1-x}Ba_xTiO_3$ piezoelectric ceramics. J Eur Ceram Soc 2008;28:843–9. https://doi.org/10.1016/j.jeurceramsoc.2007.08.007.
[236] Bai W, Chen D, Zheng P, Shen B, Zhai J, Ji Z. Composition-and temperature-driven phase transition characteristics and associated electromechanical properties in $Bi_{0.5}Na_{0.5}TiO_3$-based lead-free ceramics. Dalton Trans 2016;45:8573–86. https://doi.org/10.1039/C6DT00906A.

[237] Li P, Zhai J, Shen B, Zhang S, Li X, Zhu F, et al. Ultrahigh piezoelectric properties in textured (K, Na)NbO_3-based lead-free ceramics. Adv Mater 2018;30:1705171. https://doi.org/10.1002/adma.201705171.

[238] Lin J, Cao Y, Zhu K, Yan F, Shi C, Bai H, et al. Ultrahigh energy harvesting properties in temperature-insensitive eco-friendly high-performance KNN-based textured ceramics. J Mater Chem A 2022;10:7978–88. https://doi.org/10.1039/D2TA00203E.

[239] Zakhozheva M, Schmitt LA, Acosta M, Guo H, Jo W, Schierholz R, et al. Wide Compositional Range In Situ Electric Field Investigations on Lead-Free Ba$(Zr_{0.2}Ti_{0.8})O_3$–$x(Ba_{0.7}Ca_{0.3})TiO_3$ Piezoceramic. Phys Rev Appl 2015;3:064018. https://doi.org/10.1103/PhysRevApplied.3.064018.

[240] Damjanovic D, Demartin M. Contribution of the irreversible displacement of domain walls to the piezoelectric effect in barium titanate and lead zirconate titanate ceramics. J Phys: Condens Matter 1997;9:4943–53. https://doi.org/10.1088/0953-8984/9/23/018.

[241] Garcia JE, Perez R, Ochoa DA, Albareda A, Lente MH, Eiras JA. Evaluation of domain wall motion in lead zirconate titanate ceramics by nonlinear response measurements. J Appl Phys 2008;103:054108. https://doi.org/10.1063/1.2894595.

[242] Schaufele AB, Hardtl KH. Ferroelastic properties of lead zirconate titanate ceramics. J Am Ceram Soc 1996;79:2637–40. https://doi.org/10.1111/j.1151-2916.1996.tb09027.x.

[243] Gerber P, Böttger U, Waser R. Composition influences on the electrical and electromechanical properties of lead zirconate titanate thin films. J Appl Phys 2006;100:124105. https://doi.org/10.1063/1.2401047.

[244] Kungl H, Theissmann R, Knapp M, Baehtz C, Fuess H, Wagner S, et al. Estimation of strain from piezoelectric effect and domain switching in morphotropic PZT by combined analysis of macroscopic strain measurements and synchrotron X-ray data. Acta Mater 2007;55:1849–61. https://doi.org/10.1016/j.actamat.2006.10.046.

[245] Schönau KA, Knapp M, Kungl H, Hoffmann MJ, Fuess H. In situ synchrotron diffraction investigation of morphotropic Pb$[Zr_{1-x}Ti_x]O_3$ under an applied electric field. Phys Rev B 2007;76:144112. https://doi.org/10.1103/PhysRevB.76.144112.

[246] Hinterstein M, Schoenau KA, Kling J, Fuess H, Knapp M, Kungl H, et al. Influence of lanthanum doping on the morphotropic phase boundary of lead zirconate titanate. J Appl Phys 2010;108:024110. https://doi.org/10.1063/1.3437399.

[247] Genenko YA, Khachaturyan R, Vorotiahin IS, Schultheiß J, Daniels JE, Grünebohm A, et al. Multistep stochastic mechanism of polarization reversal in rhombohedral ferroelectrics. Phys Rev B 2020;102:064107. https://doi.org/10.1103/PhysRevB.102.064107.

[248] Hall DA, Steuwer A, Cherdhirunkorn B, Withers PJ, Mori T. Texture of poled tetragonal PZT detected by synchrotron X-ray diffraction and micromechanics analysis. Mater Sci Eng, A 2005;409:206–10. https://doi.org/10.1016/j.msea.2005.05.115.

[249] Saito Y. Hysteresis curve of X-ray diffraction peak intensity in lead zirconate titanate ceramics. Jpn J Appl Phys, Part 1997;1(36):5963–9. https://doi.org/10.1143/JJAP.36.5963.

[250] Hall DA, Steuwer A, Cherdhirunkorn B, Withers PJ, Mori T. Micromechanics of domain switching in rhombohedral PZT ceramics. Ceram Int 2008;34:679–83. https://doi.org/10.1016/j.ceramint.2007.09.001.

[251] Li FX, Zhou XL, Soh AK. An optimization-based "phase field" model for polycrystalline ferroelectrics. Appl Phys Lett 2010;96:152905. https://doi.org/10.1063/1.3377899.

[252] Hoffmann MJ, Kungl H. High strain lead-based perovskite ferroelectrics. Curr Opin Solid State Mater Sci 2004;8:51–7. https://doi.org/10.1016/j.cossms.2003.12.003.

[253] Leist T, Granzow T, Jo W, Rödel J. Effect of tetragonal distortion on ferroelectric domain switching: A case study on La-doped $BiFeO_3$-$PbTiO_3$ ceramics. J Appl Phys 2010;108:014103. https://doi.org/10.1063/1.3445771.

[254] Leist T, Webber KG, Jo W, Granzow T, Aulbach E, Suffner J, et al. Domain switching energies: Mechanical versus electrical loading in La-doped bismuth ferrite-lead titanate. J Appl Phys 2011;109:054109. https://doi.org/10.1063/1.3555599.

[255] Leist T, Webber KG, Jo W, Aulbach E, Rödel J, Prewitt AD, et al. Stress-induced structural changes in La-doped $BiFeO_3$-$PbTiO_3$ high-temperature piezoceramics. Acta Mater 2010;58:5962–71. https://doi.org/10.1016/j.actamat.2010.07.012.

[256] Tutuncu G, Li BZ, Bowman K, Jones JL. Domain wall motion and electromechanical strain in lead-free piezoelectrics: Insight from the model system (1–x)Ba$(Zr_{0.2}Ti_{0.8})O_3$–x$(Ba_{0.7}Ca_{0.3})TiO_3$ using in situ high-energy X-ray diffraction during application of electric fields. J Appl Phys 2014;115:144104. https://doi.org/10.1063/1.4870934.

[257] Zhang MH, Liu YX, Wang K, Koruza J, Schultheiß J. Origin of High Electromechanical Properties in KNN-Based Lead-Free Piezoelectrics Modified with $BaZrO_3$. Phys Rev Mater 2020:064407. https://doi.org/10.1103/PhysRevMaterials.4.064407.

[258] Seo YH, Vögler M, Isaia D, Aulbach E, Rödel J, Webber KG. Temperature-dependent R-curve behavior of Pb$(Zr_{1-x}Ti_x)O_3$. Acta Mater 2013;61:6418–27. https://doi.org/10.1016/j.actamat.2013.07.020.

[259] Vögler M, Acosta M, Brandt DRJ, Molina-Luna L, Webber KG. Temperature-dependent R-curve behavior of the lead-free ferroelectric 0.615Ba$(Zr_{0.2}Ti_{0.8})O_3$–0.385$(Ba_{0.7}Ca_{0.3})TiO_3$ ceramic. Eng Fract Mech 2015;144:68–77. https://doi.org/10.1016/j.engfracmech.2015.06.069.

[260] Li Y, Liu Y, Öchsner P-E, Isaia D, Zhang Y, Wang K, et al. Temperature dependent fracture toughness of KNN-based lead-free piezoelectric ceramics. Acta Mater 2019;174:369–78. https://doi.org/10.1016/j.actamat.2019.05.060.

[261] Glazounov AE, Kungl H, Reszat JT, Hoffmann MJ, Kolleck A, Schneider GA, et al. Contribution from Ferroelastic Domain Switching Detected Using X-ray Diffraction to R-Curves in Lead Zirconate Titanate Ceramics. J Am Ceram Soc 2001;84:2921–9. https://doi.org/10.1111/j.1151-2916.2001.tb01116.x.

[262] Uchino K, Zheng JH, Joshi A, Chen YH, Yoshikawa S, Hirose S, et al. High power characterization of piezoelectric materials. J Electroceram 1998;2:33–40. https://doi.org/10.1023/A:1009962925948.

[263] Arlt G. The Influence of Microstructure on the Properties of Ferroelectric Ceramics. Ferroelectrics 1990;104:217–27. https://doi.org/10.1080/00150199008223825.

[264] Meier W, Meyer KE, Sava Gallis DF, Blea-Kirby MA, Roth J, Felman D, et al. Highly Textured $BaTiO_3$ via Templated Grain Growth and Resulting Polarization Reversal Dynamics. J Am Ceram Soc 2016;99:922–9. https://doi.org/10.1111/jace.14048.

[265] Höfling M, Zhou X, Riemer LM, Bruder E, Liu B, Zhou L, et al. Control of polarization in bulk ferroelectrics by mechanical dislocation imprint. Science 2021;372:961–4. https://doi.org/10.1126/science.abe3810.

[266] Ghayour H, Abdellahi M. A brief review of the effect of grain size variation on the electrical properties of $BaTiO_3$-based ceramics. Powder Technol 2016;292:84–93. https://doi.org/10.1016/j.powtec.2016.01.030.

[267] Buscaglia V, Randall CA. Size and scaling effects in barium titanate. An overview. J Eur Ceram Soc 2020;40:3744–58. https://doi.org/10.1016/j.jeurceramsoc.2020.01.021.

[268] Ihlefeld JF, Harris DT, Keech R, Jones JL, Maria JP, Trolier-McKinstry S. Scaling Effects in Perovskite Ferroelectrics: Fundamental Limits and Process-Structure-Property Relations. J Am Ceram Soc 2016;99:2537–57. https://doi.org/10.1111/jace.14387.

[269] Hoshina T. Size effect of barium titanate: fine particles and ceramics. J Ceram Soc Jpn 2013;121:156–61. https://doi.org/10.2109/jcersj2.121.156.

[270] Moriana AD, Zhang SJ. Lead-free textured piezoceramics using tape casting: A review. J Materiomics 2018;4:277–303. https://doi.org/10.1016/j.jmat.2018.09.006.

[271] Messing GL, Trolier-McKinstry S, Sabolsky EM, Duran C, Kwon S, Brahmaroutu B, et al. Templated grain growth of textured piezoelectric ceramics. Crit Rev Solid State Mater Sci 2004;29:45–96. https://doi.org/10.1080/10408430490490905.

[272] Messing GL, Poterala S, Chang YF, Frueh T, Kupp ER, Watson BH, et al. Texture-engineered ceramics-Property enhancements through crystallographic tailoring. J Mater Res 2017;32:3219–41. https://doi.org/10.1557/jmr.2017.207.

[273] Kinoshita K, Yamaji A. Grain-Size Effects on Dielectric Properties in Barium-Titanate Ceramics. J Appl Phys 1976;47:371–3. https://doi.org/10.1063/1.322330.

[274] Arlt G, Hennings D, Dewith G. Dielectric-Properties of Fine-Grained Barium-Titanate Ceramics. J Appl Phys 1985;58:1619–25. https://doi.org/10.1063/1.336051.

[275] Frey MH, Xu Z, Han P, Payne DA. The role of interfaces on an apparent grain size effect on the dielectric properties for ferroelectric barium titanate ceramics. Ferroelectrics 1998;206:337–53. https://doi.org/10.1080/00150199808009168.

[276] Zheng P, Zhang JL, Tan YQ, Wang CL. Grain-size effects on dielectric and piezoelectric properties of poled $BaTiO_3$ ceramics. Acta Mater 2012;60:5022–30. https://doi.org/10.1016/j.actamat.2012.06.015.

[277] Huan Y, Wang XH, Fang J, Li LT. Grain Size Effects on Piezoelectric Properties and Domain Structure of $BaTiO_3$ Ceramics Prepared by Two-Step Sintering. J Am Ceram Soc 2013;96:3369–71. https://doi.org/10.1111/jace.12601.

[278] Huan Y, Wang XH, Fang J, Li LT. Grain size effect on piezoelectric and ferroelectric properties of $BaTiO_3$ ceramics. J Eur Ceram Soc 2014;34:1445–8. https://doi.org/10.1016/j.jeurceramsoc.2013.11.030.

[279] Tan YQ, Zhang JL, Wu YQ, Wang CL, Koval V, Shi BG, et al. Unfolding grain size effects in barium titanate ferroelectric ceramics. Sci Rep 2015;5:9953. https://doi.org/10.1038/srep09953.

[280] Ghosh D, Sakata A, Carter J, Thomas PA, Han H, Nino JC, et al. Domain Wall Displacement is the Origin of Superior Permittivity and Piezoelectricity in $BaTiO_3$ at Intermediate Grain Sizes. Adv Funct Mater 2014;24:885–96. https://doi.org/10.1002/adfm.201301913.

[281] Hoshina T, Takizawa K, Li JY, Kasama T, Kakemoto H, Tsurumi T. Domain size effect on dielectric properties of barium titanate ceramics. Jpn J Appl Phys 2008;47:7607–11. https://doi.org/10.1143/JJAP.47.7607.

[282] Choi Y-K, Hoshina T, Takeda H, Teranishi T, Tsurumi T. Effects of oxygen vacancies and grain sizes on the dielectric response of $BaTiO_3$. Appl Phys Lett 2010;97:212907. https://doi.org/10.1063/1.3508947.

[283] Dai BW, Zheng P, Bai WF, Wen F, Li LL, Wu W, et al. Direct and converse piezoelectric grain-size effects in $BaTiO_3$ ceramics with different Ba/Ti ratios. J Eur Ceram Soc 2018;38:4212–9. https://doi.org/10.1016/j.jeurceramsoc.2018.05.011.

[284] Takahashi H, Numamoto Y, Tani J, Tsurekawa S. Considerations for $BaTiO_3$ Ceramics with High Piezoelectric Properties Fabricated by Microwave Sintering Method. Jpn J Appl Phys 2008;47:8468–71. https://doi.org/10.1143/JJAP.47.8468.

[285] Hoshina T, Kigoshi Y, Hatta S, Takeda H, Tsurumi T. Domain contribution to dielectric properties of fine-grained $BaTiO_3$ ceramics. Jpn J Appl Phys 2009;48:09KC1. https://doi.org/10.1143/JJAP.48.09KC01.

[286] Zhao Z, Buscaglia V, Viviani M, Buscaglia MT, Mitoseriu L, Testino A, et al. Grain-size effects on the ferroelectric behavior of dense nanocrystalline $BaTiO_3$ ceramics. Phys Rev B 2004;70:024107. https://doi.org/10.1103/PhysRevB.70.024107.

[287] Henry E, Lllyn A. Some Relationships between Grain Size and Properties in High Purity Barium Titanate Ceramics. J Can Ceram Soc 1965;34:137.

[288] Kanata T, Yoshikawa T, Kubota K. Grain-Size Effects on Dielectric Phase-Transition of $BaTiO_3$ Ceramics. Solid State Commun 1987;62:765–7. https://doi.org/10.1016/0038-1098(87)90044-5.

[289] Takahashi H, Numamoto Y, Tani J, Tsurekawa S. Piezoelectric properties of $BaTiO_3$ ceramics with high performance fabricated by microwave sintering. Jpn J Appl Phys 2006;1(45):7405–8. https://doi.org/10.1143/JJAP.45.7405.

[290] Karaki T, Yan K, Miyamoto T, Adachi M. Lead-free piezoelectric ceramics with large dielectric and piezoelectric constants manufactured from $BaTiO_3$ nano-powder. Jpn J Appl Phys 2007;2(46):L97–8. https://doi.org/10.1143/JJAP.46.L97.

[291] Chen Y, Ye HH, Wang XS, Li YX, Yao X. Grain size effects on the electric and mechanical properties of submicro $BaTiO_3$ ceramics. J Eur Ceram Soc 2020;40:391–400. https://doi.org/10.1016/j.jeurceramsoc.2019.09.033.

[292] Lemos da Silva L, Lee K-Y, Petrick S, Etter M, Schökel A, Chaves CG, et al. Uncovering the symmetry of the induced ferroelectric phase transformation in polycrystalline barium titanate. J Appl Phys. 2021;130:234101. https://doi.org/10.1063/5.0068703.

[293] Helke G, Seifert S, Cho SJ. Phenomenological and structural properties of piezoelectric ceramics based on $xPb(Zr,Ti)O_3$-$(1–x)Sr(K_{0.25}Nb_{0.75})O_3$ (PZT/SKN) solid solutions. J Eur Ceram Soc 1999;19:1265–8. https://doi.org/10.1016/S0955-2219(98)00417-8.

[294] Helbig U. Size effect in low grain size neodymium doped PZT ceramics. J Eur Ceram Soc 2007;27:2567–76. https://doi.org/10.1016/j.jeurceramsoc.2006.09.018.

[295] Haertling GH. Hot-pressed lead zirconate-lead titanate ceramics containing bismuth. Am Ceram Soc Bull 1964;43:875–9.

[296] Webster A, Weston T. The grain-size dependence of the electromechanical properties in lead zirconate-titanate ceramics. J Can Ceram Soc 1968;47:51–4.

[297] Okazaki K, Nagata K. Effects of Grain-Size and Porosity on Electrical and Optical Properties of PLZT Ceramics. J Am Ceram Soc 1973;56:82–6. https://doi.org/10.1111/j.1151-2916.1973.tb12363.x.

[298] Yamamoto T. Optimum Preparation Methods for Piezoelectric Ceramics and Their Evaluation. Am Ceram Soc Bull 1992;71:978–85.

[299] Randall CA, Kim N, Kucera JP, Cao WW, Shrout TR. Intrinsic and extrinsic size effects in fine-grained morphotropic-phase-boundary lead zirconate titanate ceramics. J Am Ceram Soc 1998;81:677–88. https://doi.org/10.1111/j.1151-2916.1998.tb02389.x.

[300] Hoffmann M, Hammer M, Endriss A, Lupascu D. Correlation between microstructure, strain behavior, and acoustic emission of soft PZT ceramics. Acta Mater 2001;49:1301–10. https://doi.org/10.1016/S1359-6454(01)00025-8.

[301] Sakaki C, Newalkar BL, Komarneni S, Uchino K. Grain size dependence of high power piezoelectric characteristics in Nb doped lead zirconate titanate oxide ceramics. Jpn J Appl Phys 2001;40:6907–10. https://doi.org/10.1143/JJAP.40.6907.

[302] Kamel TA, de With G. Grain size effect on the poling of soft $Pb(Zr,Ti)O_3$ ferroelectric ceramics. J Eur Ceram Soc 2008;28:851–61. https://doi.org/10.1016/j.jeurceramsoc.2007.08.010.

[303] Picht G, Khansur NH, Webber KG, Kungl H, Hoffmann MJ, Hinterstein M. Grain size effects in donor doped lead zirconate titanate ceramics. J Appl Phys 2020;128:214105. https://doi.org/10.1063/5.0029659.

[304] Eriksson M, Yan HX, Viola G, Ning HP, Gruner D, Nygren M, et al. Ferroelectric Domain Structures and Electrical Properties of Fine-Grained Lead-Free Sodium Potassium Niobate Ceramics. J Am Ceram Soc 2011;94:3391–6. https://doi.org/10.1111/j.1551-2916.2011.04510.x.

[305] Kakimoto K-i, Kaneko R, Kagomiya I. Grain-size-controlled $(Li,Na,K)NbO_3$ ceramics using powder source classified by centrifugal separator. Jpn J Appl Phys 2012;51:09LD6. https://doi.org/10.1143/JJAP.51.09LD06.

[306] Yang W, Li P, Wu S, Li F, Shen B, Zhai J. A study on the relationship between grain size and electrical properties in $(K,Na)NbO_3$-based lead-free piezoelectric ceramics. Adv Electron Mater 2019;5:1900570. https://doi.org/10.1002/aelm.201900570.

[307] Cai W, Fu CL, Gao JC, Chen HQ. Effects of grain size on domain structure and ferroelectric properties of barium zirconate titanate ceramics. J Alloys Compd 2009;480:870–3. https://doi.org/10.1016/j.jallcom.2009.02.049.

[308] Hao JG, Bai WF, Li W, Zhai JW. Correlation Between the Microstructure and Electrical Properties in High-Performance $(Ba_{0.85}Ca_{0.15})$ $(Zr_{0.1}Ti_{0.9})O_3$ Lead-Free Piezoelectric Ceramics. J Am Ceram Soc 2012;95:1998–2006. https://doi.org/10.1111/j.1551-2916.2012.05146.x.

[309] Kittel C. Theory of the Structure of Ferromagnetic Domains in Films and Small Particles. Phys Rev 1946;70:965–71. https://doi.org/10.1103/PhysRev.70.965.

[310] Hungria T, Alguero M, Hungria AB, Castro A. Dense, fine-grained $Ba_{1-x}Sr_xTiO_3$ ceramics prepared by the combination of mechanosynthesized nanopowders and spark plasma sintering. Chem Mater 2005;17:6205–12. https://doi.org/10.1021/cm0514488.

[311] Amorin H, Jimenez R, Ricote J, Hungria T, Castro A, Alguero M. Apparent vanishing of ferroelectricity in nanostructured $BiScO_3$-$PbTiO_3$. J Phys D Appl Phys 2010;43:285401. https://doi.org/10.1088/0022-3727/43/28/285401.

[312] Alguero M, Ricote J, Jimenez R, Ramos P, Carreaud J, Dkhil B, et al. Size effect in morphotropic phase boundary $Pb(Mg_{1/3}Nb_{2/3})O_3$-$PbTiO_3$. Appl Phys Lett 2007;91:112905. https://doi.org/10.1063/1.2778471.

[313] Kang BS, Dong GC, Choi S. Effects of grain size on pyroelectric and dielectric properties of $Pb_{0.9}La_{0.1}TiO_3$ ceramics. J Mater Sci: Mater Electron 1998;9:139–44. https://doi.org/10.1023/A:1008865523714.

[314] Xu F, Trolier-McKinstry S, Ren W, Xu BM, Xie ZL, Hemker KJ. Domain wall motion and its contribution to the dielectric and piezoelectric properties of lead zirconate titanate films. J Appl Phys 2001;89:1336–48. https://doi.org/10.1063/1.1325005.

[315] Uchino K, Sadanaga E, Kaisha T. Particle/grain size dependence of ferroeletricity. Ceram Trans 1990;8:107–15.

[316] Chen X, Fang DN, Hwang KC. Micromechanics simulation of ferroelectric polarization switching. Acta Mater 1997;45:3181–9. https://doi.org/10.1016/S1359-6454(97)00008-6.

[317] Graham HC, Tallan NM, Mazdiyasni KS. Electrical Properties of High-Purity Polycrystalline Barium Titanate. J Am Ceram Soc 1971;54:548–53. https://doi.org/10.1111/j.1151-2916.1971.tb12204.x.

[318] Lukacs V, Airimioaei M, Padurariu L, Curecheriu L, Ciomaga C, Bencan A, et al. Phase coexistence and grain size effects on the functional properties of $BaTiO_3$ ceramics. J Eur Ceram Soc 2022;42:2230–47. https://doi.org/10.1016/j.jeurceramsoc.2021.12.024.
[319] Anliker M, Brugger HR, Kanzig W. Das Verhalten Von Kolloidalen Seignetteelektrika III, Bariumtitanat $BaTiO_3$. Helv Phys Acta 1954;27:99–124.
[320] Williamson G, Hall W. X-ray line broadening from filed aluminium and wolfram. Acta Metall 1953;1:22–31. https://doi.org/10.1016/0001-6160(53)90006-6.
[321] Rogan RC, Tamura N, Swift GA, Üstündag E. Direct measurement of triaxial strain fields around ferroelectric domains using X-ray microdiffraction. Nat Mater 2003;2:379–81. https://doi.org/10.1038/nmat901.
[322] Zhang Y, Jiang Q. Twinning-induced stress and electric field concentrations in ferroelectric ceramics. J Am Ceram Soc 1995;78:3290–6. https://doi.org/10.1111/j.1151-2916.1995.tb07967.x.
[323] Pertsev N, Arlt G. Internal stresses and elastic energy in ferroelectric and ferroelastic ceramics: Calculations by the dislocation method. Ferroelectrics 1991;123:27–44. https://doi.org/10.1080/00150199108244710.
[324] Jiang QY, Subbarao EC, Cross LE. Grain-Size Dependence of Electric Fatigue Behavior of Hot-Pressed PLZT Ferroelectric Ceramics. Acta Metall Mater 1994;42:3687–94. https://doi.org/10.1016/0956-7151(94)90434-0.
[325] Ohya Y, Nakagawa ZE, Hamano K. Grain-Boundary Microcracking Due to Thermal-Expansion Anisotropy in Aluminum Titanate Ceramics. J Am Ceram Soc 1987;70:C184–6. https://doi.org/10.1111/j.1151-2916.1987.tb05720.x.
[326] Pohanka RC, Rice RW, Walker BE. Effect of Internal Stress on Strength of $BaTiO_3$. J Am Ceram Soc 1976;59:71–4. https://doi.org/10.1111/j.1151-2916.1976.tb09394.x.
[327] Marincel DM, Zhang HR, Kumar A, Jesse S, Kalinin SV, Rainforth WM, et al. Influence of a Single Grain Boundary on Domain Wall Motion in Ferroelectrics. Adv Funct Mater 2014;24:1409–17. https://doi.org/10.1002/adfm.201302457.
[328] Pertsev NA, Arlt G. Forced Translational Vibrations of 90° Domain-Walls and the Dielectric-Dispersion in Ferroelectric Ceramics. J Appl Phys 1993;74:4105–12. https://doi.org/10.1063/1.354457.
[329] Marincel DM, Zhang HR, Britson J, Belianinov A, Jesse S, Kalinin SV, et al. Domain pinning near a single-grain boundary in tetragonal and rhombohedral lead zirconate titanate films. Phys Rev B 2015;91:134113. https://doi.org/10.1103/PhysRevB.91.134113.
[330] Rodriguez BJ, Choudhury S, Chu YH, Bhattacharyya A, Jesse S, Seal K, et al. Unraveling Deterministic Mesoscopic Polarization Switching Mechanisms: Spatially Resolved Studies of a Tilt Grain Boundary in Bismuth Ferrite. Adv Funct Mater 2009;19:2053–63. https://doi.org/10.1002/adfm.20090010.
[331] Huey BD, Premnath RN, Lee S, Polomoff NA. High Speed SPM Applied for Direct Nanoscale Mapping of the Influence of Defects on Ferroelectric Switching Dynamics. J Am Ceram Soc 2012;95:1147–62. https://doi.org/10.1111/j.1551-2916.2012.05099.x.
[332] Tan XL, Ma C, Frederick J, Beckman S, Webber KG. The Antiferroelectric ↔ Ferroelectric Phase Transition in Lead-Containing and Lead-Free Perovskite Ceramics. J Am Ceram Soc 2011;94:4091–107. https://doi.org/10.1111/j.1551-2916.2011.04917.x.
[333] Rodriguez BJ, Chu YH, Ramesh R, Kalinin SV. Ferroelectric domain wall pinning at a bicrystal grain boundary in bismuth ferrite. Appl Phys Lett 2008;93:142901. https://doi.org/10.1063/1.2993327.
[334] Gruverman A, Auciello O, Tokumoto H. Imaging and control of domain structures in ferroelectric thin films via scanning force microscopy. Annu Rev Mater Sci 1998;28:101–23. https://doi.org/10.1146/annurev.matsci.28.1.101.
[335] Stolichnov I, Malin L, Colla E, Tagantsev AK, Setter N. Microscopic aspects of the region-by-region polarization reversal kinetics of polycrystalline ferroelectric $Pb(Zr,Ti)O_3$ films. Appl Phys Lett 2005;86:012902. https://doi.org/10.1063/1.1845573.
[336] Marton P, Shimada T, Kitamura T, Elsasser C. First-principles study of the interplay between grain boundaries and domain walls in ferroelectric $PbTiO_3$. Phys Rev B 2011;83:064110. https://doi.org/10.1103/PhysRevB.83.064110.
[337] DeVries RC, Burke JE. Microstructure of Barium Titanate Ceramics. J Am Ceram Soc 1957;40:200–6. https://doi.org/10.1111/j.1151-2916.1957.tb12603.x.
[338] Takahashi H, Numamoto Y, Tani J, Tsurekawa S. Domain properties of high-performance barium titanate ceramics. Jpn J Appl Phys 2007;1(46):7044–7. https://doi.org/10.1143/JJAP.46.7044.
[339] Tsurekawa S, Ibaraki K, Kawahara K, Watanabe T. The continuity of ferroelectric domains at grain boundaries in lead zirconate titanate. Scr Mater 2007;56:577–80. https://doi.org/10.1016/j.scriptamat.2006.12.029.
[340] Jang JW, Youn HJ, Byun C, Kim IT, Hong KS. Ferroelectric domain structures of polycrystalline $PbTiO_3$ thin films prepared by MOCVD. Ferroelectrics 1999;227:15–28. https://doi.org/10.1080/00150199908224187.
[341] Cheng SY, Ho NJ, Lu HY. Crystallographic relationships of the {111} growth twins in tetragonal barium titanate determined by electron-backscatter diffraction. J Am Ceram Soc 2006;89:3470–4. https://doi.org/10.1111/j.1551-2916.2006.01231.x.
[342] Wu YC, Lee CC, Lu HY, McCauley DE, Chu MSH. The $\{\bar{1}11\}$ growth twins in tetragonal barium titanate. J Am Ceram Soc 2006;89:1679–86. https://doi.org/10.1111/j.1551-2916.2006.00948.x.
[343] Mantri S, Oddershede J, Damjanovic D, Daniels JE. Ferroelectric domain continuity over grain boundaries. Acta Mater 2017;128:400–5. https://doi.org/10.1016/j.actamat.2017.01.065.
[344] Mantri S, Daniels JE. Ferroelectric Domain Continuity Over Grain Boundaries for Tetragonal, Orthorhombic, and Rhombohedral Crystal Symmetries. IEEE T Ultrason Ferr 2018;65:1517–24. https://doi.org/10.1109/TUFFC.2018.2827406.
[345] Mantri S, Daniels J. Domain walls in ferroelectrics. J Am Ceram Soc 2021;104:1619–32. https://doi.org/10.1111/jace.17555.
[346] Yazawa K, Uchida H, Blendell JE. Origin of Grain Size Effects on Voltage-Driven Ferroelastic Domain Evolution in Polycrystalline Tetragonal Lead Zirconate Titanate Thin Film. Adv Funct Mater 2020;30:1909100. https://doi.org/10.1002/adfm.201909100.
[347] Heinzmann A, Hennig E, Kolle B, Kopsch D, Richter S, Schwotzer H, et al. Properties of PZT multilayer actuators. 8th International Conference on New Actuators, Bremen, Germany 2002.
[348] Karastamatis T, Lupascu D, Lucato S, Lynch C. The effect of grain size on the R-curve behavior of Lead Zirconate Titanate (PZT). P Soc Photo-Opt Ins 2001;4333:38–40. https://doi.org/10.1117/12.432737.
[349] Karastamatis T, Lupascu DC, Lucato SLDE, Rödel J, Lynch CS. R-curves of lead zirconate titanate (PZT). J Eur Ceram Soc 2003;23:1401–8. https://doi.org/10.1016/S0955-2219(02)00352-7.
[350] Jiang Q, Subbarao E, Cross L. Fatigue in PLZT: acoustic emission as a discriminator between microcracking and domain switching. Ferroelectrics 1994;154:113–8. https://doi.org/10.1080/00150199408017271.
[351] Carisey T, Levin I, Brandon DG. Microstructure and Mechanical-Properties of Textured Al_2O_3. J Eur Ceram Soc 1995;15:283–9. https://doi.org/10.1016/0955-2219(95)90350-R.
[352] An L. Indentation fatigue in random and textured alumina composites. J Am Ceram Soc 1999;82:178–82. https://doi.org/10.1111/j.1151-2916.1999.tb01738.x.
[353] García RE, Craig Carter W, Langer SA. The effect of texture and microstructure on the macroscopic properties of polycrystalline piezoelectrics: application to barium titanate and PZN–PT. J Am Ceram Soc 2005;88:750–7. https://doi.org/10.1111/j.1551-2916.2005.00109.x.
[354] Schultheiß J, Clemens O, Zhukov S, Seggern H, Sakamoto W, Koruza J. Effect of degree of crystallographic texture on ferro-and piezoelectric properties of $Ba_{0.85}Ca_{0.15}TiO_3$ piezoceramics. J Am Ceram Soc 2017;100:2098–107. https://doi.org/10.1111/jace.14749.
[355] Choudhury S, Li YL, Krill C, Chen LQ. Effect of grain orientation and grain size on ferroelectric domain switching and evolution: Phase field simulations. Acta Mater 2007;55:1415–26. https://doi.org/10.1016/j.actamat.2006.09.048.
[356] Liu YC, Chang YF, Li F, Yang B, Sun Y, Wu J, et al. Exceptionally High Piezoelectric Coefficient and Low Strain Hysteresis in Grain-Oriented $(Ba,Ca)(Ti,Zr)O_3$ through Integrating Crystallographic Texture and Domain Engineering. ACS Appl Mater Interfaces 2017;9:29863–71. https://doi.org/10.1021/acsami.7b08160.
[357] Sabolsky EM, Maldonado L, Seabaugh MM, Swartz SL. Textured-$Ba(Zr,Ti)O_3$ piezoelectric ceramics fabricated by templated grain growth (TGG). J Electroceram 2010;25:77–84. https://doi.org/10.1007/s10832-009-9591-x.
[358] Yan Y, Yang L, Zhou Y, Cho KH, Heo JS, Priya S. Enhanced temperature stability in <111> textured tetragonal $Pb(Mg_{1/3}Nb_{2/3})_3$-$PbTiO_3$ piezoelectric ceramics. J Appl Phys 2015;118:104101. https://doi.org/10.1063/1.4929958.

[359] Vriami D, Damjanovic D, Vleugels J, Van der Biest O. Textured $BaTiO_3$ by templated grain growth and electrophoretic deposition. J Mater Sci 2015;50:7896–907. https://doi.org/10.1007/s10853-015-9322-4.

[360] Chang Y, Wu J, Sun Y, Zhang S, Wang X, Yang B, et al. Enhanced electromechanical properties and phase transition temperatures in [001] textured $Pb(In_{1/2}Nb_{1/2})O_3$-$Pb(Mg_{1/3}Nb_{2/3})O_3$-$PbTiO_3$ ternary ceramics. Appl Phys Lett. 2015;107:082902. https://doi.org/10.1063/1.4929688.

[361] Zhang HB, Zhu YW, Fan PY, Marwat MA, Ma WG, Liu K, et al. Temperature-insensitive electric-field-induced strain and enhanced piezoelectric properties of <001> textured $(K,Na)NbO_3$-based lead-free piezoceramics. Acta Mater 2018;156:389–98. https://doi.org/10.1016/j.actamat.2018.07.005.

[362] Liu BH, Li P, Shen B, Zhai JW, Zhang Y, Li F, et al. Simultaneously enhanced piezoelectric response and piezoelectric voltage coefficient in textured KNN-based ceramics. J Am Ceram Soc 2018;101:265–73. https://doi.org/10.1111/jace.15175.

[363] Jones JL, Slamovich EB, Bowman KJ. Critical evaluation of the Lotgering degree of orientation texture indicator. J Mater Res 2004;19:3414–22. https://doi.org/10.1557/JMR.2004.0440.

[364] Jones JL, Slamovich EB, Bowman KJ, Lupascu DC. Domain switching anisotropy in textured bismuth titanate ceramics. J Appl Phys 2005;98:104102. https://doi.org/10.1063/1.2128475.

[365] Takenaka T, Sakata K, Toda K. Piezoelectric Properties of Bismuth Layer-Structured Ferroelectric $Na_{0.5}Bi_{4.5}Ti_4O_{15}$Ceramic. Jpn J Appl Phys 1985;24:730.. https://doi.org/10.7567/JJAPS.24S2.730.

[366] Muralt P. Ferroelectric thin films for micro-sensors and actuators: a review. J Micromech Microeng 2000;10:136. https://doi.org/10.1088/0960-1317/10/2/307.

[367] Nagarajan V, Roytburd A, Stanishevsky A, Prasertchoung S, Zhao T, Chen L, et al. Dynamics of ferroelastic domains in ferroelectric thin films. Nat Mater 2003;2:43–7. https://doi.org/10.1038/nmat800.

[368] Duran C, Trolier-McKinstry S, Messing GL. Dielectric and piezoelectric properties of textured $Sr_{0.53}Ba_{0.47}Nb_2O_6$ ceramics prepared by templated grain growth. J Mater Res 2002;17:2399–409. https://doi.org/10.1557/JMR.2003.0032.

[369] Haugen AB, Olsen GH, Madaro F, Morozov MI, Tutuncu G, Jones JL, et al. Piezoelectric $K_{0.5}Na_{0.5}NbO_3$ Ceramics Textured Using Needlelike $K_{0.5}Na_{0.5}NbO_3$ Templates. J Am Ceram Soc 2014;97:3818–25. https://doi.org/10.1111/jace.13223.

[370] Ma Y, Bowman KJ. Texture in Hot-Pressed or Forged Alumina. J Am Ceram Soc 1991;74:2941–4. https://doi.org/10.1111/j.1151-2916.1991.tb06870.x.

[371] Vaudin MD, Rupich MW, Jowett M, Riley G, Bingert JF. A method for crystallographic texture investigations using standard x-ray equipment. J Mater Res 1998;13:2910–9. https://doi.org/10.1557/JMR.1998.0398.

[372] Dollase WA. Correction of Intensities for Preferred Orientation in Powder Diffractometry - Application of the March Model. J Appl Crystallogr 1986;19:267–72. https://doi.org/10.1107/S0021889886089458.

[373] Lotgering FK. Topotactical Reactions with Ferrimagnetic Oxides Having Hexagonal Crystal Structures-I. J Inorg Nulc Chem 1959;9:113–23. https://doi.org/10.1016/0022-1902(59)80070-1.

[374] Seabaugh MM, Vaudin MD, Cline JP, Messing GL. Comparison of texture analysis techniques for highly oriented α-Al_2O_3. J Am Ceram Soc 2000;83:2049–54. https://doi.org/10.1111/j.1151-2916.2000.tb01510.x.

[375] Wu J, Zhang S, Li F. Prospect of texture engineered ferroelectric ceramics. Appl Phys Lett 2022;121:120501. https://doi.org/10.1063/5.0101775.

[376] Ichikawa H, Sakamoto W, Akiyama Y, Maiwa H, Moriya M, Yogo T. Fabrication and Characterization of (100), (001)-Oriented Reduction-Resistant Lead-Free Piezoelectric (Ba, Ca)TiO_3 Ceramics Using Platelike Seed Crystals. Jpn J Appl Phys 2013;52. https://doi.org/10.7567/JJAP.52.09KD08.

[377] Chang Y, Poterala SF, Yang Z, Trolier-McKinstry S, Messing GL. ⟨001⟩ textured $(K_{0.5}Na_{0.5})(Nb_{0.97}Sb_{0.03})O_3$ piezoelectric ceramics with high electromechanical coupling over a broad temperature range. Appl Phys Lett. 2009;95:232905. https://doi.org/10.1063/1.3271682.

[378] Bai W, Li H, Xi J, Zhang J, Shen B, Zhai J. Effect of different templates and texture on structure evolution and strain behavior of <001>-textured lead-free piezoelectric BNT-based ceramics. J Alloys Compd 2016;656:13–23. https://doi.org/10.1016/j.jallcom.2015.09.209.

[379] Larsen PK, Kampschoer GLM, Mark MBvd, Klee M.. Ultrafast polarization switching of lead zirconate titanate thin films. Proc IEEE Int Symp Appl Ferroelectr 1992;217–24. https://doi.org/10.1109/ISAF.1992.300668.

[380] Bellur KR, Al-Shareef H, Rou S, Gifford K, Auciello O, Kingon A. Electrical characterization of sol-gel derived PZT thin films. Proc IEEE Int Symp Appl Ferroelectr 1992:448–51. https://doi.org/10.1109/ISAF.1992.300595.

[381] Hubmann AH, Li SY, Zhukov S, von Seggern H, Klein A. Polarisation dependence of Schottky barrier heights at ferroelectric $BaTiO_3$/RuO_2 interfaces: influence of substrate orientation and quality. J Phys D Appl Phys 2016;49:295304. https://doi.org/10.1088/0022-3727/49/29/295304.

[382] Kong S, Moriana A, Zhang S, Checchia S, Daniels JE. Self-poling and electromechanical response of crystallographically textured PMN-32PT prepared by templated grain growth. J Am Ceram Soc 2022;105:3581–9. https://doi.org/10.1111/jace.18315.

[383] Li J, Shen Z, Chen X, Yang S, Zhou W, Wang M, et al. Grain-orientation-engineered multilayer ceramic capacitors for energy storage applications. Nat Mater 2020;19:999–1005. https://doi.org/10.1038/s41563-020-0704-.

[384] Li P, Fu Z, Wang F, Huan Y, Zhou Z, Zhai J, et al. High piezoelectricity and stable output in $BaHfO_3$ and $(Bi_{0.5}Na_{0.5})ZrO_3$ modified $(K_{0.5}Na_{0.5})(Nb_{0.96}Sb_{0.04})O_3$ textured ceramics. Acta Mater 2020;199:542–50. https://doi.org/10.1016/j.actamat.2020.08.058.

[385] Liu Y, Chang Y, Sun E, Li F, Zhang S, Yang B, et al. Significantly enhanced energy-harvesting performance and superior fatigue-resistant behavior in [001] c-textured $BaTiO_3$-based lead-free piezoceramics. ACS Appl Mater Interfaces 2018;10:31488–97. https://doi.org/10.1021/acsami.8b10361.

[386] Haugen AB, Morozov MI, Jones JL, Einarsrud MA. Rayleigh analysis of dielectric properties in textured $K_{0.5}Na_{0.5}NbO_3$ ceramics. J Appl Phys. 2014;116:214101. https://doi.org/10.1063/1.4902858.

[387] Yan YK, Zhou JE, Maurya D, Wang YU, Priya S. Giant piezoelectric voltage coefficient in grain-oriented modified $PbTiO_3$ material. Nat Commun. 2016;7:13089 https://www.doi.org/10.1038/ncomms13089.

[388] Wada S, Yako K, Kakemoto H, Erhart J, Tsurumi T. Enhanced piezoelectric property of $BaTiO_3$ single crystals with the different domain sizes. Key Eng Mat 2004;269:19–22. https://doi.org/10.4028/www.scientific.net/KEM.269.19.

[389] Wada S, Yako K, Kakemoto H, Tsurumi T, Kiguchi T. Enhanced piezoelectric properties of barium titanate single crystals with different engineered-domain sizes. J Appl Phys 2005;98:014109. https://doi.org/10.1063/1.1957130.

[390] Wada S, Takeda K, Muraishi T, Kakemoto H, Tsurum T, Kimura T. Preparation of [110] grain oriented barium titanate ceramics by templated grain growth method and their piezoelectric properties. Jpn J Appl Phys 2007;1(46):7039–43. https://doi.org/10.1109/MHS.2007.4420883.

[391] Padurariu L, Curecheriu L, Galassi C, Mitoseriu L. Tailoring non-linear dielectric properties by local field engineering in anisotropic porous ferroelectric structures. Appl Phys Lett 2012;100:252905. https://doi.org/10.1063/1.4729878.

[392] Gheorghiu F, Padurariu L, Airimioaei M, Curecheriu L, Ciomaga C, Padurariu C, et al. Porosity-dependent properties of Nb-doped $Pb(Zr,Ti)O_3$ ceramics. J Am Ceram Soc 2017;100:647–58. https://doi.org/10.1111/jace.14587.

[393] Padurariu L, Curecheriu LP, Mitoseriu L. Nonlinear dielectric properties of paraelectric-dielectric composites described by a 3D Finite Element Method based on Landau-Devonshire theory. Acta Mater 2016;103:724–34. https://doi.org/10.1016/j.actamat.2015.11.008.

[394] Zhang Y, Roscow J, Lewis R, Khanbareh H, Topolov VY, Xie MY, et al. Understanding the effect of porosity on the polarisation-field response of ferroelectric materials. Acta Mater 2018;154:100–12. https://doi.org/10.1016/j.actamat.2018.05.007.

[395] Indergand R, Kochmann DM. Effect of temperature on domain wall–pore interactions in lead zirconate titanate: A phase-field study. Appl Phys Lett 2021;119:222901. https://doi.org/10.1063/5.0066612.

[396] Olariu CS, Padurariu L, Stanculescu R, Baldisserri C, Galassi C, Mitoseriu L. Investigation of low field dielectric properties of anisotropic porous $Pb(Zr,Ti)O_3$ ceramics: experiment and modeling. J Appl Phys 2013;114:214101. https://doi.org/10.1063/1.4837616.

[397] Johnson-Wilke RL, Wilke RHT, Wallace M, Rajashekhar A, Esteves G, Merritt Z, et al. Ferroelectric/Ferroelastic domain wall motion in dense and porous tetragonal lead zirconate titanate films. IEEE T Ultrason Ferr 2015;62:46–55. https://doi.org/10.1109/TUFFC.2014.006562.

[398] Matavž A, Bradeško A, Rojac T, Malič B, Bobnar V. Self-assembled porous ferroelectric thin films with a greatly enhanced piezoelectric response. Appl Mater Today 2019;16:83–9. https://doi.org/10.1016/j.apmt.2019.04.008.

[399] Esteves G, Wallace M, Johnson-Wilke R, Fancher CM, Wilke RHT, Trolier-McKinstry S, et al. Effect of Mechanical Constraint on Domain Reorientation in Predominantly {111}-Textured Lead Zirconate Titanate Films. J Am Ceram Soc 2016;99:1802–7. https://doi.org/10.1111/jace.14159.

[400] Griggio F, Jesse S, Kumar A, Ovchinnikov O, Kim H, Jackson TN, et al. Substrate clamping effects on irreversible domain wall dynamics in lead zirconate titanate thin films. Phys Rev Lett 2012;108:157604. https://doi.org/10.1103/PhysRevLett.108.157604.

[401] Denis LM, Esteves G, Walker J, Jones JL, Trolier-McKinstry S. Thickness dependent response of domain wall motion in declamped {001} $Pb(Zr_{0.3}Ti_{0.7})O_3$ thin films. Acta Mater 2018;151:243–52. https://doi.org/10.1016/j.actamat.2018.03.046.

[402] Wallace M, Johnson-Wilke RL, Esteves G, Fancher CM, Wilke RHT, Jones JL, et al. In situ measurement of increased ferroelectric/ferroelastic domain wall motion in declamped tetragonal lead zirconate titanate thin films. J Appl Phys 2015;117:054103. https://doi.org/10.1063/1.4907394.

[403] Lu G, Li S, Ding X, Sun J, Salje EK. Ferroelectric switching in ferroelastic materials with rough surfaces. Sci Rep 2019;9:1–7. https://doi.org/10.1038/s41598-019-52240-3.

[404] Roscow JI, Li Y, Hall DA. Residual stress and domain switching in freeze cast porous barium titanate. J Eur Ceram Soc 2022;42:1434–44. https://doi.org/10.1016/j.jeurceramsoc.2021.11.046.

[405] Menne D, Lemos da Silva L, Rotan M, Glaum J, Hinterstein M, Willenbacher N. Giant functional properties in porous electroceramics through additive manufacturing of capillary suspensions. ACS Appl Mater Interfaces 2022;14:3027–37. https://doi.org/10.1021/acsami.1c19297.

[406] Geis S, Fricke J, Löbmann P. Electrical properties of PZT aerogels. J Eur Ceram Soc 2002;22:1155–61. https://doi.org/10.1016/S0955-2219(01)00426-5.

[407] Zhang HL, Li JF, Zhang BP. Microstructure and electrical properties of porous PZT ceramics derived from different pore-forming agents. Acta Mater 2007;55:171–81. https://doi.org/10.1016/j.actamat.2006.07.032.

[408] Li JF, Takagi K, Ono M, Pan W, Watanabe R, Almajid A, et al. Fabrication and evaluation of porous piezoelectric ceramics and porosity-graded piezoelectric actuators. J Am Ceram Soc 2003;86:1094–8. https://doi.org/10.1111/j.1151-2916.2003.tb03430.x.

[409] Barabanova E, Malyshkina O, Ivanova A, Posadova E, Zaborovskiy K, Daineko A. Effect of porosity on the electrical properties of PZT ceramics. In: IOP Conf Ser: Mater Sci. Eng: IOP Publishing; 2013. p. 012026. https://doi.org/10.1088/1757-899X/49/1/012026.

[410] Yap EW, Glaum J, Oddershede J, Daniels JE. Effect of porosity on the ferroelectric and piezoelectric properties of $(Ba_{0.85}Ca_{0.15})$ $(Zr_{0.1}Ti_{0.9})O_3$ piezoelectric ceramics. Scr Mater 2018;145:122–5. https://doi.org/10.1016/j.scriptamat.2017.10.022.

[411] Yang A, Wang CA, Guo R, Huang Y, Nan CW. Porous PZT ceramics with high hydrostatic figure of merit and low acoustic impedance by TBA-based gel-casting process. J Am Ceram Soc 2010;93:1427–31. https://doi.org/10.1111/j.1551-2916.2009.03585.x.

[412] Zeng T, Dong XL, Chen ST, Yang H. Processing and piezoelectric properties of porous PZT ceramics. Ceram Int 2007;33:395–9. https://doi.org/10.1016/j.ceramint.2005.09.022.

[413] Menge G, Lorenz H, Fu ZW, Eichhorn F, Schader F, Webber KG, et al. Paper-Derived ferroelectric ceramics: a feasibility study. Adv Eng Mater 2018;20:1800052. https://doi.org/10.1002/adem.201800052.

[414] Nagata K. Effects of porosity and grain size on hysteresis loops of piezoelectric ceramics (PbLa)(ZrTi)O_3. Electr Eng Jpn 1980;100:1–8.

[415] Bakarič T, Rojac T, Abellard AP, Malič B, Levassort F, Kuscer D. Effect of pore size and porosity on piezoelectric and acoustic properties of $Pb(Zr_{0.53}Ti_{0.47})O_3$ ceramics. Adv Appl Ceram 2016;115:66–71. https://doi.org/10.1179/1743676115Y.0000000040.

[416] Zhang Y, Xie M, Roscow J, Bao Y, Zhou K, Zhang D, et al. Enhanced pyroelectric and piezoelectric properties of PZT with aligned porosity for energy harvesting applications. J Mater Chem A 2017;5:6569–80. https://doi.org/10.1039/C7TA00967D.

[417] Wersing W, Lubitz K, Mohaupt J. Dielectric, elastic and piezoelectric properties of porous PZT ceramics. Ferroelectrics 1986;68:77–97. https://doi.org/10.1080/00150198608238739.

[418] Banno H. Effects of Shape and Volume Fraction of Closed Pores on Remanent Polarization and Coercive Force of Ferroelectric Ceramics. Jpn J Appl Phys 1987;26:50–2. https://doi.org/10.7567/JJAPS.26S2.50.

[419] Roscow JI, Zhang Y, Krasny MJ, Lewis RWC, Taylor J, Bowen CR. Freeze cast porous barium titanate for enhanced piezoelectric energy harvesting. J Phys D: Appl Phys 2018;51:225301. https://doi.org/10.1088/1361-6463/aabc81.

[420] Deville S. Freeze-Casting of porous biomaterials: structure, properties and opportunities. Materials 2010;3:1913–27. https://doi.org/10.3390/ma3031913.

[421] Schultheiß J, Dermeik B, Filbert-Demut I, Hock N, Yin X, Greil P, et al. Processing and characterization of paper-derived Ti_3SiC_2 based ceramic. Ceram Int 2015;41:12595–603. https://doi.org/10.1016/j.ceramint.2015.06.085.

[422] Zhang Y, Bao YX, Zhang D, Bowen CR. Porous PZT Ceramics with Aligned Pore Channels for Energy Harvesting Applications. J Am Ceram Soc 2015;98:2980–3. https://doi.org/10.1111/jace.13797.

[423] Bouville F, Portuguez E, Chang Y, Messing GL, Stevenson AJ, Maire E, et al. Templated grain growth in macroporous materials. J Am Ceram Soc 2014;97:1736–42. https://doi.org/10.1111/jace.12976.

[424] Behera RP, Muhammad SBS, Jiaxuan MH, Le Ferrand H. Porous textured ceramics with controlled grain size and orientation. J Eur Ceram Soc 2021;41:617–24. https://doi.org/10.1016/j.jeurceramsoc.2020.08.061.

[425] Xu R, Liu S, Saremi S, Gao R, Wang JJ, Hong Z, et al. Kinetic control of tunable multi-state switching in ferroelectric thin films. Nat Commun 2019;10:1–10. https://doi.org/10.1038/s41467-019-09207-9.

[426] Chen P, Paillard C, Zhao HJ, Íñiguez J, Bellaiche L. Deterministic control of ferroelectric polarization by ultrafast laser pulses. Nat Commun 2022;13:1–8. https://doi.org/10.1038/s41467-022-30324-5.

[427] Khachaturyan R, Dimou A, Grünebohm A. Domain Wall Acceleration by Ultrafast Field Application: An Ab Initio-Based Molecular Dynamics Study. Phys. Status Solidi RRL. 2022;16:2200038. https://doi.org/10.1002/pssr.202200038.

[428] Ghosez P, Junquera J. Modeling of Ferroelectric Oxide Perovskites: From First to Second Principles. Annu Rev Condens Matter Phys 2022;13:325–64. https://doi.org/10.1146/annurev-conmatphys-040220-045528.

[429] Grünebohm A, Marathe M, Khachaturyan R, Schiedung R, Lupascu DC, Shvartsman VV. Interplay of domain structure and phase transitions: theory, experiment and functionality. J Phys: Condens Matter 2021;34:073002. https://doi.org/10.1088/1361-648X/ac3607.

[430] Smith RC, Hom CL. Domain wall theory for ferroelectric hysteresis. J Intell Material Syst Struct 1999;10:195–213. https://doi.org/10.1177/1045389X9901000302.

[431] Smith RC, Ounaies Z. A domain wall model for hysteresis in piezoelectric materials. J Intell Material Syst Struct 2000;11:62–79. https://doi.org/10.1106/HPHJ-UJ4D-E9D0-2MDY.

[432] Smith RC, Hu ZZ. Homogenized energy model for characterizing polarization and strains in hysteretic ferroelectric materials: Material properties and uniaxial model development. J Intell Material Syst Struct 2012;23:1833–67. https://doi.org/10.1177/1045389X12453967.

[433] Leschhorn A, Djoumbou S, Kliem H. Microscopic model of domain wall motion. J Appl Phys 2014;115:114106. https://doi.org/10.1063/1.4868901.

[434] Leschhorn A, Kliem H. Influence of thermal vibrations on polarization switching in the model of local fields. J Appl Phys 2017;121:014103. https://doi.org/10.1063/1.4973586.

[435] Wang JJ, Wang B, Chen LQ. Understanding, Predicting, and Designing Ferroelectric Domain Structures and Switching Guided by the Phase-Field Method. Annu Rev Mater Res 2019;49:127–52. https://doi.org/10.1146/annurev-matsci-070218-121843.

[436] Chen LQ. Phase-field method of phase transitions/domain structures in ferroelectric thin films: A review. J Am Ceram Soc 2008;91:1835–44. https://doi.org/10.1111/j.1551-2916.2008.02413.x.

[437] Xiao Y, Shenoy VB, Bhattacharya K. Depletion layers and domain walls in semiconducting ferroelectric thin films. Phys Rev Lett 2005;95:247603. https://doi.org/10.1103/PhysRevLett.95.247603.

[438] Gu YJ, Li ML, Morozovska AN, Wang Y, Eliseev EA, Gopalan V, et al. Flexoelectricity and ferroelectric domain wall structures: Phase-field modeling and DFT calculations. Phys Rev B 2014;89:174111. https://doi.org/10.1103/PhysRevB.89.174111.

[439] Li YL, Choudhury S, Haeni JH, Biegalski MD, Vasudevarao A, Sharan A, et al. Phase transitions and domain structures in strained pseudocubic (100) $SrTiO_3$ thin films. Phys Rev B 2006;73:184112. https://doi.org/10.1103/PhysRevB.73.184112.

[440] Choudhury S, Li YL, Krill CE, Chen LQ. Phase-field simulation of polarization switching and domain evolution in ferroelectric polycrystals. Acta Mater 2005;53:5313–21. https://doi.org/10.1016/j.actamat.2005.07.040.

[441] Vidyasagar A, Tan WL, Kochmann DM. Predicting the effective response of bulk polycrystalline ferroelectric ceramics via improved spectral phase field methods. J Mech Phys Solids 2017;106:133–51. https://doi.org/10.1016/j.jmps.2017.05.017.

[442] Su Y, Kang H, Wang Y, Li J, Weng GJ. Intrinsic versus extrinsic effects of the grain boundary on the properties of ferroelectric nanoceramics. Phys Rev B 2017;95:054121. https://doi.org/10.1103/PhysRevB.95.054121.

[443] Su Y, Liu N, Weng GJ. A phase field study of frequency dependence and grain-size effects in nanocrystalline ferroelectric polycrystals. Acta Mater 2015;87:293–308. https://doi.org/10.1016/j.actamat.2015.01.015.

[444] Zhang W, Bhattacharya K. A computational model of ferroelectric domains. Part I: model formulation and domain switching. Acta Mater 2005;53:185–98. https://doi.org/10.1016/j.actamat.2004.09.016.

[445] Lich LV, Shimada T, Wang J, Masuda K, Bui TQ, Dinh VH, et al. Continuum thermodynamics of unusual domain evolution-induced toughening effect in nanocracked strontium titanate. Eng Fract Mech 2018;190:232–44. https://doi.org/10.1016/j.engfracmech.2017.12.030.

[446] Zhou JE, Yan YK, Priya S, Wang YU. Computational study of textured ferroelectric polycrystals: Texture development during templated grain growth. J Appl Phys 2017;121:064108. https://doi.org/10.1063/1.4976022.

[447] Shu WL, Wang J, Zhang TY. Effect of grain boundary on the electromechanical response of ferroelectric polycrystals. J Appl Phys 2012;112:064108. https://doi.org/10.1063/1.4752269.

[448] Ming C, Yang TN, Luan K, Chen L, Wang L, Zeng JT, et al. Microstructural effects on effective piezoelectric responses of textured PMN-PT ceramics. Acta Mater 2018;145:62–70. https://doi.org/10.1016/j.actamat.2017.11.043.

[449] Abdollahi A, Arias I. Phase-field modeling of crack propagation in piezoelectric and ferroelectric materials with different electromechanical crack conditions. J Mech Phys Solids 2012;60:2100–26. https://doi.org/10.1016/j.jmps.2012.06.014.

[450] Narita F, Kobayashi T, Shindo Y. Evaluation of dielectric and piezoelectric behavior of unpoled and poled barium titanate polycrystals with oxygen vacancies using phase field method. Int J Smart Nano Mat 2016;7:265–75. https://doi.org/10.1080/19475411.2017.1278834.

[451] Shindo Y, Narita F, Kobayashi T. Phase field simulation on the electromechanical response of poled barium titanate polycrystals with oxygen vacancies. J Appl Phys 2015;117:234103. https://doi.org/10.1063/1.4922720.

[452] Vorotiahin IS, Morozovska AN, Genenko YA. Hierarchy of domain reconstruction processes due to charged defect migration in acceptor doped ferroelectrics. Acta Mater 2020;184:267–83. https://doi.org/10.1016/j.actamat.2019.11.048.

[453] Zuo Y, Genenko YA, Klein A, Stein P, Xu B. Domain wall stability in ferroelectrics with space charges. J Appl Phys 2014;115:084110. https://doi.org/10.1063/1.4866359.

[454] Fedeli P, Kamlah M, Frangi A. Phase-field modeling of domain evolution in ferroelectric materials in the presence of defects. Smart Mater Struct 2019;28:035021. https://doi.org/10.1088/1361-665X/aafff8.

[455] Zhang W, Bhattacharya K. A computational model of ferroelectric domains. Part II: grain boundaries and defect pinning. Acta Mater 2005;53:199–209. https://doi.org/10.1016/j.actamat.2004.09.015.

[456] Richter T, Denneler S, Schuh C, Suvaci E, Moos R. Textured PMN-PT and PMN-PZT. J Am Ceram Soc 2008;91:929–33. https://doi.org/10.1111/j.1551-2916.2007.02216.x.

[457] Amorín H, Uršič H, Ramos P, Holc J, Moreno R, Chateigner D, et al. $Pb(Mg_{1/3}Nb_{2/3})O_3$–$PbTiO_3$ textured ceramics with high piezoelectric response by a novel templated grain growth approach. J Am Ceram Soc 2014;97:420–6. https://doi.org/10.1111/jace.12721.

[458] Li F, Lin DB, Chen ZB, Cheng ZX, Wang JL, Li CC, et al. Ultrahigh piezoelectricity in ferroelectric ceramics by design. Nat Mater 2018;17:349–54. https://doi.org/10.1038/s41563-018-0034-4.

[459] Gao JH, Wang Y, He ZX, Liu YB, Wang D, Jin L, et al. Laminated Modulation of Tricritical Ferroelectrics Exhibiting Highly Enhanced Dielectric Permittivity and Temperature Stability. Adv Funct Mater 2019;29:1807162. https://doi.org/10.1002/adfm.201807162.

[460] Pan H, Li F, Liu Y, Zhang QH, Wang M, Lan S, et al. Ultrahigh-energy density lead-free dielectric films via polymorphic nanodomain design. Science 2019;365:578–82. https://doi.org/10.1126/science.aaw8109.

[461] Qian JF, Peng RC, Shen ZH, Jiang JY, Xue F, Yang TN, et al. Interfacial Coupling Boosts Giant Electrocaloric Effects in Relaxor Polymer Nanocomposites: In Situ Characterization and Phase-Field Simulation. Adv Mater. 2019;31:1801949. https://doi.org/10.1002/adma.201801949.

[462] Zhao C, Gao S, Yang T, Scherer M, Schultheiß J, Meier D, et al. Precipitation Hardening in Ferroelectric Ceramics. Adv Mater 2021;33:2102421. https://doi.org/10.1002/adma.202102421.

[463] Haun MJ, Zhuang ZQ, Furman E, Jang SJ, Cross LE. Thermodynamic Theory of the Lead Zirconate-Titanate Solid-Solution System, part III: Curie Constant and Sixth-Order Polarization Interaction Dielectric Stiffness Coefficients. Ferroelectrics 1989;99:45–54. https://doi.org/10.1080/00150198908221438.

[464] Pohlmann H, Wang JJ, Wang B, Chen LQ. A thermodynamic potential and the temperature-composition phase diagram for single-crystalline $K_{1-x}Na_xNbO_3$ ($0 \leq x \leq 0.5$). Appl Phys Lett 2017;110:102906. https://doi.org/10.1063/1.4978360.

[465] Tomeno I, Tsunoda Y, Oka K, Matsuura M, Nishi M. Lattice dynamics of cubic $NaNbO_3$: An inelastic neutron scattering study. Phys Rev B 2009;80:104101. https://doi.org/10.1103/PhysRevB.80.104101.

[466] Hlinka J, Márton P. Phenomenological model of a 90° domain wall in $BaTiO_3$-type ferroelectrics. Phys Rev B 2006;74:104104. https://doi.org/10.1103/PhysRevB.74.104104.

[467] Wang JJ, Meng FY, Ma XQ, Xu MX, Chen LQ. Lattice, elastic, polarization, and electrostrictive properties of $BaTiO_3$ from first-principles. J Appl Phys 2010;108:034107. https://doi.org/10.1063/1.3462441.

[468] Rupprecht G, Bell RO. Dielectric Constant in Paraelectric Perovskites. Phys Rev 1964;135:A748. https://doi.org/10.1103/PhysRev.135.A748.

[469] Suzuki I, Gura L, Klein A. The energy level of the $Fe^{2+}/^{3+}$-transition in $BaTiO_3$ and $SrTiO_3$ single crystals. Phys Chem Chem Phys 2019;21:6238–46. https://doi.org/10.1039/C8CP07872F.

[470] Sluka T, Tagantsev AK, Damjanovic D, Gureev M, Setter N. Enhanced electromechanical response of ferroelectrics due to charged domain walls. Nat Commun 2012;3:748. https://doi.org/10.1038/ncomms1751.

[471] Sluka T, Tagantsev AK, Bednyakov P, Setter N. Free-electron gas at charged domain walls in insulating $BaTiO_3$. Nat Commun 2013;4:1808. https://doi.org/10.1038/ncomms2839.

[472] Yudin PV, Tagantsev AK. Fundamentals of flexoelectricity in solids. Nanotechnology 2013;24:432001. https://doi.org/10.1088/0957-4484/24/43/432001.

[473] Wang B, Gu YJ, Zhang SJ, Chen LQ. Flexoelectricity in solids: Progress, challenges, and perspectives. Prog Mat Sci 2019;106:100570. https://doi.org/10.1016/j.pmatsci.2019.05.003.

[474] Fleury PA, Scott JF, Worlock JM. Soft Phonon Modes and 110° K Phase Transition in $SrTiO_3$. Phys Rev Lett 1968;21:16. https://doi.org/10.1103/PhysRevLett.21.16.

[475] Johnson W, Mehl R. Reaction kinetics in processes of reaction and growth. Trans Metall Soc AIME 1939;135:42–58.

[476] Avrami M. Kinetics of Phase Change. II Transformation-Time Relations for Random Distribution of Nuclei. J Chem Phys 1940;8:212–24. https://doi.org/10.1063/1.1750631.

[477] Kolmogorov AN. On the statistical theory of the crystallization of metals. Bull Acad Sci USSR, Math Ser 1937;1:355–9.

[478] Matyjasek K. Analysis of switching process in $(CH_3NH_3)_5Bi_2Br_{11}$ single crystals based on the Avrami model. J Phys D Appl Phys 2000;33:2553–9. https://doi.org/10.1088/0022-3727/33/20/306.

[479] Rogowski RZ, Matyjasek K, Jakubas R. Polarization switching in $(CH_3NH_3)_5Bi_2Cl_{11}$ ferroelectric crystals. Cryst Res Technol 2006;41:557–61. https://doi.org/10.1002/crat.200510625.

[480] Matyjasek K. Analysis of the switching process in triglycine sulphate crystals based on the Avrami model. J Phys D Appl Phys 2001;34:2211–9. https://doi.org/10.1088/0022-3727/34/14/317.

[481] Hashimoto S, Orihara H, Ishibashi Y. Study of D-E Hysteresis Loop of TGS Based on the Avrami-Type Model. J Phys Soc Jpn 1994;63:1601–10. https://doi.org/10.1143/JPSJ.63.1601.
[482] Usher TD, Poole CP, Farach HA. Ferroelectric Polarization Reversal in Potassium Dihydrogen Phosphate as Monitored by Switching Current. Ferroelectrics 1990;110:67–75. https://doi.org/10.1080/00150199108008244.
[483] Ishibashi Y, Orihara H. Size Effect in Ferroelectric Switching. J Phys Soc Jpn 1992;61:4650–6. https://doi.org/10.1143/JPSJ.61.4650.
[484] Orihara H, Ishibashi Y. A Statistical-Theory of Nucleation and Growth in Finite Systems. J Phys Soc Jpn 1992;61:1919–25. https://doi.org/10.1143/JPSJ.61.1919.
[485] Shur V, Rumyantsev E, Makarov S. Kinetics of phase transformations in real finite systems: Application to switching in ferroelectrics. J Appl Phys 1998;84:445–51. https://doi.org/10.1063/1.368047.
[486] Furukawa T, Date M, Ohuchi M, Chiba A. Ferroelectric Switching Characteristics in a Copolymer of Vinylidene Fluoride and Trifluorethylene. J Appl Phys 1984;56:1481–6. https://doi.org/10.1063/1.334102.
[487] Dimmler K, Parris M, Butler D, Eaton S, Pouligny B, Scott JF, et al. Switching Kinetics in KNO_3 Ferroelectric Thin-Film Memories. J Appl Phys 1987;61:5467–70. https://doi.org/10.1063/1.338237.
[488] Seike A, Amanuma K, Kobayashi S, Tatsumi T, Koike H, Hada H. Polarization reversal kinetics of a lead zirconate titanate thin-film capacitor for nonvolatile memory. J Appl Phys 2000;88:3445–7. https://doi.org/10.1063/1.1288010.
[489] Scott JF, Kammerdiner L, Parris M, Traynor S, Ottenbacher V, Shawabkeh A, et al. Switching Kinetics of Lead Zirconate Titanate Sub-Micron Thin-Film Memories. J Appl Phys 1988;64:787–92. https://doi.org/10.1063/1.341925.
[490] Wu D, Vrejoiu I, Alexe M, Gruverman A. Anisotropy of domain growth in epitaxial ferroelectric capacitors. Appl Phys Lett 2010;96:112903. https://doi.org/10.1063/1.3366724.
[491] Guo EJ, Dorr K, Herklotz A. Strain controlled ferroelectric switching time of $BiFeO_3$ capacitors. Appl Phys Lett 2012;101:242908. https://doi.org/10.1063/1.4772006.
[492] Lohse O, Grossmann M, Boettger U, Bolten D, Waser R. Relaxation mechanism of ferroelectric switching in $Pb(Zr,Ti)O_3$ thin films. J Appl Phys 2001;89:2332–6. https://doi.org/10.1063/1.1331341.
[493] Tagantsev AK, Stolichnov I, Setter N, Cross JS, Tsukada M. Non-Kolmogorov-Avrami switching kinetics in ferroelectric thin films. Phys Rev B 2002;66:214109. https://doi.org/10.1103/PhysRevB.66.214109.
[494] Duiker HM, Beale PD. Grain-Size Effects in Ferroelectric Switching. Phys Rev B 1990;41:490–5. https://doi.org/10.1103/PhysRevB.41.490.
[495] Dabra N, Hundal JS, Nautiyal A, Sekhar KC, Nath R. Analysis of ferroelectric polarization switching in $(NH_4)_{0.39}K_{0.61}NO_3$ films using nucleation limited switching model. J Appl Phys 2010;108:024108. https://doi.org/10.1063/1.3457228.
[496] Nautiyal A, Sekhar KC, Pathak NP, Dabra N, Hundal JS, Nath R. Polarization switching properties of spray deposited $CsNO_3$: PVA composite films. Appl Phys A 2010;99:941–6. https://doi.org/10.1007/s00339-010-5699-8.
[497] Schütrumpf J, Zhukov S, Genenko YA, von Seggern H. Polarization switching dynamics by inhomogeneous field mechanism in ferroelectric polymers. J Phys D Appl Phys 2012;45:165301. https://doi.org/10.1088/0022-3727/45/16/165301.
[498] Lee J, van Breemen AJJM, Khikhlovskyi V, Kemerink M, Janssen RAJ, Gelinck GH. Pulse-modulated multilevel data storage in an organic ferroelectric resistive memory diode. Sci Rep 2016;6:24407. https://doi.org/10.1038/srep24407.
[499] Genenko YA, Zhang M-H, Vorotiahin IS, Khachaturyan R, Liu Y-X, Li J-W, et al. Multistep stochastic mechanism of polarization reversal in orthorhombic ferroelectrics. Phys Rev B 2021;104:184106. https://doi.org/10.1103/PhysRevB.104.184106.
[500] Chan KH, Hagood NW. Modeling of nonlinear piezoceramics for structural actuation. Smart Structures and Materials 1994: Smart Structures and Intelligent Systems. Int Soc Optics Photonics 1994:194–206. https://doi.org/10.1117/12.175181.
[501] Hwang SC, Lynch CS, McMeeking RM. Ferroelectric/Ferroelastic Interactions and a Polarization Switching Model. Acta Metall Mater 1995;43:2073–84. https://doi.org/10.1016/0956-7151(94)00379-V.
[502] Lu W, Fang DN, Li CQ, Hwang KC. Nonlinear electric-mechanical behavior and micromechanics modelling of ferroelectric domain evolution. Acta Mater 1999;47:2913–26. https://doi.org/10.1016/S1359-6454(99)00153-6.
[503] Kessler H, Balke H. On the local and average energy release in polarization switching phenomena. J Mech Phys Solids 2001;49:953–78. https://doi.org/10.1016/S0022-5096(00)00073-9.
[504] Huber JE, Fleck NA, Landis CM, McMeeking RM. A constitutive model for ferroelectric polycrystals. J Mech Phys Solids 1999;47:1663–97. https://doi.org/10.1016/S0022-5096(98)00122-7.
[505] Hwang SC, Huber JE, McMeeking RM, Fleck NA. The simulation of switching in polycrystalline ferroelectric ceramics. J Appl Phys 1998;84:1530–40. https://doi.org/10.1063/1.368219.
[506] Chen W, Lynch CS. A micro-electro-mechanical model for polarization switching of ferroelectric materials. Acta Mater 1998;46:5303–11. https://doi.org/10.1016/S1359-6454(98)00207-9.
[507] Hwang SC, McMeeking RM. Finite element model of ferroelectric/ferroelastic polycrystals. In: Smart Structures and Materials 2000: Active Materials: Behavior and Mechanics: International Society for Optics and Photonics; 2000. p. 404–18. https://doi.org/10.1117/12.388224.
[508] Li J, Weng GJ. A theory of domain switch for the nonlinear behaviour of ferroelectrics. P Roy Soc A-Math Phy 1999;455:3493–511. https://doi.org/10.1098/rspa.1999.0462.
[509] Li JY, Liu D. On ferroelectric crystals with engineered domain configurations. J Mech Phys Solids 2004;52:1719–42. https://doi.org/10.1016/j.jmps.2004.02.011.
[510] Pathak A, McMeeking RM. Three-dimensional finite element simulations of ferroelectric polycrystals under electrical and mechanical loading. J Mech Phys Solids 2008;56:663–83. https://doi.org/10.1016/j.jmps.2007.05.003.
[511] Neumeister P, Balke H. Micromechanical modelling of remanent properties of morphotropic PZT. J Mech Phys Solids 2011;59:1794–807. https://doi.org/10.1016/j.jmps.2011.05.014.
[512] Landis CM. Non-linear constitutive modeling of ferroelectrics. Curr Opin Solid State Mater Sci 2004;8:59–69. https://doi.org/10.1016/j.cossms.2004.03.010.
[513] Evans PG, Sichel-Tissot RJ. In-situ X-Ray characteirzation of piezoelectric ceramic thin films. Am Cer Soc Bull 2013;92:18–23.
[514] Lee HJ, Ahn Y, Marks SD, Landahl EC, Zhuang S, Yusuf MH, et al. Structural evidence for ultrafast polarization rotation in ferroelectric/dielectric superlattice nanodomains. Phys Rev X 2021;11:031031. https://doi.org/10.1103/PhysRevX.11.031031.
[515] Chynoweth AG. Radiation Damage Effects in Ferroelectric Triglycine Sulfate. Phys Rev 1959;113:159–66. https://doi.org/10.1103/PhysRev.113.159.
[516] Vanishri S, Reddy JNB, Bhat HL. Irradiation effects on domain dynamics in ferroelectric glycine phosphite. J Appl Phys 2007;101:054106. https://doi.org/10.1063/1.2537695.
[517] Fletcher SR, Keve ET, Skapski AC. Crystal-Structure of Triglycine Sulfate at Low X-Ray Dosage and after Irradiation/Field Treatment. Ferroelectrics 1974;8:479–82. https://doi.org/10.1080/00150197408234132.
[518] Kalinin SV, Ziatdinov M, Hinkle J, Jesse S, Ghosh A, Kelley KP, et al. Automated and Autonomous Experiments in Electron and Scanning Probe Microscopy. ACS Nano 2021;15:12604–27. https://doi.org/10.1021/acsnano.1c02104.
[519] Kelley KP, Kalinin SV, Ziatdinov M, Paull O, Sando D, Nagarajan V, et al. Probing polarization dynamics at specific domain configurations: Computer-vision based automated experiment in piezoresponse force microscopy. Appl Phys Lett 2021;119:132902. https://doi.org/10.1063/5.0062046.
[520] Bencan A, Drazic G, Ursic H, Makarovic M, Komelj M, Rojac T. Domain-wall pinning and defect ordering in $BiFeO_3$ probed on the atomic and nanoscale. Nat Commun 2020;11:1762. https://doi.org/10.1038/s41467-020-15595-0.
[521] Lee W, Salje E, Bismayer U. Influence of point defects on the distribution of twin wall widths. Phys Rev B 2005;72:104116. https://doi.org/10.1103/PhysRevB.72.104116.
[522] Gault B, Chiaramonti A, Cojocaru-Mirédin O, Stender P, Dubosq R, Freysoldt C, et al. Atom probe tomography. Nat Rev Met Primers 2021;1:1–30. https://doi.org/10.1038/s43586-021-00047-w.

[523] Riemer LM, Lalitha KV, Jiang XJ, Liu N, Dietz C, Stark RW, et al. Stress-induced phase transition in lead-free relaxor ferroelectric composites. Acta Mater 2017;136:271–80. https://doi.org/10.1016/j.actamat.2017.07.008.

[524] Lalitha KV, Riemer LM, Koruza J, Rödel J. Hardening of electromechanical properties in piezoceramics using a composite approach. Appl Phys Lett 2017;111:022905. https://doi.org/10.1063/1.4986911.

[525] Ren P, Höfling M, Koruza J, Lauterbach S, Jiang X, Frömling T, et al. High temperature creep-mediated functionality in polycrystalline barium titanate. J Am Ceram Soc 2020;103:1891–902. https://doi.org/10.1111/jace.16881.

[526] Meier D, Seidel J, Gregg M, Ramesh R. Domain walls: from fundamental properties to nanotechnology concepts. New York, NY, USA: Oxford University Press; 2020.

[527] Puntigam L, Schultheiß J, Strinic A, Yan Z, Bourret E, Altthaler M, et al. Insulating improper ferroelectric domain walls as robust barrier layer capacitors. J Appl Phys 2021;129:074101. https://doi.org/10.1063/5.0038300.

[528] Ruff E, Krohns S, Lilienblum M, Meier D, Fiebig M, Lunkenheimer P, et al. Conductivity Contrast and Tunneling Charge Transport in the Vortexlike Ferroelectric Domain Patterns of Multiferroic Hexagonal $YMnO_3$. Phys Rev Lett 2017;118:036803. https://doi.org/10.1103/PhysRevLett.118.036803.

[529] Rojac T, Ursic H, Bencan A, Malic B, Damjanovic D. Mobile Domain Walls as a Bridge between Nanoscale Conductivity and Macroscopic Electromechanical Response. Adv Funct Mater 2015;25:2099–108. https://doi.org/10.1002/adfm.201402963.

[530] Makarovic M, Bayir MC, Ursic H, Bradesko A, Rojac T. Domain wall conductivity as the origin of enhanced domain wall dynamics in polycrystalline $BiFeO_3$. J Appl Phys 2020;128:064104. https://doi.org/10.1063/5.0017374.

[531] Liu LS, Rojac T, Damjanovic D, Di Michiel M, Daniels J. Frequency-dependent decoupling of domain-wall motion and lattice strain in bismuth ferrite. Nat Commun 2018;9:4928. https://doi.org/10.1038/s41467-018-07363-y.

[532] Nataf GF, Guennou M, Gregg JM, Meier D, Hlinka J, Salje EKH, et al. Domain-wall engineering and topological defects in ferroelectric and ferroelastic materials. Nat Rev Phys 2020;2:662. https://doi.org/10.1038/s42254-020-0235-z.

[533] Mundy JA, Schaab J, Kumagai Y, Cano A, Stengel M, Krug IP, et al. Functional electronic inversion layers at ferroelectric domain walls. Nat Mater 2017;16:622–7. https://doi.org/10.1038/nmat4878.

[534] Schaab J, Skjærvø SH, Krohns S, Dai XY, Holtz ME, Cano A, et al. Electrical half-wave rectification at ferroelectric domain walls. Nat Nanotechnol 2018;13:1028–34. https://doi.org/10.1038/s41565-018-0253-5.

[535] Schultheiß J, Lysne E, Puntigam L, Bourret E, Yan Z, Krohns S, et al. Charged ferroelectric domain walls for deterministic ac signal control. Nano Lett 2021;21:9560–6. https://doi.org/10.1021/acs.nanolett.1c03182.

[536] Lemanov V. Phase Transitions in Incipient Ferroelectrics of Perovskite Structure with Impurities. Defects and Surface-Induced Effects in Advanced Perovskites: Springer 2000:329–40.

[537] Randall CA, Fan Z, Reaney I, Chen LQ, Trolier-McKinstry S. Antiferroelectrics: History, fundamentals, crystal chemistry, crystal structures, size effects, and applications. J Am Ceram Soc 2021;104:3775–810. https://doi.org/10.1111/jace.17834.

[538] Fu Z, Chen X, Li Z, Hu T, Zhang L, Lu P, et al. Unveiling the ferrielectric nature of $PbZrO_3$-based antiferroelectric materials. Nat Commun 2020;11:1–8. https://doi.org/10.1038/s41467-020-17664-w.

[539] Bokov A, Ye Z-G. Recent progress in relaxor ferroelectrics with perovskite structure. J Mater Sci 2006;41:31–52. https://doi.org/10.1007/s10853-005-5915-7.

[540] Liu Z, Lu T, Ye J, Wang G, Dong X, Withers R, et al. Antiferroelectrics for energy storage applications: a review. Adv Mater Technol 2018;3:1800111. https://doi.org/10.1002/admt.201800111.

[541] Dvořák V. Improper ferroelectrics. Ferroelectrics 1974;7:1–9. https://doi.org/10.1080/00150197408237942.

[542] Levanyuk AP, Sannikov DG. Improper ferroelectrics. Sov Phys Uspekhi. 1974;17:199. https://doi.org/10.1070/PU1974v017n02ABEH004336.

[543] Meier D, Seidel J, Cano A, Delaney K, Kumagai Y, Mostovoy M, et al. Anisotropic conductance at improper ferroelectric domain walls. Nat Mater 2012;11:284–8. https://doi.org/10.1038/nmat3249.

[544] Wu W, Horibe Y, Lee N, Cheong SW, Guest JR. Conduction of Topologically Protected Charged Ferroelectric Domain Walls. Phys Rev Lett 2012;108:077203. https://doi.org/10.1103/PhysRevLett.108.077203.

[545] Zhang HB, Xu PW, Patterson E, Zang JD, Jiang SL, Rödel J. Preparation and enhanced electrical properties of grain-oriented $(Bi_{1/2}Na_{1/2})TiO_3$-based lead-free incipient piezoceramics. J Eur Ceram Soc 2015;35:2501–12. https://doi.org/10.1016/j.jeurceramsoc.2015.03.012.

[546] Bai W, Zhao X, Ding Y, Wang L, Zheng P, Hao J, et al. Giant field-induced strain with low hysteresis and boosted energy storage performance under low electric field in $(Bi_{0.5}Na_{0.5})TiO_3$-based grain orientation-controlled ceramics. Adv Electron Mater. 2020;6:2000332. https://doi.org/10.1002/aelm.202000332.

[547] Bai W, Zhao X, Huang Y, Ding Y, Wang L, Zheng P, et al. Integrating chemical engineering and crystallographic texturing design strategy for the realization of practically viable lead-free sodium bismuth titanate-based incipient piezoceramics. Dalton Trans 2020;49:8661–71. https://doi.org/10.1039/D0DT01334J.

[548] Fiebig M, Lottermoser T, Meier D, Trassin M. The evolution of multiferroics. Nat Rev Mater 2016;1:16046. https://doi.org/10.1038/natrevmats.2016.46.

[549] Zhang QH, Wang LJ, Wei XK, Yu RC, Gu L, Hirata A, et al. Direct observation of interlocked domain walls in hexagonal $RMnO_3$ (R = Tm, Lu). Phys Rev B 2012;85:020102(R). https://doi.org/10.1103/PhysRevB.85.020102.

[550] Harunsani MH, Li J, Qin YB, Tian HT, Li JQ, Yang HX, et al. Spontaneous formation of circular and vortex ferroelectric domain structure in hexagonal $YMnO_3$ and $YMn_{0.9}Fe_{0.1}O_3$ prepared by low temperature solution synthesis. Appl Phys Lett. 2015;107:062905. https://doi.org/10.1063/1.4928565.

[551] Baghizadeh A, Vieira JM, Vaghefi PM, Willinger MG, Amaral VS. Development of ferroelectric domains and topological defects in vacancy doped ceramics of h-$LuMnO_3$. J Appl Phys 2017;122:044102. https://doi.org/10.1063/1.4996349.

[552] Baghizadeh A, Vieira J, Stroppa D, Vaghefi PM, Graça M, Amaral J, et al. Interaction of multiferroic properties and interfaces in hexagonal $LuMnO_3$ ceramics. J Phys D: Appl Phys 2017;50:055304. https://doi.org/10.1088/1361-6463/50/5/055304.